High Resolution Modelling of Post-Glacial Rebound and Sea-Level Change

Anthony Patrick Purcell

A thesis submitted for the degree of Doctor of Philosophy of the Australian National University

The work in this thesis was carried out while I was a full-time student at the Research School of Earth Sciences at the Australian National University, between March 1991 and April 1997. Except where mentioned in the text, the research here is my own and is believed to be original. No part of this thesis has been submitted to any other university or similar institution.

Anthony Purcell,
September 1997.

Acknowledgements

I would like to take this opportunity to thank those who have made this thesis possible. The patience, advice, encouragement and support of my long-suffering supervisor, Prof. Kurt Lambeck, were invaluable, and I am deeply indebted for his insight and perseverance. During the course of my studies I was fortunate enough to share offices with Dr. Paul Johnston and Dr. Dan Zwartz, both of whom share an extraordinary enthusiasm for science and a flair for keeping life interesting, I am very grateful to both for their comments and support, which were freely given and always constructive. Special thanks also goes to Dr. Claudine Stirling for her encouragement and for being there to vent to, even though she well and truly beat me to the printers. I owe many thanks to Herb McQueen, Jean Braun, Cathy Smither, Georg Kaufmann, Malcolm Sambridge, Brian Kennett, and Patrick Wu, all of whom took the time to help me wrestle with problems theoretical and practical. Vivien Gleeson, Clementine Krayshek and Janine Dolton helped with administrative detail and encouragement, and saved me more angst than I care to contemplate. The companionship and support of my fellow students is also greatly appreciated, particularly Melita Keywood, Adam Kent, Leesa Carson, Julie Quinn, Yusuke Yokoyama, and Kevin Fleming.

Outside of the school, the understanding and tolerance of my family and friends has been nothing short of outstanding, for all they have given and have endured I extend my warmest thanks. In particular, I have been extremely fortunate to count Anthony Bushell, Andrew Hide, Lisa, Alyson, Gwen Morse, Neville Smythe, Brett Evill, Kenneth Beaton, and Takako Toda-Knight among my friends, and each is in no small part responsible for the completion of this work. Finally I thank God for all that he has granted, most especially the love and support of my parents, my grandmother, my sister Kerrie, and my brothers, Michael, Thomas and Paul.

ABSTRACT

The history of deformation of the earth's surface due to the removal of the Holocene and latest Pleistocene ice sheets is recorded in the global sea-level record. Recent advances in collection and dating of sea-level data, and computing technology have made possible high-resolution, high-precision numerical modelling of deglaciation events. Currently available mathematical formulations for the earth's response to surface loading are ill-suited to such high-resolution modelling however, suffering from numerical instability or excessive computational cost. In this thesis, the suitability of established techniques for modelling short wavelength surface load problems is closely examined. Achieving high resolution with the conventional spherical harmonic scheme has previously been shown to be prohibitively expensive computationally, the numerical instability or physical inappropriateness of associated harmonic analysis procedures is demonstrated here. The earth is then modelled as a flat, semi-infinite half-space and a new formalism developed that is exceptionally stable at depth, based on the wave propagation technique of seismology. This formalism is extended to include the effect of pre-stress and dilatation and their relative effects considered in detail. In the visco-elastic case, pre-stress advection is demonstrated to be critical in forcing deformation toward equilibrium with the load, and dilatation is shown to be largely negligible provided pre-stress is included. The new formulation is then tested numerically to establish its stability as part of a large super-position problem. The stability of numerical inversion schemes for the Fourier and Laplace transforms is also established, and their impact on the implementation of the wave propagation technique found to be small provided sufficient care is taken in choosing the inversion procedure to be used and their various input parameters.

Contents

INTRODUCTION

This thesis is concerned with theoretical aspects of the earth's response to surface loading on time scales of 10^3 yr to 10^5 yr. The motivation for this investigation is to provide a high accuracy formalism for modelling the Earth's response to cycles of glacial loading and unloading, from which the Earth's viscosity structure and response parameters may be inferred. A secondary motivation, not examined in this thesis, is the development of a high resolution inversion scheme to infer a detailed history of the deglaciation process from observations of the associated rebound.

Our understanding of the physical properties of the earth is severely limited by the fact that direct measurements can only be made at or near the earth's surface. Careful observation in a diverse range of fields has however made it possible to infer constraints on many of the processes at work in the earth's interior and their various interactions, though there is still much that we do not know with any certainty.

The earth's response to loading cycles of high frequency (less than a few years) is well established, the earth behaving essentially as an elastic body with parameters inferred from the analysis of seismic travel time data. At these frequencies the earth is shown to have a liquid core of radius 3 480 km with a semi-solid 1 250 km inner core, and to undergo a rapid change in elastic parameters from a depth of 410 km until a sharp discontinuity at 670 km marks the boundary between upper and lower mantle.

Apart from seismological phenomena, the most significant body of available observational data comes from the interaction of the continental plates. Plate tectonics is the largest scale geophysical phenomenon whose effects are directly observable at the surface and is therefore fundamental to our understanding of the earth as a whole. Any theory concerning the physical processes at work in the earth's interior must be consistent with the observed behaviour and properties of the continental plates.

On the time-scales of continental drift ($\sim 10^6$ yr) much of the earth may be treated as a fluid under an elastic or visco-elastic lithosphere, the motion of the continental plates being attributed to convection of the mantle material beneath. The nature of this mantle convection is of great importance to the field of earth science and is very strongly dependent on the viscosity of mantle material. If it were possible to determine the rate of mantle convection and whether it takes place throughout the entire mantle or occurs separately in the upper and lower mantle we would be able to place important constraints on the properties and behaviour of mantle material, such as the degree of mixing that occurs throughout the mantle, temperature distribution, the origin and composition of mantle plumes, the nature of hotspots, and the genesis of material from mid-ocean ridges. These properties themselves have far reaching consequences in a wide range of

geophysical and geochemical researches from the nature and behaviour of the earth's magnetic field through to the origin of the moon.

Mantle viscosity is constrained by the response through time of the earth under a surface load. The deformation that results form this loading is a function of both the rheology of the earth and the nature of the load, so that if the loading history is well understood then the relaxation process provides important data on the properties of the earth over the time-scale of the load. The results of such studies may not be directly applicable to the problem of mantle convection which takes place over particularly long time-scales ($\sim 10^6 - 10^7$), but it may be possible to extrapolate such data to longer time-scales.

At intermediate frequencies the earth cannot be satisfactorily modelled as either an elastic or fluid body and a theoretical treatment is required that spans these two limiting cases. This thesis attempts to develop an appropriate mathematical formalism, addressing in particular, methods that have the potential for very high spatial resolution. These techniques may then be applied to glacial rebound data to constrain both the history of the deglaciation process and the visosity profile of the earth.

A large body of high-quality rebound data is preserved in the sea-level record of the Holocene and Late Pleistocene. Geomorphological evidence indicates that over the last 2 million years the earth has been undergoing periodic glaciation and de-glaciation. The glaciation process seems to take place over a period of approximately 90 000 years and is followed by a rapid deglaciation which is complete after about 15 000 years. There then ensues an interglacial period of around 15 000 years before the cycle is repeated.

During the last glacial maximum, which occurred approximately 23 000 years ago, there were substantial glaciers over North America, Fennoscandia, Antarctica, Great Britain and the Barents Sea. These glaciers represented extremely large volumes of ice, the Laurentide ice sheet for example was about 3 000 metres thick and covered a large portion of North America. The melting of the glaciers and concomitant addition of melt-water to the oceans therefore resulted in substantial changes in the moment of inertia of the earth, and the shape of both the geoid and the earth's surface.

When a large load is placed on the surface of the earth it will displace material in the mantle and so deform the earth's surface and gravitational field. If the distribution of the load is subsequently altered the displaced material will move towards equilibrium with the new load distribution, resulting again in a change in the shape of the earth's surface and the geoid.

The relative position of the earth's surface and the shape of the geoid at times during and since the last period of deglaciation are preserved in the global sea level record and geoid observations. Direct geoid measurements are only available for a small fraction

of the period since the last glacial maximum so that the vast majority of detailed post-glacial rebound data are obtained from observations of sea level.

The change in sea level around the globe resulting from the melting of latest Pleistocene ice sheets is a function of both the change in load and the rheological properties of the earth. Sea-level is measured relative to the position of the shoreline so that the effect of all up-lift and subsidence events will be preserved in sea-level signals. For many sites it is possible to remove the contribution to sea-level change due to tectonic processes and other loading events however, and observations from such sites may then be used in conjunction with the theory developed for the problem of glacial rebound and sea-level change to constrain both the rheological properties of the earth and the melting history of the ice sheets.

The theoretical development for the deformation of the earth under surface loading is quite involved but has been extensively developed by a number of different investigators (Haskell 1935, McConnell 1965, Peltier 1974, Cathles 1975, Farrell & Clark 1976). In the simplest case sea level is altered simply by the volume of meltwater that is added to the oceans, this so-called eustatic sea level change is quite a large effect contributing 105-140m to global sea level depending on the ice model used. Farrell & Clark (1976) demonstrated that even if the earth is assumed to be completely rigid, post-glacial sea level change will be affected by changes in the gravitational attraction of the ice sheets and gravitational self-attraction of the water in the ocean basins.

If we allow the earth to deform under surface loads then calculation of sea level change is further complicated by the earth's response to the change in distribution of the surface load as the ice sheets are removed and water is added to the ocean basins (Bloom 1967). The change in geometry of the ocean basins due to the volume of meltwater added and loading effects result in the integral equation for sea level change being implicit. That is, sea level change at a particular point is dependent on the amount of sea level change at that point so that an iterative procedure is required to find a solution (Peltier & Andrews 1976). Johnston (1993) showed that for realistic earth models the effect of the ice load on the geometry of the ocean basins is accurately determined after two iterations.

A change in surface load results in a redistribution of mass within the earth to achieve equilibrium with the new load. The resulting change in the earth's gravitational field must be considered since both the mean shape of the surface of the ocean (which will be an equipotential function) and the deformation caused by a given surface load will vary if there is a change in the earth's gravitational field (Farrell & Clark 1976).

Various models for the earth's rheology have been considered, their complexity increasing as data, computational resources, and theoretical development allowed. Haskell (1935) and others modelled the earth as being completely viscous while Love (1911, 1927) and Longman (1962) developed the theoretical techniques necessary to

model the deformation of an elastic sphere. McConnell (1965) considered the deformation of a stratified, semi-infinite half-space with Maxwell rheology and Peltier (1974) developed the formalism for a radially symmetric spherical Maxwell body.

Having developed the theory for the deformation of a self-gravitating visco-elastic sphere under a surface load past investigators have used the resulting forward modelling procedures to invert post-glacial rebound data and constrain both the rheology of the earth (e.g. Cathles 1975, Peltier 1976, Nakada & Lambeck 1987, Gasperini & Sabadini 1989, Mitrovica & Peltier 1991, Johnston 1993) and the melting history of the Holocene ice sheets (e.g. Lambeck 1993a,b, Quinlan & Beaumont 1982).

Determining the melting history of the ice sheets since the last glacial maximum is a difficult problem in its own right. The extent of the glaciers as a function of time can often be determined from various geomorphological indicators but the thickness of the ice sheets cannot usually be determined directly except at a few isolated points where nanatuks were formed. Isotopic records broadly indicate the total amount of water that was removed from the oceans to form the ice sheets while palaeoclimatic data give some indication as to when and where the climate was most favourable for the formation and thickening of glaciers, there are of course also mechanical constraints on the shape of the glaciers but still many details of the melting history of the holocene ice sheets are relatively poorly known. For example, the vast majority of the land on which the Barents sea ice sheet rested is now submerged, obliterating much of the geomorphological evidence of its extent and progress, this is also a problem in many other areas such as the Irish sea, the North sea, the gulf of Bothnia, and the coastal fringes of the Laurentide and Antarctic ice sheets. Even where the geomorphological evidence is intact it is usually only possible to determine the direction and time of transit of the most recent ice sheet, all evidence of previous ice sheet transitions being overwritten.

The rapid improvement of the distribution and quality of sea-level observations throughout the Holocene and latest Pleistocene has made detailed modelling of ice sheets possible for the first time (Lambeck 1993b, Lambeck et. al. 1996). The vast majority of the formalism developed for the problem of glacial rebound has however been devoted to forward modelling, so that attempted inversions of the sea-level record to constrain the deglatiation process have been largely restricted to an iterative procedure of forward modelling and adjustment of the ice model. The detail that may be achieved with such a scheme is limited by the resolution of the modelling procedure being used which in some cases has proven inadequate.

Throughout the British Isles the sea-level record is generally of very high quality, particularly on the east coast of Scotland where past shorelines are preserved along the shores of firths and river valleys, in particular the Forth estuary, the valleys of the Tay and Earn Rivers, and the firths of Beauly, Cromarty, Inverness and Moray. In this

region the indicators of past sea-level mostly take the form of preserved shorelines extending substantial distances along inlets and estuaries, allowing very accurate determination of gradients.

One feature of particular interest is the relationship between the Main Late-glacial, High Buried, Main Buried and Low Buried shorelines. Age constraints from pollen and carbon-dating place these shorelines at approximately 10 300, 10 100, 9600, and 8700 years BP respectively (Haggart 1986, Firth & Haggart 1989) and their elevations indicate that sea-level in this region oscillated over that period. The nature of these oscillations is uncertain since available sea-level observations from other regions during this period are dominated by either addition of meltwater or post-glacial uplift, the sheer magnitude of these contributions is enough to completely mask any small amplitude features so that it is impossible to judge whether this is a global, regional, or local feature.

One possibility is that the oscillations are due to rebound associated with the Loch Lomond stadial, an extended climatic deterioration from 12 000 years BP onward during which a small ice sheet extended back into the upper valleys of the Forth and Tay rivers and down into the Clyde estuary (Sissons 1974, 1981). The readvance seems to have reached its maximum extent between about 11 000 and 10 500 years BP before retreating once again to vanish completely by 9 000 years BP.

It is equally possible however that they are a feature of the global sea-level, and if this is the case, their nature and behaviour could be significant in understanding the climate of the late Pleistocene and the mechanism of sea-level change. To distinguish between these two possibilities requires a technique for accurately modelling the rebound due to the ice sheet over these time periods. The lateral extent of the ice sheet in this period is significantly smaller than for earlier phases of the deglaciation process and attempts to model its effect have so far been unsuccessful due to poor resolution of the global modelling procedure for surface features of this wavelength.

The purpose of the current work is to investigate the various techniques by which rebound data may be used to infer details of the surface load at very high resolutions, and particularly techniques appropriate to incorporation into a direct inversion scheme.

The power and flexibility of the spherical harmonic scheme of Cathles (1975), and Farrell & Clark (1976) is such that it should not be completely discarded without first examining the possibility of extending it to the high-resolution case. Chapter 1 reviews the formalism of loading problems and particularly the analytical techniques developed for the case of a spherical body. The performance of this global spherical harmonic scheme is generally poor when applied to short wavelength loads however, since the power spectra for earth models are heavily biased toward harmonics of low degree, and high resolution features such as the Loch Lomond readvance require extremely high degree approximations to achieve even moderate definition.

Spherical harmonic analysis is a common tool in modelling the potential of the earth's magnetic field and several techniques (Haines 1985, De Santis 1991, 1992) have been developed to extend the global formalism to regional scale problems. The formalism of these techniques will be developed and their suitability to high resolution rebound problems closely examined.

For short to medium wavelength features such as the Fennoscandian and British ice sheets the sphericity of the earth may be neglected and it may be modelled as a flat semi-infinite body (Wolf 1984, 1985a, Amelung & Wolf 1994). Chapter 2 details the analytical development of three distinct techniques for modelling the deformation of a flat, stratified, elastic half-space in three-dimensional Cartesian coordinates.

Theoretically, the results of these techniques are equally valid but in practice the formalism of propagator matrix procedures is very susceptible to numerical instability with depth. This is particularly undesirable if the technique is to be used to model a larger ice sheet through superposition since the larger ice sheet will stress the earth to far greater depths than the component loads. Chapter 2 closes with a discussion of the relative analytical and numerical properties of each of the flat earth procedures, and a comparison of each against the analytical results for a uniform half-space.

Propagator matrix procedures rely implicitly on the use of Fourier transforms, and the extension to the visco-elastic regime is achieved with the use of the Laplace transform. The final results of flat earth modelling procedures are therefore obtained only after numerical inversions from the Fourier and Laplace transform domains. Numerical inversion of integral transforms carries significant risk of computational error and inversion routines and associated parameters must be chosen carefully to guarantee that the accuracy and stability of the propagator matrix procedures are not undermined by either of the inversions required.

The Fourier transform is a powerful and widely used numerical tool that is generally well understood but requires particular attention when applied to propagator matrix procedures of this type. In contrast, inversion of the Laplace transform is a very complex issue, particularly for compressible earth models, and though the collocation technique of Schapery (1962) provides good results for a large variety of earth models, it is prone to introduce small amplitude oscillations over long time-scales and there has previously been no means of comparison for its results for rheologies where the normal analysis scheme fails (which includes a large class of plausible earth models).

Chapter 3 examines the implementation of both Fourier and Laplace transform inversion schemes and possible sources of error for each, as well as providing several means of comparison for the collocation and normal mode techniques for compressible and incompressible earth models.

The analytical complexity of the propagator matrix techniques developed in chapter 2 is initially reduced by neglecting pre-stress advection and dilatation. These terms are indispensable if the results of our modelling are to have any physical validity however, and are reintroduced into the formalism for the propagator matrix procedures in Chapter 4. The effect of each term singly and combined is considered in the visco-elastic regime, the analysis is also extended to the the incompressible case, and finally the procedure is tested for stability as part of a superposition scheme.

Chapter 5 summarises the results of the previous chapters and discusses their consequences and potential applications. The chapter and thesis close by considering possible refinements that may be made in future implementations to the techniques developed here.

Chapter 1

DEFORMATION OF A SPHERICAL BODY BY SURFACE LOADING

1.0 Introduction

Deformation of the earth's surface due to loading by the ice sheets and changes in loading of the ocean basins is an important factor in calculating the sea-level change associated with the exchange of ice and water volumes. Accordingly, an extensive formalism has been developed to deal with this problem. For loads of small lateral extent, however, this global modelling procedure may not be particularly appropriate or efficient and it may be necessary to either adapt the procedure or develop new ones to accurately model the high-resolution case. In this chapter, I will briefly review the relevant formalism of continuum mechanics and the global modelling procedure itself with particular attention to its applicability to small-scale problems, and introduce the Spherical Cap Harmonic Analysis (SCHA) procedure developed by Haines (1985) and the Adjusted Spherical Harmonic Analysis (ASHA) scheme of De Santis (1992). Although these procedures were initially developed to model the regional behaviour of the earth's magnetic potential they may both be adapted and used with the global formalism to model local deformation.

The first step in developing a mathematical formalism for the deformation of the earth is to infer some of the *a priori* physical properties of the earth at the time scales we will be considering. The most obvious of these properties is of course the earth's shape. Neglecting ellipticity, topography, and diurnal rotation we may consider the earth as a static, spherical body and model its response to surface loading accordingly once we have determined the nature of its rheology.

Seismic travel time data indicate that the earth's elastic properties vary with depth and that there are layers within the earth throughout which these properties vary smoothly and some depths at which the physical properties change quite sharply (usually thought to correspond to chemical boundaries or mineralogical phase transitions). For mathematical convenience we will neglect lateral heterogeneities and assume that the various rheological parameters are a function only of depth. This allows us to model the earth as a stratified sphere whose rheological properties are prescribed throughout a series of layers. In some formulations the gradients of density and the elastic moduli are taken to be zero which is obviously not the case in the real earth although any function of depth may be closely approximated by a step-function if the layering is taken to be fine enough. Neglecting the local density gradient has a number of consequences for the validity of our modelling procedures and the interpretation of our results (see for example Kaufmann 1991,

Johnston 1993) but a detailed discussion of these considerations is beyond the scope of the current work.

On seismic time scales the crust and mantle behave as elastic solids while the outer core acts as a liquid and the inner core as some sort of slurry. On longer time scales (of about 10^6 yrs) the mantle seems to convect as a liquid. Rebound data indicate that for deformations over glacial time scales (of $10^3 - 10^5$ years) there is an initial 'elastic' component of deformation followed by an extended period of viscous creep indicating some sort of viscoelastic rheology (Lambeck, Smither & Johnston 1997). In fact we will assume that the earth (with the exception of the fluid core) is a Maxwell viscoelastic body since for such a body the constitutive equations have the simplest possible form consistent with the properties discussed above. Petrological and laboratory evidence indicates that mantle material actually has a more complicated non-linear rheology (see for example Ranalli 1982) but model results obtained assuming the earth to be 'effectively' a Maxwell viscoelastic body have so far proven sufficiently accurate to obviate the need to consider more complicated models (see for example Lambeck 1993a,b, Peltier & Andrews 1976, Wu & Peltier 1983).

Mindful of these assumptions, in this chapter we will review the theory for the deformation of a radially stratified, spherical, Maxwell viscoelastic body under surface loading from its foundations in continuum mechanics, paying particular attention to the Love number derivation (bearing in mind that the SCHA technique uses associated Legendre functions of non-integral degree). We will then discuss the global technique's applicability to short wavelength problems and perform a similar derivation and analysis of the SCHA and ASHA procedures.

1.1 The Field Equations

For the moment we consider a general body subject to some surface or body force. We will assume that the resulting deformation is small and occurs slowly and steadily, ensuring the system is in equilibrium at all times. We will also assume that the system is closed to any other external thermodynamic contributions and that there are no chemical changes in the system itself.

Under these assumptions the continuum form of Newton's second law (otherwise known as the inertia equation) is:

$$\nabla \cdot t + \rho^{(0)} f = \rho^{(0)} \ddot{u} \qquad (1.1.1)$$

where the $^{(0)}$ superscript indicates the initial value of the relevant function (in this case density but this convention will be adopted throughout for other functions) prior to the application of the force under consideration. The double dot over the *u* term indicates second derivative with respect to time.

Equation (1.1.1) is the Lagrangian form of the inertia equation, where *t* is the Piola-Kirchoff stress tensor, *f* is the body force per unit mass, ρ is the density, and *u* is the displacement. We will restrict our attention to the Lagrangian formulation rather than the Eulerian since it is most easily adapted to the modelling of glacial loading problems.

These equations are valid for a reference frame that rotates with the earth. The body forces in this instance include gravitation, centrifugal force, and the Coriolis force. We will neglect the latter two effects since diurnal and annual contributions are unlikely to have a significant impact on deformation occurring on a glacial time frame (c. 10^3 - 10^5 yrs), so that we are effectively considering a stationary sphere.

The second of the field equations is the continuity equation which enforces conservation of mass within the earth:

$$\nabla \cdot \left(\rho u \right) = 0 \qquad (1.1.2)$$

The last of the relevant field equations is that governing the earth's gravitational field. Gravitational acceleration is taken to be the gradient of the gravitational potential ϕ which satisfies the equation:

$$\nabla^2 \phi = -4\pi G \rho \qquad (1.1.3)$$

where G is Newton's gravitational constant.

§1.1.1 The Initial State

We assume that the body we are considering is initially in hydrostatic equilibrium. This is not entirely the case in the earth today as is demonstrated by the existence of gravity anomalies, but should be a reasonable assumption for the most part. If we also assume that initially the only force acting on our body is self-gravitation then the initial field satisfies the relations:

$$t^{(0)} = - p^{(0)} \, I \tag{1.1.4a}$$

$$\nabla p^{(0)} = \rho^{(0)} \, \nabla \, \phi^{(0)} \tag{1.1.4b}$$

$$\nabla^2 \phi^{(0)} = - 4 \pi G \rho^{(0)} \tag{1.1.4c}$$

where p is pressure and I is the Kronecker delta tensor (see Wolf 1991).

§1.1.2 The Incremental Field Equations

Rather than modelling the total response of the body to a force it is useful to consider only perturbations or increments from the initial state. The various properties of a body may be expressed as functions of either current position (the Eulerian formulation) or initial state (the Lagrangian formulation). It is easier to express boundary conditions using the Lagrangian framework but both are capable of expressing perturbations in the quantities we are interested in.

We will adopt the incremental notation of Wolf (1991) given in table 1.1 below:

Property	Lagrangian Formulation	Eulerian Formulation
particle position	x $l(x,t)$	$x(l, t)$ l
displacement	$u(x, t) = l(x, t) - x$	$U(x, t) \; U(x, t) = l - x(l, t)$
function	$f(x, t)$	$F(l, t)$
initial value	$f^{(0)}(x) = f(x, 0)$	$F^{(0)}(l) = F(l, 0)$
material increment	$f^{(\delta)}(x) = f(x, t) - f^{(0)}(x)$	$F^{(\delta)}(l) = F(l, t) - F^{(0)}(x(l, t))$
local increment	$f^{(\Delta)}(x) = f(x, t) - f^{(0)}(l(x, t))$	$F^{(\Delta)}(l) = F(l, t) - F^{(0)}(l)$

Table 1.1: Notation for local and material increments in Eulerian and Lagrangian forms.

Given a function f the material increment $f^{(\delta)}(X)$ is the change in the function for the particle X while the local increment $f^{(\Delta)}(X)$ is the change in the function at the position currently occupied by X. Assuming infinitesimal perturbations the material and local increments may be related using a Taylor series expansion:

$$f^{(\delta)} = f^{(\Delta)} + u \cdot \nabla f^{(0)} \qquad (1.1.5)$$

which is accurate to first order.

Substituting this expression into the inertial and gravitational equations (1.1.1) and (1.1.3), and noting that for the problem of glacial rebound the acceleration term on the right hand side of the inertia equation may be neglected, yields the incremental forms of the equations:

$$\nabla \cdot t^{(\delta)} + \nabla \left(\rho^{(0)} g^{(0)} \cdot u \right) + \rho^{(\Delta)} g^{(0)} + \rho^{(0)} g^{(\Delta)} = 0 \qquad (1.1.6)$$

$$\nabla^2 \phi^{(\Delta)} = -4\pi G \rho^{(\Delta)} \qquad (1.1.7)$$

where g is the acceleration due to gravity and is given by:

$$g = \nabla \phi \qquad (1.1.8)$$

and is taken to point upwards.

The local increment in density is given by the incremental form of the continuity equation (1.1.2):

$$\rho^{(\Delta)} = -\nabla \cdot \left(\rho^{(0)} u \right) \qquad (1.1.9)$$

This term assumes a particular convenient form inside a region of uniform density where it becomes the product of the original density field and the divergence of the deformation (also called the dilatation). I will hereafter refer to the component of (1.1.6) containing $\rho^{(\Delta)}$ as the internal buoyancy term.

The second term in equation (1.1.6) is the pre-stress advection term which represents the fact that before the current stress field was applied the body under consideration was already under stress due to its own weight as a result of its hydrostatic initial condition. The pre-existing stress field (the pre-stress) advects with the deformed material within the body and is super-imposed by the new stress field.

The pre-stress and internal buoyancy terms are both crucially important in assuring the physical meaningfulness of our modelling, particularly for deformations of the scale that typically occur in analyses of glacial rebound. The nature and magnitude of their

effect will be discussed extensively when we come to model the deformation of a flat semi-infinite half-space in chapter 4.

The incremental field equations take a simpler form inside a liquid since an inviscid material cannot support any shear stresses and there is no dilatation since a fluid can instantaneously move to dissipate any increase in pressure (except in the case where the increase is hydrostatic). Since there is no dilatation there will be a local density gradient (radial in the case of a sphere, vertical in the case of a flat semi-infinite half-space). From (1.1.9) we see that for a spherical body the local change in density is given by:

$$\rho^{(\Delta)} = -\left(\frac{\partial \rho^{(0)}}{\partial r}\right) u_r = -\rho^{(0)'} u_r$$

(1.1.10)

where we have used the prime (') to denote differentiation with respect to r.

Using (1.1.6), (1.1.7) and (1.1.10), noting that there is no dilatation, and setting $t^{(\delta)} = 0$ yields the incremental field equations for an inviscid body such as the core:

$$\nabla \cdot \boldsymbol{u} = 0$$

(1.1.11)

$$-\nabla\left(\rho^{(0)} \boldsymbol{g}^{(0)} \cdot \boldsymbol{u}\right) + \rho^{(0)'} u_r \boldsymbol{g}^{(0)} - \rho^{(0)} \boldsymbol{g}^{(\Delta)} = 0$$

(1.1.12)

$$\nabla^2 \phi^{(\Delta)} = 4\pi G \rho^{(0)'} u_r$$

(1.1.13)

1.2 Boundary Conditions

Throughout an elastic body the absence of cavitation, cracking and slip requires that the deformation, gravitational potential, and normal stress be everywhere continuous. At a layer boundary, the partition between two different rheological regimes, there may be a discontinuity in the density or elastic moduli of the material. Regardless of any such inhomogeneity, given the vector normal to the boundary, n, the quantities u_i, $\phi^{(\Delta)}$, and $\sum_j n_j^{(0)} t_{ij}^{(\Delta)}$, and $n^{(0)} \cdot \left(\nabla \phi^{(\Delta)} - 4\pi G \rho^{(0)} u \right)$ must be continuous across the boundary. The third of these boundary conditions is obtained by integrating the inertia equation (equation (1.1.6)) and letting the thickness of the pillbox approach zero while the last is given by repeating this integration, applying the convergence theorem, using the form for the internal buoyancy term given in (1.1.9), and letting the thickness of the pillbox again approach zero (see Cathles 1975, p17). Doing so yields:

$$0 = \int_v \nabla \cdot \left(\nabla \phi^{(\Delta)} - 4\pi G \rho^{(0)} u \right) dV = \int_s \left(\nabla \phi^{(\Delta)} - 4\pi G \rho^{(0)} u \right) \cdot da$$

$$= dA \, n \cdot \left[\nabla \phi^{(\Delta)} - 4\pi G \rho^{(0)} u \right]_-^+$$

(1.2.1)

Letting the height of the pillbox approach zero causes the area of the side of the cylinder to vanish and we get the boundary condition we require. Note that for a phase boundary the boundary conditions are different since (1.1.9) no longer applies the effect of this contribution has been considered for the spherical case by Johnston, Lambeck & Wolf (1996) but is beyond the scope of the present work.

We will assume that these boundary conditions hold at all internal boundaries except the core-mantle and free surface boundaries which we will discuss shortly.

It should be noted that in the case of a stratified sphere, the normals to the layer boundaries are simply radial vectors so that the third of the boundary conditions given above corresponds simply to continuity of the radial components of shear stress, $t_{r\theta}$ and $t_{r\varphi}$, and the radial stress itself, t_{rr}. Analogously, for a flat, stratified half-space the condition guarantees continuity of the vertical components of shear stress, t_{xz} and t_{yz}, and the vertical component of stress t_{zz}.

At the core-mantle boundary the situation is complicated (Dahlen 1974, Dahlen and Fels 1978) by the presence of a thin boundary layer inside which the dilatation is non-zero and the radial and tangential components of deformation change rapidly. If this layer is neglected then the deformation appears to be discontinuous across the core-mantle boundary. The perturbation to the gravitational potential and its gradient are continuous and smooth through the boundary layer so that the potential is continuous across the boundary. Since the core-mantle boundary layer represents a chemical transition and is

therefore governed by (1.1.9), the effective discontinuity in the gravity perturbation is a function of the effective discontinuities in density and radial deformation. The mathematical implementation of these boundary conditions will be discussed in greater detail during the spherical harmonic formulation in section 1.5.

For a flat semi-infinite half-space additional internal boundary conditions are given by a simple physical principle: all perturbations must tend to zero as distance from the source of deformation tends toward infinity.

At the surface we will restrict our attention to the case of an external force applied normal to the surface of the body for which there is no traction, in particular a surface load whose initial force per unit mass would be $g_S^{(0)}$, the gravitational acceleration of the body at the surface (in both the spherical and the flat earth cases this value will be constant over the free surface). Outside the body we also have that $\rho^{(\Delta)} = 0$ and the local increment in gravitational potential satisfies Laplace's equation ($\nabla^2 \phi^{(\Delta)} = 0$). Our other surface boundary conditions are given by observing that perturbations to gravity and potential must tend towards zero with increasing distance from the body. The mathematical formulation of the surface boundary conditions for a spherical body will be discussed in more detail in section 1.5.3.

1.3 Constitutive Equations

§1.3.1 Constitutive Equation for an Elastic Body

For deformations with sufficiently small gradients of displacement in a Cartesian coordinate system the various components of strain, ε_{ij}, are defined:

$$\varepsilon_{ij} = \frac{1}{2}\left(\frac{\partial u_i}{\partial x_j} + \frac{\partial u_j}{\partial x_i}\right)$$

(1.3.1)

where the u_i represent the corresponding components of displacement (see for example Fung 1965). The material increment in stress, $t^{(\delta)}$, is related to the strain by the constitutive equation. For an elastic solid the constitutive equation has the form:

$$t^{(\delta)} = \lambda\left(\nabla \cdot u\right)I + 2\mu\varepsilon$$

(1.3.2)

where λ and μ are the Lamé parameters of the body. Noting from (1.3.1) that $\nabla \cdot u = \sum_{k=1}^{3} \varepsilon_{kk}$ we may rewrite (1.3.2) in component form:

$$t_{ij}^{(\delta)} = \lambda\left(\delta_{ij}\,\varepsilon_{kk}\right) + 2\mu\,\varepsilon_{ij}$$

(1.3.3)

where we have adopted the Einstein summation convention $\varepsilon_{kk} = \sum_{k=1}^{3} \varepsilon_{kk}$.

Setting $i = j$ in (1.3.3) and summing, we see that:

$$t_{kk}^{(\delta)} = \left(3\lambda + 2\mu\right)\varepsilon_{kk}$$

(1.3.4)

which shows the effect of the bulk modulus of the body $K = \lambda + 2\mu/3$

§1.3.2 Constitutive Equation for a Maxwell Visco-elastic Body

We wish to model the deformation of the earth which initially has shear strength like an elastic body but under continuous stress loses its rigidity and behaves something like a Newtonian fluid. For such a material the constitutive equation has the form:

$$\dot{t}_{ij}^{(\delta)} + \frac{\mu}{\eta}\left(t_{ij}^{(\delta)} - \frac{\delta_{ij}t_{kk}^{(\delta)}}{3}\right) = \lambda\left(\delta_{ij}\,\dot{\varepsilon}_{kk}\right) + 2\mu\,\dot{\varepsilon}_{ij}$$

(1.3.5)

where η is the viscosity of the fluid.

Setting $i = j$ in (1.3.6) and summing yields a system directly equivalent to (1.3.4):

$$\dot{t}_{kk}^{(\delta)} = \left(3\lambda + 2\mu\right)\dot{\varepsilon}_{kk}$$

(1.3.6)

§1.3.3 Integral transforms

A useful tool in the solution of differential equations of the form of (1.3.5) is the integral transform. Using integral transforms translates a differential equation into a corresponding algebraic equation which may be solved using standard techniques and the resulting expression inverted to yield the desired function. In the time domain for example, it is often more convenient to mathematically model the behaviour of the Laplace transform of a function in the frequency domain rather than the function itself and then invert to yield the desired result in the time domain, particularly to model the behaviour of a Maxwell fluid (see for example Biot 1965, Peltier 1974). Similarly, in the spatial domain Fourier and Hankel transforms are used to simplify the problem being considered, particularly when modelling the behaviour of an elastic solid (see for example, Sneddon 1951, McConnell 1968).

The Fourier and Laplace transforms of a function f and their corresponding inverses are defined (see for example Spiegel 1968):

$$\mathcal{F}(f(x)) = \hat{f}(v) = \int_{-\infty}^{\infty} f(x)e^{-ivx}\,dx \qquad \mathcal{F}^{-1}(\hat{f}(v)) = \frac{1}{2\pi}\int_{-\infty}^{\infty} \hat{f}(v)e^{ivx}\,dv = f(x)$$

(1.3.7)

$$\mathcal{L}(f(t)) = \tilde{f}(s) = \int_{0}^{\infty} f(t)e^{-st}\,dt \qquad \mathcal{L}^{-1}(\tilde{f}(s)) = \frac{1}{2\pi i}\lim_{T\to\infty}\int_{c-iT}^{c+iT} \tilde{f}(s)e^{st}\,ds = f(t)$$

where the constant c used in the bounds of the last integral is chosen to be larger than $\mathrm{Re}\left(s_i\right)$ for all the singular points, s_i, of $\tilde{f}(s)$.

These transforms have the very desirable property of transforming differentiation into an algebraic operation (again see for example Spiegel 1968):

$$\mathcal{F}\left(\frac{df}{dx}\right) = iv\,\hat{f}(v) \qquad\qquad \mathcal{L}\left(\frac{df}{dt}\right) = s\,\tilde{f}(s) - f(0) \qquad (1.3.8)$$

where it should be noted that for any incremental quantity f, we have $f(0) = 0$.

The singular points or poles of the transform function, $\tilde{f}$, are the points in the complex plane at which the function becomes undefined (that is, its magnitude becomes arbitrarily large as it approaches the pole). A pole s_i of $\tilde{f}$ is said to be of order m_i if m_i is the smallest integer such that $\lim_{s\to s_i} \tilde{f}(s)(s-s_i)^{m_i}$ is finite; it is said to be an essential singularity of $\tilde{f}$ if there is no finite value of m_i for which this condition holds. The corresponding residue, r_i, of $\tilde{f}$ is then defined:

$$r_i = \frac{1}{(m_i - 1)!} \lim_{s \to s_i} \frac{d^{m_i - 1}}{ds^{m_i - 1}} \left(\tilde{f}(s)(s - s_i)^{m_i} \right) \tag{1.3.9}$$

Residues are particularly important in the calculation of the inverse Laplace transform since the most convenient technique for evaluating the inverse integral given in (1.3.7) is by closing a path to include all of the poles of the function (assuming that they are distributed through a bounded region), and then invoking the residue theorem (see for example Kreyszig 1983). The residue theorem states that the integral of a function around a closed curve is equal to the sums of the residues of the poles of the function that lie inside it (this assumes that they are distinct and that none of the singularities are essential).

In the case of the inverse Laplace transform the function e^{st} has no poles so all of the poles of the integrand must be due to $\tilde{f}(s)$. Using a Bromwich path (see for example Krylov and Skoblya 1977) to close the curve of integration means that the inverse integral is simply the sum of the residues of the integrand, which are themselves related to the residues of $\tilde{f}(s)$ (the integral around the closure approaches zero for sufficiently large values of T by the Jordan Lemma).

§1.3.4 Applying the Correspondence Principle to a Maxwell Fluid

Laplace transforming (1.3.5) and (1.3.6) yields the alternative form for the constitutive equations for a Maxwell visco-elastic body:

$$\tilde{t}_{ij}^{(\delta)}(s) - \frac{\delta_{ij}\,\tilde{t}_{kk}^{(\delta)}(s)}{3} = \frac{2\mu s}{s + \mu/\eta}\left(\tilde{\varepsilon}_{ij}(s) - \frac{\delta_{ij}\,\tilde{\varepsilon}_{kk}(s)}{3} \right) = 2\tilde{\mu}^{*}(s)\left(\tilde{\varepsilon}_{ij}(s) - \frac{\delta_{ij}\,\tilde{\varepsilon}_{kk}(s)}{3} \right) \tag{1.3.10}$$

$$\tilde{t}_{kk}^{(\delta)}(s) = (3\lambda + 2\mu)\,\tilde{\varepsilon}_{kk}(s) \tag{1.3.11}$$

where s is the Laplace transform variable.

Substituting (1.3.11) into (1.3.10) yields the transformed constitutive equation for a Maxwell fluid:

$$\tilde{t}_{ij}^{(\delta)}(s) = \tilde{\lambda}^{*}(s)\left(\delta_{ij}\,\tilde{\varepsilon}_{kk}(s) \right) + 2\tilde{\mu}^{*}(s)\tilde{\varepsilon}_{ij}(s) \tag{1.3.12}$$

which may be re-written:

$$\tilde{t}^{(\delta)}(s) = \tilde{\lambda}^{*}(s)\left(\nabla \cdot \tilde{u}(s) \right)\boldsymbol{I} + 2\tilde{\mu}^{*}(s)\tilde{\varepsilon}(s) \tag{1.3.13}$$

This is directly analogous to (1.3.2) so that the constitutive equation for a Maxwell fluid may be transformed to a form identical to that of an elastic solid with Lamé parameters dependent on s and related to the original values by the equations:

$$\tilde{\mu}^{*}(s) = \frac{\mu s}{s + \mu/\eta} \qquad (1.3.14)$$

$$\tilde{\lambda}^{*}(s) = \frac{\lambda s + \mu/\eta\left(\lambda + \frac{2}{3}\mu\right)}{s + \mu/\eta} \qquad (1.3.15)$$

Comparing (1.3.6) with (1.3.4) we see that the bulk modulus of the material is unchanged and that the constitutive equation for a Maxwell viscoelastic fluid is equivalent to that of an elastic solid with s-dependent Lamé parameters.

Numerically inverting from the frequency domain back to the time domain is however not so straightforward in the case of the Laplace transform. From the form of the inverse transform given in (1.3.7) we see that a direct inversion is only possible if the transformed function is known to have a particular form for which an inverse has been calculated analytically or if all the singularities of the transformed function and its residues at the poles are known.

From the form of the Laplace transform in (1.3.7) we see that if the function under consideration, $f(t)$, is changed dramatically over some appropriately small region then the value of the transform function, $\tilde{f}(s)$, will not be significantly affected. The value of the inverse transform at any point is therefore very strongly dependent on the exact nature of the transform function, small changes in the behaviour of $\tilde{f}(s)$ may result in significant changes in $f(t)$ (see for example Krylov & Skoblya 1977). This property of Laplace transforms makes the problem of numerically calculating the inverse transform particularly delicate and every effort must be made to ensure that any numerical error in the calculation of the transform function is as small as possible.

Since the exact form of a function and the nature and position of all its singularities are both rather difficult to determine numerically the problem is often simplified by making a series of assumptions about the form of the transform function (see for example Mitrovica & Peltier 1992). By calculating the value of the Laplace transformed deformation, $\tilde{u}(s)$, of the body for a number of different values of s we can approximate the s-dependence of $\tilde{u}(s)$ and invert to get the original time dependent function $u(t)$. The problem of determining the deformation of a Maxwell visco-elastic body can therefore be simplified to that of determining the deformation of an elastic solid under a surface load for a range of different Lamé parameters and inverting to the time domain. The numerical inversion of the Laplace transform will be discussed in greater detail in section 3.2.

1.4 Properties of Spherical Harmonic Functions

Mathematically modelling the behaviour of a spherical body is most conveniently done in spherical polar coordinates (see for example Farrell & Clark 1976). One of the most natural tools for such an analysis are the spherical harmonic functions. We shall follow the development of Johnston (1993)

§1.4.1 Spherical Harmonic Functions

The normalised spherical surface harmonics are a set of orthogonal harmonic functions on the surface of sphere. They arise naturally in the mathematical analysis of gravitational and magnetic potentials or any conservative field.

By separation of variables we see that Laplace's equation in spherical polar coordinates is

$$\Delta f(r, \theta, \varphi) = \nabla^2 f = \frac{1}{r^2}\left[\frac{\partial}{\partial r}\left(r^2 \frac{\partial f}{\partial r}\right) + \frac{1}{\sin \theta}\frac{\partial}{\partial \theta}\left(\sin \theta \frac{\partial f}{\partial \theta}\right) + \frac{1}{\sin^2 \theta}\frac{\partial^2 f}{\partial \varphi^2}\right] \quad (1.4.1)$$

where r is radial distance from the origin, θ is co-latitude, and φ is longitude. This equation has linearly independent solutions of the form:

$$f_{nm}(r, \theta, \varphi) = \left(a_{nm} r^n + b_{nm} r^{-(n+1)}\right)\left[A_{nm} \cos\left(m\varphi\right) + B_{nm} \sin\left(m\varphi\right)\right] P_{nm}(\cos \theta) \quad (1.4.2)$$

where a_{nm}, b_{nm}, A_{nm}, and B_{nm} are arbitrary constants, and P_{nm} is the associated Legendre function of degree n and order m (see for example Abramowitz & Stegun 1972) which satisfies Legendre's associated differential equation:

$$\frac{d}{dx}\left(\left(1 - x^2\right)\frac{dy}{dx}\right) + \left(n(n+1) - \frac{m^2}{1 - x^2}\right)y = 0 \quad (1.4.3)$$

The f_{nm} given in (1.4.2) are finite, continuous and single-valued at all points inside a sphere only if all b_{nm} are zero and both m and n are positive integers. In this instance the P_{nm} are in fact polynomials (see for example Spiegel 1968) and have the property that for $|m| > n$, $P_{nm}(x) = 0$. Restricting our attention to the case $b_{nm} = 0$, m and n integers such that $|m| \le n$ we may define fully normalised spherical surface harmonics:

$$Y_{nm}(\theta, \varphi) = K_{nm} P_{nm}(\cos \theta) \begin{array}{c} \cos m\varphi \\ \sin |m|\varphi \end{array} \qquad \begin{array}{c} n \ge m \ge 0 \\ 0 > m \ge -n \end{array} \quad (1.4.4)$$

where the constant term K_{nm} is defined

$$K_{nm} = \left[\frac{(2n+1)(2-\delta_{m0})\Gamma(n-|m|+1)}{\Gamma(n+|m|+1)} \right]^{\frac{1}{2}} \tag{1.4.5}$$

By the theory of Sturm-Liouville boundary value problems (see for example Boyce & DiPrima 1977) these functions satisfy the relation:

$$\int_0^\pi d\theta \sin\theta \int_0^{2\pi} d\varphi \, Y_{n_1 m_1}(\theta, \varphi) Y_{n_1 m_1}(\theta, \varphi) = 4\pi \delta_{n_1 n_2} \delta_{m_1 m_2} \tag{1.4.6}$$

which makes them particularly convenient when trying to approximate a function over the surface of a sphere using least squares (see for example Kreyszig 1983).

Another important property of Legendre polynomials (which correspond to the case $m = 0$) is their generating function (see for example Spiegel 1968). Given two scalar quantities, t and x, with x lying in the region $[-1, 1]$, the following equivalence holds

$$\frac{1}{\sqrt{1 - 2tx + t^2}} = \sum_{n=0}^\infty P_n(x) t^n \tag{1.4.7}$$

From the theory of harmonic functions we have that any suitably well-behaved function (i.e. continuous, differentiable and non-singular almost everywhere) over a closed, regular region may be approximated to arbitrary accuracy in that region with an harmonic function (see, for example, Gilbarg & Trudinger 1983). So that over the surface of a sphere any such function may be written as an infinite sum of surface harmonics, i.e. there exist coefficients F_{nm} such that:

$$\lim_{N \to \infty} \int_0^\pi d\theta \sin\theta \int_0^{2\pi} d\varphi \left(F_N(\theta, \varphi) - F(\theta, \varphi) \right)^2 = 0 \tag{1.4.8}$$

where the functions F_N have the form:

$$F_N(\theta, \varphi) = \sum_{n=0}^N \sum_{m=-n}^n F_{nm} Y_{nm}(\theta, \varphi) \tag{1.4.9}$$

In fact using the method of least squares to minimise (1.4.8) for each value of N and applying (1.4.6) we see that the F_{nm} are given by the relation:

$$F_{nm} = \frac{1}{4\pi} \int_0^\pi d\theta \sin\theta \int_0^{2\pi} d\varphi \, Y_{nm}(\theta, \varphi) F(\theta, \varphi) \tag{1.4.10}$$

and are notable for being independent of N.

A spherical surface harmonic of degree n is defined as any function of the form:

$$Y_n(\theta, \varphi) = \sum_{m=-n}^{n} c_{nm} Y_{nm}(\theta, \varphi) \tag{1.4.11}$$

where the coefficients c_{nm} satisfy the constraint:

$$\sum_{m=-n}^{n} c_{nm}^2 = 1 \tag{1.4.12}$$

The gradient of a spherical harmonic function may be written:

$$\nabla Y_n(\theta, \varphi) = \frac{\hat{\theta}}{r} \frac{\partial Y_n}{\partial \theta} + \frac{\hat{\varphi}}{r \sin \theta} \frac{\partial Y_n}{\partial \varphi} \tag{1.4.13}$$

(see for example Spiegel 1968), where $\hat{\theta}$ and $\hat{\varphi}$ are the unit latitudinal and longitudinal vectors respectively and we have used the fact that surface spherical harmonic functions do not vary radially and so have no radial component to their gradient.

From (1.4.2), (1.4.3) and (1.4.4) we have the following properties of surface spherical harmonic functions:

$$\nabla^2 \left(r^n Y_n(\theta, \varphi) \right) = 0 \tag{1.4.14}$$

$$\nabla^2 Y_n(\theta, \varphi) = \frac{1}{r^2} \left[\frac{1}{\sin \theta} \frac{\partial}{\partial \theta} \left(\sin \theta \frac{\partial Y_n}{\partial \theta} \right) + \frac{1}{\sin^2 \theta} \frac{\partial^2 Y_n}{\partial \varphi^2} \right]$$

$$= -\frac{n(n+1)}{r^2} Y_n(\theta, \varphi) \tag{1.4.15}$$

$$\nabla^2 \left(\frac{\partial Y_n}{\partial \theta} \right) = -\frac{n(n+1)}{r^2} \frac{\partial Y_n}{\partial \theta} + \frac{1}{\sin^2 \theta} \left(\frac{\partial Y_n}{\partial \theta} + 2 \cot \theta \frac{\partial^2 Y_n}{\partial \varphi^2} \right) \tag{1.4.16}$$

1.5 Calculating the Deformation of an Elastic Sphere

In spherical polar coordinates the most general vector field (and in particular the displacement field for a given surface loading over a spherical body) may be written:

$$u(x) = \hat{r}\, U(x) + \nabla V(x) + \hat{r} \times W(x) \tag{1.5.1}$$

where $\hat{r}$ is the unit vector in the radial direction. The three components of the field are known respectively as the spheroidal, poloidal and toroidal modes. In the case of a radial load with no shear stress the toroidal component of the displacement field must be zero.

§1.5.1 The Spherical Harmonic Formulation for an Elastic Solid

Since any finite, differentiable scalar function may be written as a sum of components of the form of (1.4.2), using the notation of (1.4.9) we may substitute this result into (1.5.1) to show that the displacement field of a spherically symmetric body may be written as an infinite sum of the form:

$$u(r, \theta, \varphi) = \sum_{n=0}^{\infty} \left(\frac{r}{a}\right)^n \left[\hat{r}\, u_n(r)\, Y_n(\theta,\varphi) + r\, v_n(r) \nabla Y_n(\theta,\varphi)\right] \tag{1.5.2}$$

where a is the radius of the sphere being considered, in our case the earth. The functions $u_n(r)$ and $v_n(r)$ are, respectively, the radial and tangential spherical harmonic coefficients of deformation.

Being a suitably well behaved scalar function, the local increment in potential may be written as an infinite sum of the form:

$$\phi^{(\Delta)}(r, \theta, \varphi) = \sum_{n=0}^{\infty} \left(\frac{r}{a}\right)^n \phi_n(r)\, Y_n(\theta,\varphi) \tag{1.5.3}$$

From (1.5.2) and the form for the divergence of a vector field in spherical polar coordinates (see for example Spiegel 1968) we see that the dilatation, $\Delta = \nabla \cdot u$, may be written as the infinite sum:

$$\Delta = \nabla \cdot u = \sum_{n=0}^{\infty} \left(\frac{r}{a}\right)^n Y_n \left[u_n' + \frac{n+2}{r}\, u_n - \frac{n(n+1)}{r}\, v_n\right] \tag{1.5.4}$$

where, as in equation (1.1.10) we have used the prime $(')$ to represent differentiation with respect to r.

Similarly, we may substitute (1.5.2) into the spherical polar representations of the various components of strain (see for example Goodbody 1982) to show that they may also be expressed as infinite sums of the form:

$$\varepsilon_{rr} = \sum_{n=0}^{\infty} \left(\frac{r}{a}\right)^n Y_n \left(u_n' + \frac{n}{r} u_n\right) \tag{1.5.5a}$$

$$\varepsilon_{r\theta} = \frac{1}{2} \sum_{n=0}^{\infty} \left(\frac{r}{a}\right)^n \frac{\partial Y_n}{\partial \theta} \left(\frac{u_n}{r} + v_n' + \frac{n-1}{r} v_n\right) \tag{1.5.5b}$$

$$\varepsilon_{r\varphi} = \frac{1}{2\sin\theta} \sum_{n=0}^{\infty} \left(\frac{r}{a}\right)^n \frac{\partial Y_n}{\partial \varphi} \left(\frac{u_n}{r} + v_n' + \frac{n-1}{r} v_n\right) \tag{1.5.5c}$$

$$\varepsilon_{\theta\theta} = \sum_{n=0}^{\infty} \left(\frac{r}{a}\right)^n \frac{1}{r} \left(u_n Y_n + v_n \frac{\partial^2 Y_n}{\partial \theta^2}\right) \tag{1.5.5d}$$

$$\varepsilon_{\varphi\varphi} = \sum_{n=0}^{\infty} \left(\frac{r}{a}\right)^n \frac{1}{r} \left(u_n Y_n + v_n \cot\theta \frac{\partial Y_n}{\partial \theta} + \frac{v_n}{\sin^2\theta} \frac{\partial^2 Y_n}{\partial \varphi^2}\right) \tag{1.5.5e}$$

$$\varepsilon_{\theta\varphi} = \sum_{n=0}^{\infty} \left(\frac{r}{a}\right)^n \frac{v_n}{r\sin\theta} \left(\frac{\partial^2 Y_n}{\partial \varphi \partial \theta} - \cot\theta \frac{\partial Y_n}{\partial \varphi}\right) \tag{1.5.5f}$$

The radial component of the strain tensor, $\hat{r} \cdot \varepsilon$, contains no toroidal component and since the material comprising the body has a linear rheology, the radial component of the stress tensor must also have no toroidal component. The radial component of the material increment in stress may therefore also be written as an infinite sum of spherical harmonic components:

$$\hat{r} \cdot t^{(\delta)} = \sum_{n=0}^{\infty} \left(\frac{r}{a}\right)^n \left(T_{rn}(r) Y_n(\theta, \varphi)\hat{r} + r T_{\theta n}(r) \nabla Y_n(\theta, \varphi)\right) \tag{1.5.6}$$

In practice we are interested only in the problem of calculating the deformation of a Maxwell visco-elastic body which, as we saw in the previous section, may be reduced to that of calculating the deformation of an elastic body for a range of Lamé parameter values in the frequency domain and then inverting back to the time domain. From (1.5.5), (1.5.6), and the constitutive equation for an elastic body (1.3.2), we see that the spherical harmonic coefficients of stress must satisfy the relations:

$$T_{rn} = \lambda\left(u_n' + \frac{n+2}{r} u_n - \frac{n(n+1)}{r} v_n\right) + 2\mu\left(u_n' + \frac{n}{r} u_n\right) \tag{1.5.7}$$

$$T_{\theta n} = \mu\left(\frac{u_n}{r} + v_n' + \frac{n-1}{r} v_n\right) \tag{1.5.8}$$

Substituting (1.5.3) into the incremental gravitational equation (1.1.7), using (1.1.9), and noting that in a stratified body the initial density field does not vary laterally (so that in the spherical case $\rho^{(\Delta)} = -\rho^{(0)} \nabla \cdot u - \rho^{(0)'} u_r$), yields the following second order differential equation governing the spherical harmonic coefficients of gravitational potential:

$$\phi_n'' + \frac{2(n+1)}{r}\phi_n' = 4\pi G\rho^{(0)}\left(u_n' + \frac{\rho^{(0)'}}{\rho^{(0)}} u_n + \frac{n+2}{r} u_n - \frac{n(n+1)}{r} v_n \right) \qquad (1.5.9)$$

This may be converted into two first order differential equations by introducing a new quantity, q (see for example Longman 1962, 1963, Peltier 1982 and Wu & Peltier 1982), associated with the perturbation in gravitational acceleration. The form for this perturbation is given by the incremental form for the equation for gravitational acceleration (1.1.8) and may be expressed in terms of spherical harmonic components:

$$g^{(\Delta)} = \hat{r} \cdot \nabla \phi^{(\Delta)} = \sum_{n=0}^{\infty} \left(\frac{r}{a}\right)^n g_n(r) Y_n(\theta, \varphi) \qquad (1.5.10)$$

The form for the spherical harmonic components of the related quantity q are then:

$$q_n = \frac{\phi_n}{r} - g_n - 4\pi G\rho^{(0)} u_n = \phi_n' + \frac{n+1}{r}\phi_n - 4\pi G\rho^{(0)} u_n \qquad (1.5.11)$$

which, when substituted back into (1.5.9) yields:

$$q_n' = \frac{n(n+1)}{r}\left(\frac{\phi_n}{r} - 4\pi G\rho^{(0)} v_n\right) + 4\pi G\rho^{(0)}\frac{u_n}{r} - \frac{n+1}{r}q_n \qquad (1.5.12)$$

The form for this equation is different from that given by Longman (1962, 1963), and Wu & Peltier (1982) because a factor of $\left(\frac{r}{a}\right)^n$ has been removed from all spherical harmonic coefficients.

Applying the general form for the divergence of a tensor in spherical polar coordinates (see, for example, Goodbody 1982) to the material increment in stress given in (1.5.6), using the identities (1.5.7) and (1.5.8), and applying the properties of spherical harmonic functions given in (1.4.11-14), results in:

$$\hat{r}\cdot\left(\nabla\cdot t^{(\delta)}\right) = \sum_{n=0}^{\infty}\left(\frac{r}{a}\right)^n Y_n\left(T_{rr}' + \frac{n}{r}T_{rr} - \frac{n(n+1)}{r}T_{\theta n} + \frac{4\mu(n-1)}{r^2}u_n + \frac{4\mu}{r}u_n' + \frac{2\mu n(n+1)}{r^2}v_n \right)$$

$$(1.5.13)$$

$$\hat{\boldsymbol{\theta}} \cdot \left(\nabla \cdot t^{(\delta)} \right) = \sum_{n=0}^{\infty} \left(\frac{r}{a} \right)^n \frac{\partial Y_n}{\partial \theta} \left(T'_{\theta n} + \frac{n+3}{r} T_{\theta n} + \frac{T_{rn}}{r} + \frac{2\mu(1-n)}{r^2} u_n - \frac{2\mu}{r} u'_n - \frac{2\mu(n^2+n-1)}{r^2} v_n \right)$$

$$(1.5.14)$$

These expressions may be substituted back into the incremental form of the inertial equation (1.1.6) to give:

$$T'_{rn} + \frac{n}{r} T_{rn} - \frac{n(n+1)}{r} T_{\theta n} + \frac{4\mu(n-1)}{r^2} u_n + \frac{4\mu}{r} u'_n + \rho^{(0)} \left(q_n + 4\pi G \rho^{(0)} u_n - \frac{\phi_n}{r} \right)$$

$$+ \rho^{(0)} u_n \left(\frac{2}{r} g^{(0)} - g^{(0)'} \right) + \frac{n(n+1)}{r} v_n \left(\frac{2\mu}{r} - g^{(0)} \rho^{(0)} \right) = 0$$

$$(1.5.15)$$

$$T'_{\theta n} + \frac{n+3}{r} T_{\theta n} + \frac{T_{rn}}{r} + \frac{2\mu(1-n)}{r^2} u_n - \frac{2\mu}{r} u'_n - \frac{2\mu(n^2+n-1)}{r^2} v_n - \frac{\rho^{(0)} g^{(0)}}{r} u_n + \frac{\rho^{(0)}}{r} \phi_n = 0$$

$$(1.5.16)$$

where we have used equation (1.5.11) to substitute for the perturbation in gravitational acceleration, and $g^{(0)}$ is the initial value for the magnitude of the acceleration due to gravity which we may see from (1.1.8) is given by $g^{(0)} = -\phi^{(0)'}$ for a radially symmetric earth. This may be substituted into the initial gravitational equation (1.1.4c) to show that:

$$g^{(0)'} = 4\pi G \rho^{(0)} - \frac{2 g^{(0)}}{r} \qquad (1.5.17)$$

This expression may in turn be substituted back into (1.5.15) and (1.5.16) to produce a closed set of differential equations comprising (1.5.7), (1.5.8), (1.5.11), (1.5.12), (1.5.15), and (1.5.16).

This form for the system of equations is almost identical to that given for the fully non-adiabatic case by Johnston (1993), whose derivation we have largely followed, and is analogous to that given by Longman (1962).

The system of equations may be re-written in Runge-Kutta form by defining the vector:

$$y_n = \left(u_n, v_n, T_{rn}, T_{\theta n}, \phi_n, q_n \right)^T \qquad (1.5.18)$$

which satisfies the differential equation:

$$\frac{d\mathbf{y}_n}{dr} = \mathbf{A}_n(r)\,\mathbf{y}_n \tag{1.5.19}$$

The entries of $\mathbf{A}_n$ may be calculated from the formulae given above:

$$\mathbf{A}_n = \begin{bmatrix} -\dfrac{2\lambda}{\beta r} - \dfrac{n}{r} & \dfrac{\lambda n(n+1)}{\beta r} & \dfrac{1}{\beta} & 0 & 0 & 0 \\[2ex] -\dfrac{1}{r} & \dfrac{1-n}{r} & 0 & \dfrac{1}{\mu} & 0 & 0 \\[2ex] \dfrac{4\gamma}{r^2} - \dfrac{4\rho^{(0)}g^{(0)}}{r} & \dfrac{n(n+1)}{r^2}\left(\rho^{(0)}g^{(0)}r - 2\gamma\right) & -\dfrac{4\mu}{\beta r} - \dfrac{n}{r} & \dfrac{n(n+1)}{r} & \dfrac{\rho^{(0)}}{r} & -\rho^{(0)} \\[2ex] \dfrac{\rho^{(0)}g^{(0)}r - 2\gamma}{r^2} & \dfrac{1}{r^2}\left(n(n+1)(\gamma+\mu) - 2\mu\right) & -\dfrac{\lambda}{\beta r} & -\dfrac{n+3}{r} & -\dfrac{\rho^{(0)}}{r} & 0 \\[2ex] 4\pi G\rho^{(0)} & 0 & 0 & 0 & -\dfrac{n+1}{r} & 1 \\[2ex] \dfrac{4\pi G\rho^{(0)}}{r} & -\dfrac{n(n+1)4\pi G\rho^{(0)}}{r} & 0 & 0 & \dfrac{n(n+1)}{r} & -\dfrac{n+1}{r} \end{bmatrix}$$

$$\tag{1.5.20}$$

where $\beta = K + {}^{4}\mu/_3$ and $\gamma = 3K\mu/\beta$.

§1.5.2 Spherical Harmonic Formulation for a Liquid Core

Applying the spherical harmonic coefficient notation to the incremental core equations (1.1.11), (1.1.12) and (1.1.13) yields the following system of differential equations for the spherical harmonic coefficients in the core:

$$\phi'_n = q_n - \left(\frac{n+1}{r} + \frac{4\pi G\rho^{(0)}}{g^{(0)}}\right)\phi_n \tag{1.5.21}$$

$$q'_n = \left(\frac{n(n+1)}{r^2} - \left[\frac{4\pi G\rho^{(0)}}{g^{(0)}}\right]^2\right)\phi_n - \left(\frac{(n+1)}{r^2} + \frac{4\pi G\rho^{(0)}}{g^{(0)}}\right)q_n \tag{1.5.22}$$

$$T_{rn} = 0 \tag{1.5.23}$$

$$T_{\theta n} = 0 \tag{1.5.24}$$

$$u_n = \frac{\phi_n}{g^{(0)}} \tag{1.5.25}$$

$$v_n = \frac{r}{n(n+1)}u'_n + \frac{n+2}{n(n+1)}u_n \tag{1.5.26}$$

These equations do not apply if the increase in pressure is hydrostatic (i.e. for the case where $n = 0$) where the dilatation and material increment in the stress tensor are both non-zero.

Equations (1.5.21) and (1.5.22) may be solved as a Runge-Kutta system with two independent solutions. One of these solutions produces a singularity at the origin when substituted into (1.5.25) and so may be neglected. Assuming that for small values of r the solutions take the form of a power series gives the following form for the bounded solution:

$$\phi_n = C_1 \qquad\qquad q_n = C_1\left(\frac{n}{r} - \frac{4\pi G \rho^{(0)}}{g^{(0)}}\right) \qquad (1.5.27)$$

where C_1 is a constant to be determined from the boundary conditions at the surface via the core-mantle boundary. Although the form for g_n given in (1.5.27) is not bounded at the origin, the local increment of gravitational acceleration, which from (1.5.10) has the form $g_n r^n$, is well-defined for all values of r for $n \geq 1$ (again the case $n = 0$ must be considered separately).

The behaviour of the solutions in the mantle and at the surface is insensitive to the properties of the inner core so that the simplifying assumption that the inner core is comprised of an inviscid fluid will have a negligible effect on the predicted deformation of the mantle and lithosphere.

§1.5.3 Boundary Conditions

Our assumption of radial symmetry means that the boundaries between layers with different rheological properties will be a series of concentric spheres centred for convenience on the origin.

As was discussed in section 1.2 the boundary conditions within an elastic body consist of the requirement of continuity in the radial stress, gravitational potential, and displacement throughout the body, and the gravitational boundary condition given in equation (1.2.1). The first three conditions translate to continuity of the corresponding spherical harmonic coefficients defined in equations (1.5.2), (1.5.3) and (1.5.6). If we then consider the continuity of the spherical harmonic components of the quantity q defined in equation (1.5.11) we see that:

$$\left[q_n(r)\right]_-^+ = \left[\phi_n(r)r^{-1}\right]_-^+ - \left[g_n(r)\right]_-^+ - 4\pi G\left[\rho^{(0)}(r)u_n(r)\right]_-^+ \qquad (1.5.28)$$

which is equal to zero from equation (1.2.1)

At the core-mantle boundary however the situation is slightly more complex. The fact that the core is incapable of supporting shear-stress leads to an apparent discontinuity in displacement and radial stress across the boundary. This apparent inconsistency between the governing equations in the core and mantle can be reconciled by inserting a thin boundary layer just below the core-mantle boundary in which the dilatation is non-zero and both the radial and tangential components of deformation change rapidly. We still have smoothness and continuity of the gravitational potential, however, and the perturbation to gravitational acceleration is given by the discontinuity in density and the radial deformation as in equation (1.5.28) (see for example Dahlen 1974, Dahlen & Fels 1982).

Under the conditions given above for the boundary layer, the incremental form of the field equation (1.1.6) within this region will be dominated by the divergence of the stress tensor and the pre-stress advection term. Neglecting the other terms in the equation, integrating and using the fact that the stress perturbation below the boundary layer is zero gives the boundary condition for radial stress, giving us a complete system of core-mantle boundary conditions:

$$u_n(b^+) = \frac{\phi_n(b^-)}{g^{(0)}(b)} + C_3 \tag{1.5.29a}$$

$$v_n(b^+) = C_2 \tag{1.5.29b}$$

$$T_{rn}(b^+) = T_{rn}(b^-) + \rho^{(0)}(b^-)g^{(0)}(b)\left[u_n(b^+) - u_n(b^-)\right] = \rho^{(0)}(b^-)g^{(0)}(b)C_3 \tag{1.5.29c}$$

$$T_{\theta n}(b^+) = 0 \tag{1.5.29d}$$

$$\phi_n(b^+) = \phi_n(b^-) \tag{1.5.29e}$$

$$q_n(b^+) = q_n(b^-) \tag{1.5.29f}$$

The constants C_2 and C_3 represent the apparent discontinuity in the radial and tangential components of displacement across the boundary layer. Their values and the value of C_1 will be determined by the boundary conditions applied at the surface of the sphere.

We will restrict our attention to the case of a unit load applied to the surface of the body, larger loads may be modeled by scaling the results of our analysis accordingly. Such a load will exert no horizontal traction at the free surface and we have continuity of radial stress, yielding the surface boundary conditions:

$$T_{\theta n}(a) = 0 \tag{1.5.30}$$

$$T_{rn}(a) = -g^{(0)}(a) \tag{1.5.31}$$

Outside the body $\rho^{(\Delta)} = 0$ so that the local increment in potential satisfies Laplace's equation. Substituting into (1.5.9), integrating, applying the condition that the increment in potential must approach zero as radial distance tends to infinity, and using the definition of g_n yields the following equations outside the body (i.e. for $r > a$):

$$\phi_n' = -\frac{2n+1}{r}\,\phi_n \tag{1.5.32}$$

$$g_n = \frac{n+1}{r}\,\phi_n \tag{1.5.33}$$

To calculate the local increment in density at the Earth's surface under a load of magnitude $Y_n(\theta, \varphi)$, we assume that the added mass of the load lies inside a layer of negligible thickness just above the earth's surface. We then calculate the change in density for a small pillbox of material of height Δh and volume $\Delta V = \Delta h\,\Delta A$ (where ΔA is the area of the ends of the pillbox) that includes the added mass but lies mostly below the earth's surface. The mass of the load material is, to first order, $Y_n(\theta, \varphi)\Delta A$. Letting the volume of the pillbox become arbitrarily small but keeping the mass added constant we may substitute back into (1.1.9) to show that the local increment in density is given:

$$\rho_n^{(\Delta)} = -\nabla \cdot \left(\rho^{(0)} u_n\right) + Y_n(\theta, \varphi)\frac{\Delta A}{\Delta V} \tag{1.5.34}$$

Substituting this into the gravitational equation, (1.1.7), allowing the dimensions of the pillbox to approach zero, integrating, and applying the divergence theorem gives:

$$-4\pi G\,dA\,Y_n(\theta, \varphi) = \int_V \nabla \cdot \left((\nabla\phi)_n - 4\pi G\rho^{(0)} u_n\right)dV \tag{1.5.35}$$

$$= dA\,n \cdot \left[(\nabla\phi)_n - 4\pi G\rho^{(0)} u_n\right]^+$$

We can use equations (1.5.11) and (1.5.32) to rewrite (1.5.35) entirely in terms of spherical harmonic coefficients. Doing so yields:

$$g_n(a^-) + 4\pi G\rho^{(0)}(a^-)u_n(a) - \tfrac{1}{r}\phi_n(a^-) = q_n(a^-) = -4\pi G \tag{1.5.36}$$

Equations (1.5.30), (1.5.31) and (1.5.36) comprise the surface boundary conditions for a load on the surface of a sphere and may be combined with the boundary

conditions at the core mantle boundary given in (1.5.27) and (1.5.29). There will be three linearly independent vector solutions and the solution we want will be a linear combination of these three. For example let y_i be the solution to the system for the case when $C_j = \delta_{ij}$ then our solution vector y may be written $y = C_i y_i$.

§1.5.4 Love Numbers

Love numbers are a useful tool in modelling the response of a spherical body to loading by surface harmonic functions. They are a set of independent, dimensionless, depth-dependent quantities defined in terms of the gravitational potential of the surface load. If the gravitational potential of the load may be written as a sum of spherical harmonic components $\psi_n(r)\left(\frac{r}{a}\right)^n Y_n(\theta, \varphi)$ then the Love numbers (see for example Love 1927) satisfy the relations:

$$u(r, \theta, \phi) = \sum_{n=0}^{\infty} \frac{\psi_n(r)}{g^{(0)}(r)} \left(\frac{r}{a}\right)^n \left[h_n(r) Y_n(\theta, \varphi)\hat{r} + l_n(r) \nabla Y_n(\theta, \varphi) \right] \qquad (1.5.37)$$

$$\phi^{(\Delta)}(r, \theta, \phi) = \sum_{n=0}^{\infty} \left(1 + k_n(r) \right) \psi_n(r)\left(\frac{r}{a}\right)^n Y_n(\theta, \varphi) \qquad (1.5.38)$$

where the $k_n \psi_n Y_n$ term represents the contribution of the perturbation in gravitational potential due to the load.

The gravitational potential at a point (r, θ, φ) due to a distribution of mass with spherical harmonic components $Y_n(\theta', \varphi')$ over the surface of a sphere of radius a is:

$$\sum_{n=0}^{\infty} \psi_n(r)\left(\frac{r}{a}\right)^n Y_n(\theta, \varphi) = Ga^2 \int_0^{\pi} d\theta' \sin\theta' \int_0^{2\pi} \frac{Y_n(\theta', \varphi')d\varphi'}{\sqrt{a^2 + r^2 - 2r\cos\alpha}} \qquad (1.5.39)$$

where α is the angle between the rays from the origin that pass through the points (a, θ', φ') and (r, θ, φ). The form of the cosine of α may be deduced from the law of cosines for a spherical triangle (see for example Spiegel 1968) and is given in equation (1.5.44) below.

Substituting (1.4.6) for the denominator in the integrand in equation (1.5.39) and applying the orthogonality relation for spherical harmonic functions yields:

$$\psi_n(r)\left(\frac{r}{a}\right)^n Y_n(\theta, \phi) = Ga\int_0^\pi d\theta' \sin\theta' \int_0^{2\pi} d\phi' Y_n(\theta', \phi')\sum_{n'=0}^\infty \left(\frac{r}{a}\right)^{n'} P_{n'}(\cos\alpha)$$

$$= Ga\left(\frac{r}{a}\right)^n \int_0^\pi d\theta' \sin\theta' \int_0^{2\pi} d\phi' Y_n(\theta', \phi') P_n(\cos\alpha)$$

$$= \frac{4\pi aG}{2n+1}\left(\frac{r}{a}\right)^n Y_n(\theta, \phi) \tag{1.5.40}$$

By direct comparison with (1.5.2) and (1.5.3) we see that the Love numbers may be related to the spherical harmonic coefficients of deformation and gravitation by the equation:

$$\begin{pmatrix} h_n(r) \\ l_n(r) \\ 1 + k_n(r) \end{pmatrix} = \frac{2n+1}{4\pi aG}\begin{pmatrix} g^{(0)}(r)u_n(r) \\ g^{(0)}(r)v_n(r) \\ \phi_n(r) \end{pmatrix} \tag{1.5.41}$$

§1.5.5 Loads of degree 1 or 0

Surface loads of degree 1 require separate treatment (Farrell 1972) since for such a load the earth's centre of mass is translated. The combined centre of mass of the earth and load remains stationary however, and surface deformation can only be measured relative to the earth's centre of mass. This is not a problem for loads of other order since the centre of mass of such loads coincides with the centre of mass of the earth.

For the degree 1 problem the differential equations have a non-trivial solution to the homogeneous boundary value problem (the case where at the surface of the sphere $T_{rn} = 0$ and $\rho^{(\Delta)} = -\nabla\cdot\left(\rho^{(0)}u\right)$, and at the core-mantle boundary the C_i are all taken to be zero). This solution, y_1^H, has the form:

$$y_1^H = \left(\frac{1}{r}, \frac{1}{r}, 0, 0, \frac{g^{(0)}(r)}{r}, -\frac{4\pi G\rho^{(0)}(r)}{r} + \frac{2g^{(0)}(r)}{r}\right)^T \tag{1.5.42}$$

Given a solution to a particular non-homogeneous boundary value problem, y_1^S, we may construct a new solution to the boundary value problem, $y_1^G = y_1^S + cy_1^H$, where c is an arbitrary constant. We may use this extra degree of freedom to choose c such that the displacement of the centre of mass of the load-earth system is zero. For the degree 1 boundary value problem any solution to the system of differential equations (1.5.19) that satisfies any two of the boundary conditions (1.5.30), (1.5.31), and (1.5.36) will automatically satisfy the third.

Given an arbitrary degree 1 surface harmonic defined:

$$Y_1(\theta, \varphi) = \sum_{n=-1}^{1} c_{1\,n} Y_{1\,n}(\theta, \varphi) \tag{1.5.43}$$

there is a point (a, θ^*, φ^*) on the surface of the sphere such that $Y_1(\theta, \varphi) = \sqrt{3} \cos \alpha$ where α here represents the same quantity as defined for equation (1.5.39). The form for the cosine may be deduced from the law of cosines for spherical triangles:

$$\cos \alpha = \cos \theta \cos \theta^* + \sin \theta \sin \theta^* \cos(\varphi - \varphi^*) \tag{1.5.44}$$

which in turn allows us to express the coefficients of $Y_1(\theta, \varphi)$ in the following form:

$$c_{1\,-1} = \sin \varphi^* \sin \theta^* \qquad c_{1\,0} = \cos \theta^* \qquad c_{1\,1} = \cos \varphi^* \sin \theta^* \tag{1.5.45}$$

So that the load and its associated deformation are symmetric about the radial position vector r^* of the point (a, θ^*, φ^*).

The shift in the centre of mass of the earth must balance the shift in the centre of mass of the load which is given by (Farrell 1972):

$$u_{com} = \hat{r}^* Y_1(\theta, \varphi) \frac{\psi_1(a) - \phi_1(a)}{g^{(0)}(a)} \tag{1.5.46}$$

where $\hat{r}^*$ is the unit vector in the direction of r^*.

To calculate the Love numbers relative to the centre of the earth rather than some generalised origin we must subtract the shift in the earth's centre of mass from the displacement coefficients. Doing so, and retaining the notation we introduced earlier, yields the expressions (again due to Farrell 1972):

$$h_1 = h_1^S + k_1^S \qquad l_1 = l_1^S + k_1^S \qquad k_1 = 0 \tag{1.5.47}$$

which define the displacement due to the degree 1 load.

A degree 0 load corresponds to a force applied uniformly over the surface of the body. The resulting surface deformation will correspondingly be uniform and entirely due to hydrostatic compression of the material within the body. We are interested primarily in modelling surface loading of the earth by ice sheets and their associated waterloads, which, because of conservation of mass of the ice and water within the system, will never have a component degree 0 so that a detailed analysis of this case is unnecessary in this particular instance.

1.6   Spherical Cap Harmonic Analysis

As we discussed in sections 1.4 and 1.5, in a conventional spherical harmonic analysis we obtain solutions to Laplace's equation by translating into spherical polar coordinates, the solutions are sums of components of the form given in (1.4.2). These components are finite, continuous, and single-valued over the surface of a sphere centred on the origin only if the quantities n and m are both positive integers.

In this section we will examine the theoretical foundations of this spherical harmonic analysis technique with slightly more rigour with a view to adapting the procedure to the high resolution problems we wish to consider. In particular we will employ surface harmonics of non-integral degree to model appropriately well-behaved scalar functions over a spherical cap close to the pole. The price of this technique is loss of orthogonality and increased computational cost per spherical harmonic coefficient. The benefit is a dramatic reduction in the number of coefficients required to achieve a given resolution.

In our analysis of the deformation of a sphere under a load we represent the loading function, and response as a sum of surface harmonics, Y_{nm}. From the theory of harmonic functions (see for example Gilbarg & Trudinger 1983) we see that we can accurately model any suitably well behaved scalar function by summing such terms to sufficiently high degree. Changing the region of interest from the entire surface of the sphere to a small spherical cap centred at the pole does not affect the validity of our mathematical formulation, simply the details of its implementation.

§1.6.1 Solving Laplace's Equation

In solving Laplace's equation in spherical polar coordinates (equation 1.4.1) we employ separation of variables, that is we assume that the function in question, f, has the form $f(r, \theta, \varphi) = R(r)\Theta(\theta)\vartheta(\varphi)$, where R is taken to be a function only of r, completely independent of θ and φ, and Θ and ϑ are taken to be dependent only on θ and φ respectively. Substituting this form for f back into Laplace's equation, (1.4.1), multiplying by r^2 and then dividing through by f yields:

$$\left(\frac{r^2 R'' + 2rR'}{R}\right) + \frac{1}{\sin\theta}\left(\frac{\Theta''\sin\theta + \Theta'\cos\theta}{\Theta}\right) + \frac{1}{\sin^2\theta}\left(\frac{\vartheta''}{\vartheta}\right) = 0 \qquad (1.6.1)$$

where in this case the prime ($'$) denotes differentiation by the corresponding variable.

The first term in the equation is a function only of r but each of the other grouped terms is independent of r, so that for them to sum to zero they must be constant. That is, there exists a constant χ_1 such that:

$$\frac{1}{\sin\theta}\left(\frac{\Theta''\sin\theta+\Theta'\cos\theta}{\Theta}\right)+\frac{1}{\sin^2\theta}\left(\frac{\vartheta''}{\vartheta}\right)=-\left(\frac{r^2R''+2rR'}{R}\right)=-\chi_1 \quad (1.6.2)$$

Using an analogous line of reasoning we see that there exists a second constant quantity, χ_2, such that:

$$\left(\frac{\vartheta''}{\vartheta}\right)=\chi_2 \quad (1.6.3)$$

which may be substituted back into (1.6.2) to yield:

$$\frac{\Theta''\sin\theta+\Theta'\cos\theta}{\sin\theta}+\left(\frac{\chi_2}{\sin^2\theta}+\chi_1\right)\Theta=0 \quad (1.6.4)$$

By substituting $\eta=\cos\theta$ into this equation we obtain the governing differential equation for η:

$$\frac{d}{d\eta}\left((1-\eta^2)\frac{d\Theta}{d\eta}\right)+\left(\upsilon_1(\upsilon_1+1)-\frac{\upsilon_2^2}{1-\eta^2}\right)\Theta=0 \quad (1.6.5)$$

where $\chi_1=\upsilon_1(\upsilon_1+1)$ and $\chi_2=-\upsilon_2^2$. This is simply Legendre's associated differential equation which has as its solutions the associated Legendre functions of the first and second kind of degree υ_1 and order υ_2, $P_{\upsilon_1\upsilon_2}(\eta)$ and $Q_{\upsilon_2\upsilon_1}(\eta)$ respectively (see for example Abramowitz & Stegun 1972). Associated Legendre functions of the second kind, $Q_{\upsilon_2\upsilon_1}(\eta)$, are undefined at the poles and are therefore neglected when modelling physical quantities.

If the order υ_2 is imaginary or non-integral then the solution, ϑ_{υ_2}, of equation (1.6.3) is either aperiodic or has a period that is not an integral fraction of 2π, so that $\vartheta_{\upsilon_2}(\varphi)\neq\vartheta_{\upsilon_2}(\varphi+2\pi)$, which is clearly undesirable since it implies that ϑ_{υ_2} is multi-valued on the surface of a sphere. We therefore require that υ_2 be an integer (due to the symmetry of the trigonometric functions we can without loss of generality assume υ_2 is positive) so that equation (1.6.3) has solutions of the form:

$$\vartheta_{\upsilon_2}(\varphi)=A_{\upsilon_2}\cos\upsilon_2\varphi+B_{\upsilon_2}\sin\upsilon_2\varphi \quad (1.6.6)$$

where A_{υ_2} and B_{υ_2} are arbitrary constants determined by boundary conditions. These functions are clearly mutually orthogonal over the interval $[0,2\pi]$.

When the form for χ_1 used in (1.6.5) is substituted back into (1.6.2) we see that the equation has solutions:

$$R_{\upsilon_1}(r) = C_{\upsilon_1} r^{\upsilon_1} + D_{\upsilon_1} r^{-(\upsilon_1 + 1)} \tag{1.6.7}$$

The second term in this expression is undefined at the origin when $\mathrm{Re}(\upsilon_1) > -1$ while the first term is undefined for $\mathrm{Re}(\upsilon_1) < 0$ so that for most of the quantities we model we require $\mathrm{Re}(\upsilon_1) \geq 0$ and $D_{\upsilon_1} = 0$. With appropriately defined constants our solutions to equation (1.6.1) will therefore be sums of components of the form:

$$f_{\upsilon_1 \upsilon_2}(r, \theta, \varphi) = C_{\upsilon_1} r^{\upsilon_1} \Big(A_{\upsilon_2} \cos \upsilon_2 \varphi + B_{\upsilon_2} \sin \upsilon_2 \varphi \Big) P_{\upsilon_1 \upsilon_2}(\cos \theta)$$

$$= C_{\upsilon_1} r^{\upsilon_1} \Big(A_{\upsilon_2} Y_{\upsilon_1 \upsilon_2} + B_{\upsilon_2} Y_{\upsilon_1 - \upsilon_2} \Big) \tag{1.6.8}$$

The usefulness of this formulation is largely dependent on the orthogonality of terms of this type over the region $[0, \pi] \times [0, 2\pi]$. This orthogonality is a result of the orthogonality of both the trigonometric functions on $[0, 2\pi]$ (this establishes mutual orthogonality for different values of υ_2) and the associated Legendre functions on $[0, \pi]$ (which establishes mutual orthogonality for different values of υ_1).

The orthogonality of trigonometric functions whose periods are integral fractions of 2π is an elementary identity of calculus and forms the basis of Fourier analysis (see for example Kreyszig 1983). The orthogonality of the associated Legendre functions is a similar though rather more complicated issue we will examine in slightly greater detail to utilise some of its more general properties.

§1.6.2 Theory of Sturm-Liouville Boundary Value Problems

A complete set of solutions to equation (1.6.5) is generated by solutions to the associated boundary value problems. Requiring that our solution be continuous and finite throughout the region $[0, \pi]$ constrains υ_1 to be a positive integer. We also apply two boundary conditions, one at the pole, $\theta = 0$:

$$\Theta_{\upsilon_1 \upsilon_2}(0) = 0 \quad \text{for } \upsilon_2 \neq 0$$

$$\left. \frac{\partial \Theta_{\upsilon_1 0}}{\partial \theta} \right|_{\theta = 0} = 0 \tag{1.6.9}$$

and at the equator, $\theta = {}^{\pi}\!/_{2}$:

$$\Theta_{\upsilon_1 \upsilon_2}\left(\frac{\pi}{2}\right) = 0 \qquad \text{for } \upsilon_1 + \upsilon_2 \text{ odd}$$

$$(1.6.10)$$

$$\frac{\partial \Theta_{\upsilon_1 \upsilon_2}}{\partial \theta}\bigg|_{\theta = \pi/2} = 0 \qquad \text{for } \upsilon_1 + \upsilon_2 \text{ even}$$

Equation (1.6.4) can be recast into the form:

$$\left(\Theta' \sin \theta\right)' - \frac{\upsilon_2^2}{\sin \theta}\, \Theta = -\chi_1\, \Theta \sin \theta \qquad (1.6.11)$$

restricting our attention to the interval $\left[0, \pi/2\right]$, this is the traditional form for a Sturm-Liouville problem with eigenvalue χ_1 (see for example Boyce & DiPrima 1977) with corresponding separated boundary conditions given by equations (1.6.9) and (1.6.10).

For the purposes of this discussion we may take the order of the the Legendre functions as being fixed since orthogonality between surface harmonic functions of different order is inherited from the trigonometric terms. The order of the functions is therefore taken here to have a fixed positive integer value, υ_2.

We now define two sets of solutions to equation (1.6.11), for a given value of υ_2, we will denote by $\mathcal{E}_{\upsilon_2}$ the set of functions for which (1.6.11) holds, with associated integers υ_1 such that $\upsilon_1 + \upsilon_2$ is even, the corresponding set of functions for which $\upsilon_1 + \upsilon_2$ is odd we will denote $\mathcal{G}_{\upsilon_2}$. It should be noted that each of these sets has its own distinct set of boundary conditions that apply to their respective member functions.

From the theory of Sturm-Liouville eigenvalue problems (see again Boyce & DiPrima 1977), given any two distinct eigenvalues of equation (1.6.11), $\chi_{10} \neq \chi_{11}$, then provided the corresponding eigenfunctions $\Theta_{\upsilon_{10} \upsilon_2}$ and $\Theta_{\upsilon_{11} \upsilon_2}$ both lie in either $\mathcal{E}_{\upsilon_2}$ or $\mathcal{G}_{\upsilon_2}$ (i.e. as long as both functions satisfy the same set of boundary conditions) they are orthogonal on the interval $\left[0, \pi/2\right]$.

Orthogonality between the two sets of eigenfunctions, $\mathcal{E}_{\upsilon_2}$ and $\mathcal{G}_{\upsilon_2}$, is not guaranteed by Sturm-Liouville since functions from one set do not have common boundary conditions with the members of the other. In this instance orthogonality results from the symmetry properties of the two sets. The element functions of $\mathcal{E}_{\upsilon_2}$ are either symmetric or anti-symmetric about $\theta = \pi/2$, depending on the parity of υ_2 (see for example Abramowitz & Stegun 1972), if υ_2 is even then they will be symmetric, otherwise anti-symmetric. The members of $\mathcal{G}_{\upsilon_2}$ have a converse relation, they are anti-symmetric about $\theta = \pi/2$ when υ_2 is even and symmetric otherwise. That is:

$$\Theta_{\upsilon_1 \upsilon_2}\left(\frac{\pi}{2} - \theta\right) = \left(-1\right)^{\upsilon_1} \Theta_{\upsilon_1 \upsilon_2}\left(\frac{\pi}{2} + \theta\right) \tag{1.6.12}$$

so that the two sets of functions will have opposite symmetry relations. This in turn implies that the integral from 0 to π of the product of two given eigenfunctions, one from $\mathcal{E}_{\upsilon_2}$ and the second from $\mathcal{G}_{\upsilon_2}$, will be identically zero. This is very similar to the relationship between the trigonometric functions over $\left[0, 2\pi\right]$ though orthogonality in that case is more easily deduced from direct analytical computation of the integrals.

Orthogonality of the associated Legendre polynomials over the region $\left[0, \pi\right]$ for fixed values of υ_2 is therefore a consequence of their symmetry properties, and in turn grants the surface harmonics complete mutual orthogonality over the surface of a sphere, $\left[0, \pi\right] \times \left[0, 2\pi\right]$.

The most significant consequence of mutual orthogonality is that when we attempt to approximate a given function over the surface of a sphere with a sum of surface harmonics, the coefficient of each harmonic component is independent of the degree of the approximation and takes a quite convenient form given in equation (1.4.9).

The formalism of Sturm-Liouville boundary problems is worth considering in some detail in this case since it illustrates very clearly the effects of altering the boundary conditions. In the case of spherical cap harmonic analysis we do this not by applying different conditions but by changing the boundaries themselves as will be discussed in section 1.6.4.

§1.6.3 Resolution of Surface Features

The resolution of a surface harmonic of degree n, Y_n, is given by the distance between consecutive zeroes, so that if we want to model a feature of diameter ε on the surface of the sphere whose radius is a then we will need to sum to degree N given by:

$$N = \frac{\pi a}{\varepsilon} \tag{1.6.13}$$

For this reason 2ε is often called the minimum representable wavelength of a surface harmonic of degree N.

From the form of equation (1.4.7) we see that in order to calculate the coefficients of a spherical harmonic approximation F_N we must perform $\left(N + 1\right)\left(N + 2\right)$ integrals of the form given in equation (1.4.8). If, for example, we wanted to model a feature of diameter 100km on the surface of the Earth ($a = 6371$km) we would have to sum to degree 200. If we use standard spherical harmonic procedures to achieve this accuracy we will need to calculate some 40 601 coefficients (remembering that we need coefficients

for both the sine and cosine terms), which makes high resolution modelling using this technique quite expensive computationally.

§1.6.4 Spherical Cap Harmonic Analysis

The Spherical Cap Harmonic Analysis (SCHA) technique was first developed by Haines (1985) as a means of modelling variations in a regional geomagnetic field. In this procedure we restrict our attention to some small area, A, on the surface of the sphere, in particular a cap of angular radius ξ which we may without loss of generality assume to be centred on the pole $\theta = 0$.

We intend to use this technique to model deformation of the earth within a spherical cap due to an ice sheet centred around the pole. We will therefore (see for example Johnston 1993) require spherical harmonic expansions for the ice sheet, and the earth's rheology (in terms of Love numbers). These are all well behaved scalar functions and can be approximated to arbitrary accuracy using surface harmonics, but by changing the region of interest we also change the nature of the Sturm-Liouville problem for the associated Legendre functions.

In our cap analysis it is natural to use boundary conditions analogous to those applied in the spherical case:

$$\Theta_{\upsilon_1 \upsilon_2}(\xi) = 0 \quad \text{for } \upsilon_1 + \upsilon_2 \text{ odd}$$

$$\left. \frac{\partial \Theta_{\upsilon_1 \upsilon_2}}{\partial \theta} \right|_{\theta = \xi} = 0 \quad \text{for } \upsilon_1 + \upsilon_2 \text{ even}$$

(1.6.14)

In general however, these boundary conditions will require υ_1 to be non-integral. Since we are modelling functions that are everywhere finite we would normally avoid using Legendre functions of non-integral degree since they become indeterminate for various values of θ. We are only interested in the area inside the cap however, and the quantities we are modelling may be taken to be zero outside A, so that we can use Legendre functions of non-integral order provided their singularities are far enough removed from the centre of the cap (the pole of the sphere).

If we let m be a fixed positive integer value for υ_2, then from the theory of Sturm-Liouville problems we have that the eigenvalues of the corresponding boundary value problem are real and form a countably infinite sequence. If we denote the k-th eigenvalue for which there exists an eigenfunction that satisfies equations (1.6.11), (1.6.9) and (1.6.14) by n_k then our boundary conditions become:

$$\frac{d}{d\theta}P_{n_k m}(\cos\theta)\bigg|_{\theta=\xi} = 0 \quad \text{for } k+m \text{ even}$$

(1.6.15)

$$P_{n_k m}(\cos\xi) = 0 \quad \text{for } k+m \text{ odd}$$

where we should note that in general the exact value of n_k is dependent on the order m, and that in the standard spherical harmonic analysis scheme we have $\xi = \frac{\pi}{2}$ and $n_k = k$.

The advantage of this type of analysis is that for small values of ξ the values of n_k are quite widely spread as we see from the approximate relations (De Santis 1985):

$$n_k \approx \frac{\pi}{2\xi}(k+0.5) - 0.5$$

(1.6.16)

$$n_{k+1} - n_k \approx \frac{\pi}{2\xi}$$

So that the number of coefficients that need to be calculated in order to model a surface feature to a given resolution is greatly reduced. For example, as we have already seen, if we want to model a feature of radius 100 km we would have to expand to at least degree 200. If we were to use spherical cap analysis over a cap of angular radius ξ then we would need to expand our functions to degree $n_{k_{\max}}$ where $k_{\max}$ is the smallest integer such that:

$$k_{\max} \geq 200.5\,\frac{2\xi}{\pi} - 0.5 \approx 128\,\xi - 0.5$$

(1.6.17)

The latitudinal resolution of a given surface harmonic expansion is determined by the maximum degree of the expansion while the longitudinal resolution is a function of the maximum order of the expansion. In a conventional spherical harmonic analysis these two quantities are the same. But more generally, the order of expansion required to resolve a feature of diameter ε (as in equation (1.6.13)) at colatitude θ is given by:

$$m_{\max}(\theta) \approx \frac{\pi a \sin\theta}{\varepsilon}$$

(1.6.18)

In general though the features being modelled will be closer to the centre of the cap than the edge, otherwise the assumption that deformation and stress due to the load are zero at the edge of the cap may not apply. This being the case it is normally adequate to set $m_{\max} = k_{\max}$, the maximum value taken by the index k.

The number of coefficients that need to be calculated to achieve a given resolution is therefore substantially smaller than in the conventional spherical harmonic analysis for the same resolution. Modelling a 100 km diameter feature inside a cap of angular radius 10°

gives $k_{max} = 23$ yielding a total of 601 coefficients, less than two percent of that required to achieve comparable resolution in the conventional analysis.

The price of this reduction in the number of coefficients is two-fold. Firstly, the associated Legendre functions of non-integral degree are simply more expensive to calculate numerically than the associated Legendre polynomials of integral degree, requiring significant numerical effort even to determine appropriate values of n_k. More importantly, moving to the Legendre functions of non-integral degree results in a loss of orthogonality between functions from $\mathcal{E}_{v_2}$ and $\mathcal{G}_{v_2}$ over the region $[0, \xi] \times [0, 2\pi]$. We still have orthogonality within each set, since this is still a Sturm-Liouville problem but the symmetry property that gave us a completely orthogonal system is no longer guaranteed, a result of the singularities outside the cap. As a result of this there is a significant increase in the computational cost of calculating the coefficients of the surface harmonics since many of the cross-multiplication terms in the least squares problem are non-zero.

In this instance, the difference between our spherical harmonic approximation and the function being approximated is represented by the integral in equation (1.4.8):

$$\int_0^{\pi} d\theta \sin \theta \int_0^{2\pi} d\varphi \left(F_N(\theta, \varphi) - F(\theta, \varphi) \right)^2 = \mathcal{D}_N \qquad (1.6.19)$$

where the approximating function, F_N, is given:

$$F_N(\theta, \varphi) = \sum_{n=0}^{N} \sum_{m=-n}^{n} F_{nm}^N Y_{nm}(\theta, \varphi) \qquad (1.6.20)$$

The coefficients of the approximating series are chosen to minimise the quantity $\mathcal{D}_N$ in equation (1.6.19), so that for each value of n and m the coefficients of our spherical harmonic expansion are given by the relation:

$$\frac{\partial \mathcal{D}_N}{\partial F_{nm}^N} = 2 \sum_{i=0}^{N} \int_0^{\pi} d\theta \sin \theta \int_0^{2\pi} d\varphi \, Y_{nm}(\theta, \varphi) Y_{im}(\theta, \varphi)$$

$$(1.6.21)$$

$$- 2 \int_0^{\pi} d\theta \sin \theta \int_0^{2\pi} d\varphi \, Y_{nm}(\theta, \varphi) F(\theta, \varphi) = 0$$

In the case considered in equation (1.4.9) only one of the integrals in the summation in this expression is non-zero. Removing orthogonality between surface harmonics introduces the linear system above, making the coefficients dependent on the degree, N, of the approximation, and prone to numerical error due to the instability of the system of linear equations.
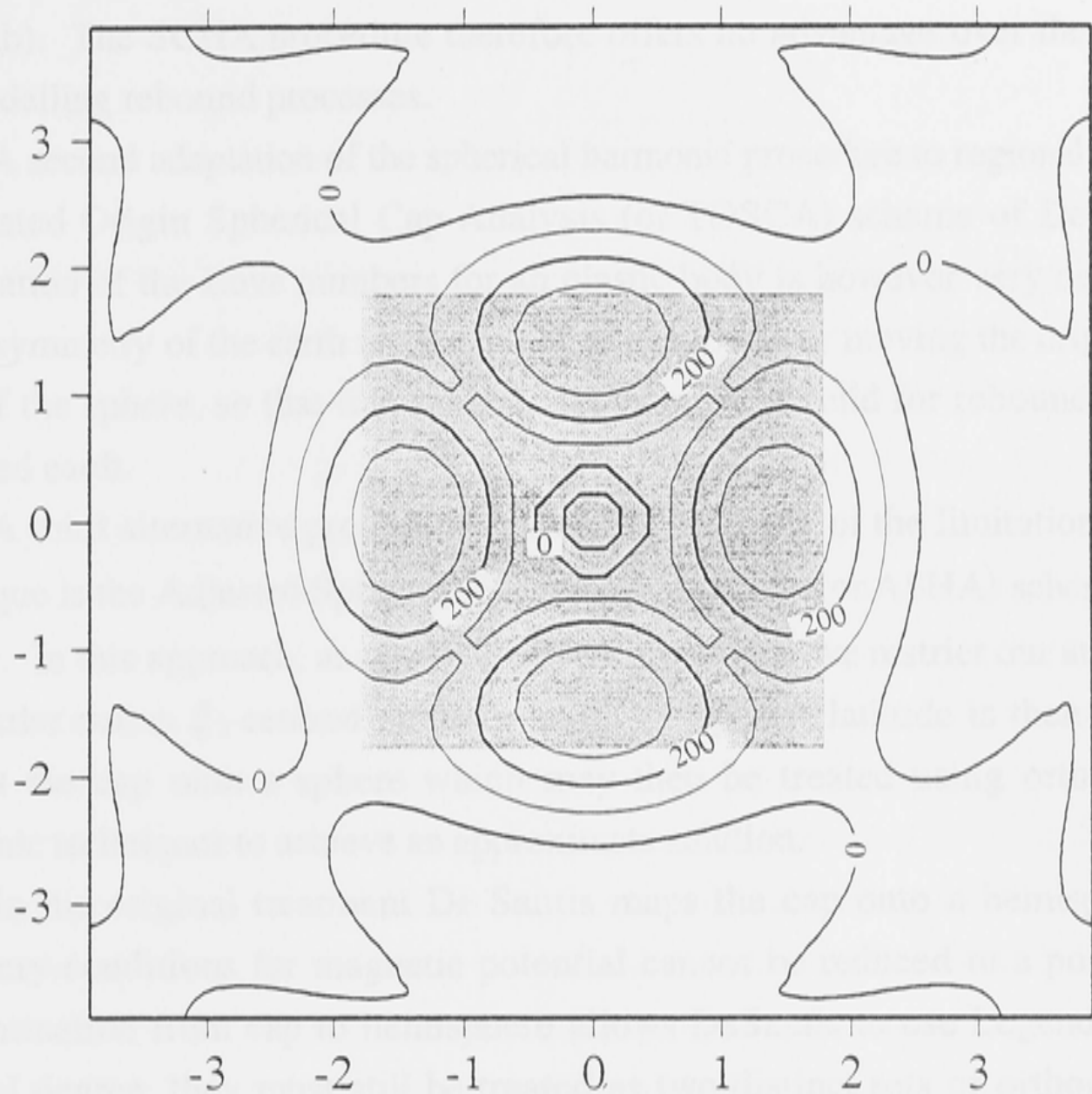
Figure 1.1: Results for the SCHA approximation of a square ice sheet of side 400 km and 400 m thick (indicated by the dashed line). Units on axes are degrees, contour spacing is 100 m.

The formalism given earlier for calculating the Love numbers of a spherical elastic body does not depend on them being of integral degree so that it is valid to apply the formalism of the SCHA technique to the problem of surface deformation. The increased analytical and computational complexity of the procedure raises the possibility of reduced numerical stability however and its suitability to very high resolution problems remains untested.

Figure 1.1 illustrates the results of SCHA analysis used to model a 400 m thick square ice sheet of side 400 km. The cap used had an angular radius of 10° and the harmonic approximation was continued to order 20, maximum degree 185. Attempts to go to a higher order approximation failed as the least squares problem became subject to catastrophic numerical instability.

The resulting computational saving with the change from the conventional to the SCHA technique was undeniably significant, but the fit of the resulting approximation was unsatisfactory, particularly at the centre of the load itself. The instability of the SCHA technique at high degrees severely reduces its usefulness for modelling very high resolution surface features, while the performance of the global spherical harmonic scheme when applied to regional scale rebound problems is more than adequate (Lambeck

1993a,b). The SCHA procedure therefore offers no advantage over the global scheme for modelling rebound processes.

A second adaptation of the spherical harmonic procedure to regional problems is the Translated Origin Spherical Cap Analysis (or TOSCA) scheme of De Santis (1991). Calculation of the Love numbers for an elastic body is however very dependent on the radial symmetry of the earth model, which is destroyed by moving the origin closer to the pole of the sphere, so that this analysis scheme is not valid for rebound problems on a stratified earth.

A third alternative procedure that addresses many of the limitations of the SCHA technique is the Adjusted Spherical Harmonics Analysis (or ASHA) scheme of De Santis (1992). In this approach, as with the SCHA procedure, we restrict our attention to a cap of angular radius ξ, centred on the pole of the sphere, latitude is then scaled so as to project the cap onto a sphere which may then be treated using orthodox spherical harmonic techniques to achieve an approximate solution.

In his original treatment De Santis maps the cap onto a hemisphere since the boundary conditions for magnetic potential cannot be reduced to a point. While this transformation from cap to hemisphere allows DeSantis to use Legendre functions of integral degree, they must still be treated as two distinct sets of orthogonal functions satisfying different boundary conditions with no orthogonality holding between the sets. Determining the coefficients of the spherical harmonic expansion in this instance therefore still requires that a large least squares problem of the form given in equation (1.6.21) be solved.

In the case of deformation due to a load of small lateral extent we may apply a simple zero boundary condition to the edge of the cap, so that in our application the boundary may be mapped onto the pole and the zero boundary condition applied there. This allows us to map the cap onto a sphere and apply the full mutual orthogonality of the Legendre polynomials of integral degree, making it ideal in principle for use in this class of application.

The ASHA technique relies on the approximation $\theta = \sin \theta$ holding throughout the region of the cap, which is valid for caps of angular radius less than $14°$ degrees, and reasonably accurate for radii of up to $22°$. Substituting this approximate relation back into equation (1.6.4) yields:

$$\frac{d^2\Theta}{d\theta^2} + \frac{1}{\theta}\frac{d\Theta}{d\theta} + \left(\frac{\chi_2}{\theta^2} + \chi_1\right)\Theta = 0 \qquad (1.6.22)$$

Introducing a new scaled variable for latitude, θ', defined such that, $\theta' = s\theta = \frac{\pi}{\xi}\theta$, then yields:

$$\frac{d^2\Theta}{d\theta'^2} + \frac{1}{\theta'}\frac{d\Theta}{d\theta'} + \left(\frac{\chi_2}{\theta'^2} + \frac{\chi_1}{s^2}\right)\Theta = 0 \qquad (1.6.23)$$

The solutions to this equation are finite and continuous over the surface of the sphere only when $\chi_1 = s^2 k(k+1)$ and $\chi_2 = -m^2$ for k, m positive integers. An approximate solution to equation (1.6.23) is then given by the associated Legendre polynomial $P_k^m(\cos\theta')$. De Santis acknowledges that the new latitude θ' is no longer always small enough for the approximation $\theta' = \sin\theta'$ to hold so that equation (1.6.23) is not strictly equivalent to equation (1.6.4), but uses the associated Legendre polynomials as approximate solutions to achieve reasonable agreement with the SCHA technique.

Mapping from a cap onto a sphere is a powerful analytical tool that would allow us to very conveniently perform calculations over small regions with great accuracy and speed but its validity needs to be closely examined. In the case of modelling the earth's geomagnetic potential the problem is largely a mathematical one of approximating a given function by surface harmonics with only a few constraints placed by the physical processes involved. The problem of calculating the deformation of a spherical body under a surface load is however rather different, the physics of the processes involved must be faithfully reproduced in the mathematical model for the results obtained to have any significance.

Figure 1.2 illustrates the effect of magnifying the region of interest. The mapping from cap to hemisphere has two immediate and completely artificial consequences, it greatly exaggerates the effect of sphericity and alters the lateral scale of the problem.
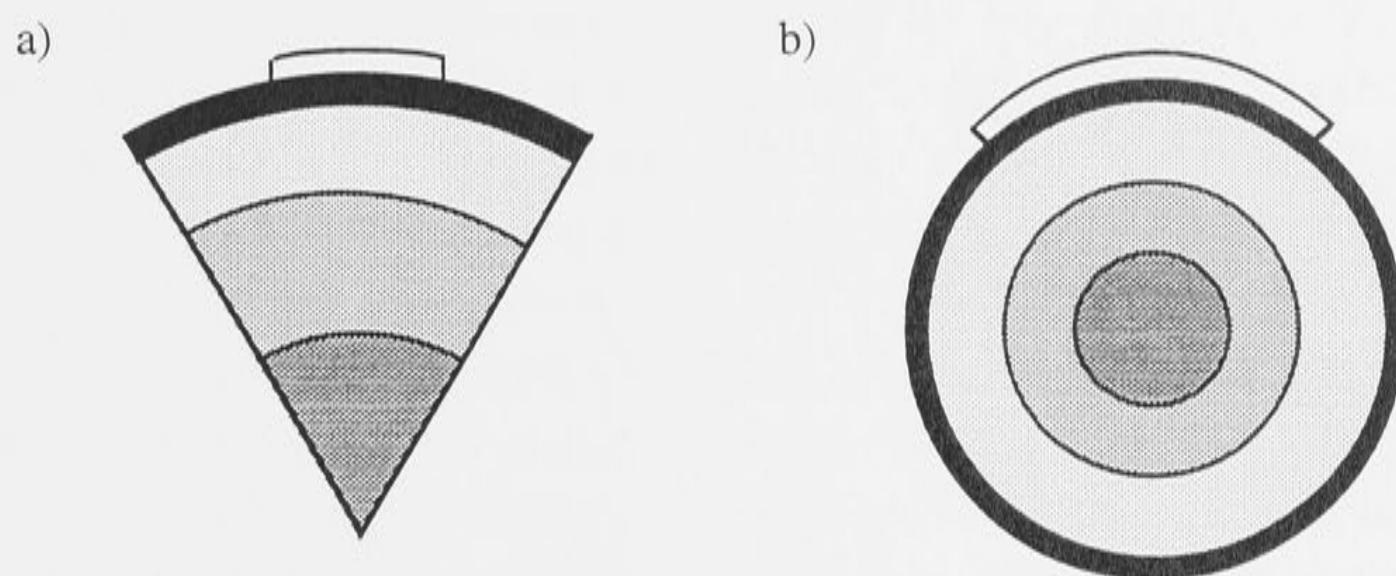

Figure 1.2: Illustration of the effect of the ASHA technique, the spherical cap (fig. a) is mapped onto the sphere (fig. b) with consequent lateral expansion of the load, exaggerated sphericity, and anisotropy.

The stresses due to a surface load are significant to depths comparable to the lateral extent of the load, translation from a cap onto a sphere greatly increases the apparent width of the load and therefore the depth to which it will stress the earth, so that the ASHA technique immediately produces unphysical behaviour when applied to the problem of surface deformation. The most significant effect of the mapping however, is that it renders the body in question anisotropic, severely complicating the form of the constitutive equation, and invalidating much of the formalism developed for the Love number calculations.

As with the TOSCA scheme, the mathematical convenience of the ASHA procedure is undermined by the physical inappropriateness of its formulation. The price of the promised numerical convenience is that the procedure requires fundamental modifications to the mathematical formalism of the problem, modifications that render the system analytically intractable.

1.7 Discussion

The mathematical formalism for calculating the deformation of an elastic sphere under a surface load has been the subject of extensive development and now provides an extremely powerful tool for the calculation of glacial rebound and associated sea-level change. The nature of this procedure is such however, that modelling the contribution of high resolution surface features is computationally very expensive, so that incorporation into a direct inversion procedure is not entirely feasible.

Surface harmonics are commonly applied whenever an approximation of a conservative field is required over the surface of a sphere, two particular examples being the modelling of the earth's geomagnetic and gravitational potentials. The failure of the conventional spherical harmonic technique at high resolution has prompted workers in these fields to develop several alternative variations for use in regional modelling such as the SCHA and ASHA techniques examined here.

The SCHA scheme of Haines (1985) does not offer significant improvement over the global spherical harmonic procedure for high resolution or regional scale modelling and suffers from significant numerical instability at very high degrees.

Fitting a series of surface harmonics to observational data is a predominantly mathematical problem, while numerical modelling of rebound processes relies heavily on the physical accuracy of the underlying theory. In the case of both the TOSCA and ASHA procedures of De Santis (1991, 1992), analytical tools that may validly be applied to the former class of problem undermine the theory developed for rebound problems on a spherical body.

High resolution modelling of surface loading therefore remains inconvenient and expensive in the spherical case, despite the undoubted power and flexibility of the analytical techniques discussed in this chapter. One of the most natural adaptations of the techniques discussed here is to neglect the effect of sphericity entirely and model the earth as a flat, stratified, semi-infinite Maxwell body. For loads of small lateral extent the effect of sphericity will not be significant, this approach has been employed by many workers (see for example McConnell 1965, 1968, Jeffreys 1976, Wolf 1985a,b) and offers significant advantages over the spherical formulation for high resolution modelling.

In the next chapter we will adapt the basic theory of loading problems to the case of a flat earth, and introduce three distinct techniques for modelling the deformation due to a surface load. Using the correspondence principle discussed in section 1.3, a Maxwell body may be modelled mathematically as elastic with frequency-dependent Lamé parameters so that we may restrict our analysis in the first instance to the deformation of a stratified, elastic half-space.

Chapter 2

DEFORMATION OF A STRATIFIED SEMI-INFINITE ELASTIC BODY

2.0   Introduction

If we restrict our attention to an ice sheet whose radius is very small compared with that of the earth then we may take the earth to be a semi-infinite solid, the upper boundary of which is a flat plane. In such an analysis it is usually more convenient to approximate the complex geometry of an ice sheet by a set of superimposed loads of reasonably simple geometry (such as cylinders or rectangular prisms), just as in our global analysis we approximate the load by superimposing surface harmonics. It is obviously more useful, though slightly more difficult, to consider rectangular loads since they may more conveniently be used to approximate complex load geometries. Previous workers have favoured the 2-dimensional case of cylindrical loads (Nakiboglu & Lambeck 1982, Wolf 1985a,b), though some attempts have been made to model ice sheets by superposition of prism loads over a square grid (Quinlan & Beaumont 1982).

Our aim ultimately is to model the deformation of a visco-elastic body under a surface load but, as discussed in section 1.3, by invoking the correspondence principle we may use the theory for an elastic body to derive the deformation of a corresponding Maxwell visco-elastic half-space. This chapter is devoted to the development of a number of procedures for modelling the deformation of a stratified, semi-infinite elastic half-space.

In the case of a semi-infinite elastic half-space, the majority of the deformation caused by a given surface load occurs above a depth approximately equal to the lateral extent of the load. The smaller the load, the smaller the depth to which the load significantly deforms the elastic body. When we superimpose a set of small loads to model a much larger surface load we superimpose their deformation and stress contributions at depths much larger than the lateral extent of the individual loads. While individually these contributions may be negligible they will become significant upon summation and it is therefore important that the deformation and stress at depth due to these individual loads are calculated as accurately as possible.

In this chapter I will examine three approaches to the problem of calculating the deformation of an elastic half-space by a surface load. All three techniques use Fourier transforms to translate the problem into one of solving a set of linear equations over a region of transform space and then inverting to the spatial domain.

The first and oldest of these techniques is an early approach developed by McConnell (1965) that relies on explicitly solving the equilibrium equations throughout the body, while the second is a slightly more conventional propagator matrix approach discussed by Cathles (1975) that uses McConnell's direct solution technique to apply the boundary condition in the bottom layer of the stratification but propagates the solution to the surface using a slightly more elegant and theoretically convenient technique from the theory of differential equations. The third is a variation of this traditional propagator matrix technique developed by Kennett (1981) originally designed to model elastic wave propagation through a stratified medium.

I will adapt each of these techniques to three dimensional Cartesian coordinates (the most convenient regime for examining the deformation due to a rectangular load), and examine their numerical stability and suitability to the problem we wish to discuss, with particular attention to the accuracy of the calculations at depth. The final section of the chapter will be devoted to a detailed discussion and comparison of the numerical performance of each of the techniques introduced and an analysis of their numerical stability. Our ultimate goal of course is to use the most appropriate numerical technique as part of a formal inverse procedure.

We will start with a reformulation of the problem of the surface deformation of an elastic body using Cartesian coordinates.

2.1 Formulation of the Problem

We will consider a homogeneous, semi-infinite, elastic body with boundary $x_3 = 0$, with x_3 increasing in the downward direction (into the solid). We will denote the component of displacement in the direction of the axis e_i by u_i and the various components of material incremental stress by $t_{ij}^{(\delta)}$. The form of the components of stress are given by the constitutive equation for an elastic body:

$$t_{ij}^{(\delta)} = \lambda \delta_{ij} \frac{\partial u_k}{\partial x_k} + \mu \left(\frac{\partial u_i}{\partial x_j} + \frac{\partial u_j}{\partial x_i} \right) \tag{2.1.1}$$

with repeated indices indicating summation as per the Einstein convention and δ_{ij} representing the Kronecker delta function.

As in chapter 1 (equation 1.5.4) we define the dilatation, Δ, to be the divergence of the deformation field:

$$\Delta = \frac{\partial u_k}{\partial x_k} = \frac{\partial u_1}{\partial x_1} + \frac{\partial u_2}{\partial x_2} + \frac{\partial u_3}{\partial x_3} \tag{2.1.2}$$

If we once again assume that the acceleration terms are small enough to be neglected (as discussed in section 1.1) and neglect the effect of pre-stress and internal buoyancy (to be reintroduced in chapter 4), then the equations of motion may be written (e.g. Love 1927):

$$\left(\lambda + \mu \right) \frac{\partial \Delta}{\partial x_j} + \mu \nabla^2 u_j = -\rho f_j \tag{2.1.3}$$

for all values of j, where ∇^2 denotes the Laplacian operator, the f_j are the various components of the body force per unit mass, and λ and μ are the Lamé parameters of the elastic body.

2.2 Basic Propagator Matrix Analysis

This analysis is based on obtaining direct analytical solutions to the governing system of differential equations throughout the body and applying the appropriate boundary conditions as discussed by McConnell (1965). We now follow his analysis and transform the problem into that of solving a set of 3 simultaneous first order differential equations using Fourier transforms. We Fourier transform all of the quantities in equations (2.1.2) and (2.1.3) with respect to x_1 and x_2 using transform variables v_1 and v_2 respectively.

Let X_i be the Fourier transform of u_i, let $\tilde{\Delta}$ denote the Fourier transform of Δ, and let τ_{ij} be the Fourier transform of $t_{ij}^{(\delta)}$. Then make the following definitions:

$$Z_1 = -iX_1 \; ; \; Z_2 = -iX_2 \; ; \; Z_3 = -X_3 \; ; \; P = (\lambda + \mu)\tilde{\Delta}$$

$$T_{13} = -i\tau_{13} \; ; \; T_{23} = -i\tau_{23} \; ; \; T_{33} = -\tau_{33}$$

(2.2.1)

where i in this case is defined by the relation $i^2 = -1$. We assume in this case that there is no body force acting inside the body we are considering (i.e. that the components of the body force, f_j in (2.1.3), are everywhere zero throughout the body). Then, upon transforming equations (2.1.2) and (2.1.3), substituting the quantities defined above into the resulting expressions and rearranging we see that within the body:

$$\left[\partial_{33} - \left(v_1^2 + v_2^2\right)\right]Z_1 = -\frac{v_1 P}{\mu}$$

(2.2.2a)

$$\left[\partial_{33} - \left(v_1^2 + v_2^2\right)\right]Z_2 = -\frac{v_2 P}{\mu}$$

(2.2.2b)

$$\left[\partial_{33} - \left(v_1^2 + v_2^2\right)\right]Z_3 = \frac{1}{\mu}\frac{\partial P}{\partial x_3}$$

(2.2.2c)

$$v_1 Z_1 + v_2 Z_2 + \frac{\partial Z_3}{\partial x_3} = -\frac{P}{\lambda + \mu}$$

(2.2.3)

where ∂_{33} represents the second order linear differential operator $\dfrac{\partial^2}{\partial x_3^2}$.

§2.2.1 Solving the Equilibrium Equations

We want to evaluate the stress and deformation terms throughout the body by solving this set of simultaneous differential equations and then inverting from the transform domain. We begin by defining the quantity $k_0 = 1 + \frac{\lambda}{\mu}$, rearranging (2.2.3) and substituting into equations (2.2.2) to yield:

$$\left[\partial_{33} - \left((k_0 + 1)v_1^2 + v_2^2 \right) \right] Z_1 - k_0 v_1 v_2 Z_2 = k_0 v_1 \frac{\partial Z_3}{\partial x_3} \tag{2.2.4a}$$

$$\left[\partial_{33} - \left(v_1^2 + (k_0 + 1)v_2^2 \right) \right] Z_2 - k_0 v_1 v_2 Z_1 = k_0 v_2 \frac{\partial Z_3}{\partial x_3} \tag{2.2.4b}$$

$$\left[(k_0 + 1) \partial_{33} - \left(v_1^2 + v_2^2 \right) \right] Z_3 = -k_0 \left[v_1 \frac{\partial Z_1}{\partial x_3} + v_2 \frac{\partial Z_2}{\partial x_3} \right] \tag{2.2.4c}$$

where . Rearranging (2.2.4b), substituting into (2.2.4c) and simplifying gives:

$$v_1 \left[\frac{\partial^2 Z_1}{\partial x_3^2} - \left(v_1^2 + v_2^2 \right) Z_1 \right] = \frac{1}{k_0 v_2} \left\{ \left(v_1^2 + v_2^2 \right) \left[v_1^2 + (k_0 + 1)v_2^2 \right] Z_2 \right.$$

$$\left. - \left[(k_0 + 2)v_1^2 + 2(k_0 + 1)v_2^2 \right] \frac{\partial^2 Z_2}{\partial x_3^2} + (k_0 + 1) \frac{\partial^4 Z_2}{\partial x_3^4} \right\} \tag{2.2.5}$$

Equations (2.2.4a) and (2.2.4b) may be combined to yield the following equivalence:

$$v_2 \left[\frac{\partial^2 Z_1}{\partial x_3^2} - \left(v_1^2 + v_2^2 \right) Z_1 \right] = v_1 \left[\frac{\partial^2 Z_2}{\partial x_3^2} - \left(v_1^2 + v_2^2 \right) Z_2 \right] \tag{2.2.6}$$

which may be incorporated back into (2.2.5). Collecting like terms, simplifying and removing unnecessary constant factors yields the biharmonic equation:

$$\frac{\partial^4 Z_2}{\partial x_3^4} - 2 \left(v_1^2 + v_2^2 \right) \frac{\partial^2 Z_2}{\partial x_3^2} + \left(v_1^2 + v_2^2 \right)^2 Z_2 = 0 \tag{2.2.7}$$

We may immediately see that equation (2.2.7) has solutions of the form:

$$Z_2 = B\,e^{\alpha x_3} + C v_2 x_3\,e^{\alpha x_3} + E\,e^{-\alpha x_3} + F v_2 x_3\,e^{-\alpha x_3} \tag{2.2.8a}$$

where B, C, E, and F are arbitrary constants to be determined by the boundary conditions, and α is defined such that: $\alpha^2 = v_1^2 + v_2^2$.

Using the definition of P, substituting (2.2.8a) back into (2.2.4a) and (2.2.4c), and then solving the resulting differential equations, yields the additional results:

$$Z_1 = A\,e^{\alpha x_3} + C v_1 x_3\,e^{\alpha x_3} + D\,e^{-\alpha x_3} + F v_1 x_3\,e^{-\alpha x_3} \tag{2.2.8b}$$

$$Z_3 = -\left(\frac{v_1 A + v_2 B}{\alpha}\right) e^{\alpha x_3} + \left[\left(\frac{\lambda + 3\mu}{\lambda + \mu}\right) - \alpha x_3\right] C e^{\alpha x_3}$$

$$\tag{2.2.8c}$$

$$+ \left(\frac{v_1 D + v_2 E}{\alpha}\right) e^{-\alpha x_3} + \left[\left(\frac{\lambda + 3\mu}{\lambda + \mu}\right) + \alpha x_3\right] F e^{-\alpha x_3}$$

$$P = -2\alpha x_3 \left[C e^{\alpha x_3} + F e^{-\alpha x_3}\right] \tag{2.2.8d}$$

where A and D are also arbitrary constants. Substituting these expressions back into (2.1.1) and using (2.2.1) yields the forms for the components of stress:

$$T_{13} = \frac{\mu}{\alpha}\left\{\left(2v_1^2 + v_2^2\right)e^{\alpha x_3} A + v_1 v_2\,e^{\alpha x_3} B + 2\alpha v_1\left[\alpha x_3 - \left(\frac{\mu}{\lambda + \mu}\right)\right]e^{\alpha x_3} C\right.$$

$$\tag{2.2.9a}$$

$$\left. -\left(2v_1^2 + v_2^2\right)e^{-\alpha x_3} D - v_1 v_2\,e^{-\alpha x_3} E - 2\alpha v_1\left[\alpha x_3 + \left(\frac{\mu}{\lambda + \mu}\right)\right]e^{-\alpha x_3} F\right\}$$

$$T_{23} = \frac{\mu}{\alpha}\left\{v_1 v_2\,e^{\alpha x_3} A + \left(v_1^2 + 2v_2^2\right)e^{\alpha x_3} B + 2\alpha v_2\left[\alpha x_3 - \left(\frac{\mu}{\lambda + \mu}\right)\right]e^{\alpha x_3} C\right.$$

$$\tag{2.2.9b}$$

$$\left. - v_1 v_2\,e^{-\alpha x_3} D - \left(v_1^2 + 2v_2^2\right)e^{-\alpha x_3} E - 2\alpha v_2\left[\alpha x_3 + \left(\frac{\mu}{\lambda + \mu}\right)\right]e^{-\alpha x_3} F\right\}$$

$$T_{33} = -2\mu \left\{ v_1 e^{\alpha x_3} A + v_2 e^{\alpha x_3} B - \alpha \left[\left(\frac{\lambda + 2\mu}{\lambda + \mu} \right) - \alpha x_3 \right] e^{\alpha x_3} C \right.$$

$$\left. + v_1 e^{-\alpha x_3} D + v_2 e^{-\alpha x_3} E + \alpha \left[\alpha x_3 + \left(\frac{\mu}{\lambda + \mu} \right) \right] e^{-\alpha x_3} F \right\}$$

(2.2.9c)

If we let w be the deformation and stress vector $\left(Z_1, Z_2, Z_3, T_{13}, T_{23}, T_{33} \right)^T$ and let y be the vector $\left(A, B, C, D, E, F \right)^T$ then we have $My = w$ where the entries of M are given by equations (2.2.8) and (2.2.9) above and more explicitly in section A.1. If we set $v_2 = 0$ in M the resulting matrix is equivalent to that given for the two dimensional case by McConnell (1965), as would be expected.

§2.2.2 Application to a Stratified Body

We will now assume that our elastic halfspace is stratified into N uniform layers as illustrated in Figure 2.1, where the Lamé parameters for the n-th layer are λ_n and μ_n, and the lower boundary is the plane $x_3 = h_n$. We will take the upper boundary of the first layer to be the surface of the body $x_3 = h_0 = 0$, while the bottom layer is taken to be semi-infinite so that $h_N = \infty$.

$$x_3 = h_0 = 0$$
$$\lambda_1, \mu_1$$
$$x_3 = h_1$$
$$\lambda_2, \mu_2$$
$$x_3 = h_2$$
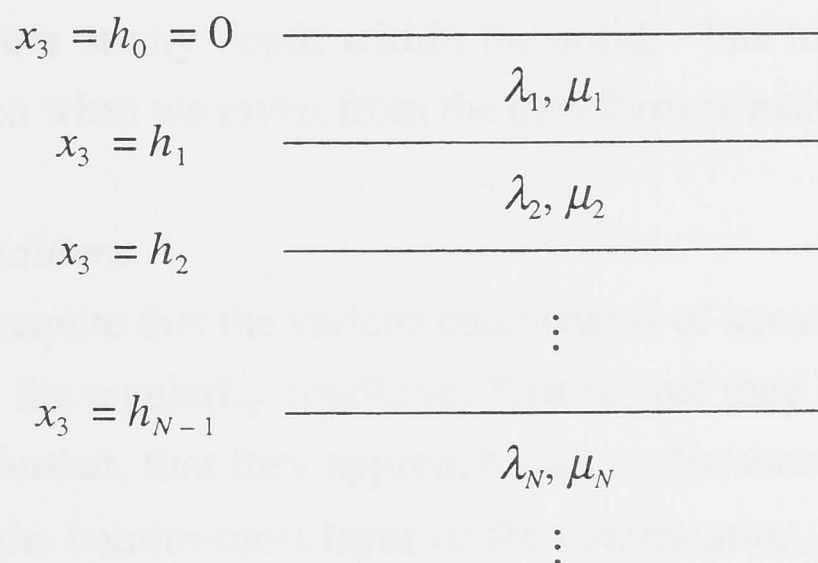$$\vdots$$
$$x_3 = h_{N-1}$$
$$\lambda_N, \mu_N$$
$$\vdots$$

Figure 2.1: Side on view of a layered elastic half-space. The bottom of the n-th layer has depth $x_3 = h_n$, the top of the first layer is the upper boundary of the half-space $x_3 = 0$.

Using the analysis outlined in section 2.2.1 we see that at any point inside the n-th layer (i.e. if $h_{n-1} \leq x_3 \leq h_n$) $w(x_3) = M_n(x_3)y_n$, where $y_n = \left(A_n, B_n, C_n, D_n, E_n, F_n \right)^T$ and the entries of $M_n(x_3)$ are obtained by substituting x_3, λ_n, and μ_n into A.1. It should be remembered that the entries of the matrices M_n are in fact functions of v_1 and v_2 and that we have temporarily suppressed this dependence for ease of notation.

As discussed in section 1.3 the boundary conditions between layers are simply continuity of the various components of stress and displacement, this continuity is inherited by the Fourier transforms of these functions as a matter of course. Mathematically, this may be expressed

$$M_n(h_n)y_n = M_{n+1}(h_n)y_{n+1} \tag{2.2.10a}$$

and may be rewritten:

$$y_n = \left[\left(M_n(h_n) \right)^{-1} M_{n+1}(h_n) \right] y_{n+1} \tag{2.2.10b}$$

Applying (2.2.10b) recursively we see that at the surface:

$$w(0) = M_1(0) \left[\prod_{n=1}^{N-1} \left(M_n(h_n) \right)^{-1} M_{n+1}(h_n) \right] y_N$$

$$= L\, y_N \tag{2.2.11}$$

Once we have determined y_N we can use (2.2.10) to evaluate the components of displacement and stress at any depth within the solid. The lateral variation of these quantities will be given when we invert from the transform domain.

§2.2.3 Boundary Conditions

Physically, we require that the various components of stress and deformation due to the surface load obey the regularity condition. That is, that they be finite and continuous inside the body and further, that they approach zero as distance from the load becomes arbitrarily large. In the bottom-most layer of the stratification, $x_3 \geq h_{N-1}$, depth may become arbitrarily large, we therefore require that the magnitude of the various components of stress and displacement decrease with depth within this layer (this need not necessarily be the case near the surface of the body but it is certainly true inside the

bottom-most layer of the stratification). Applied to our formulation this requirement means that A_N, B_N, and C_N must all be equal to zero.

At the surface the vertical stress, $t_{33}^{(\delta)}$, will be specified by the normal loading function, and the shearing stresses, $t_{13}^{(\delta)}$ and $t_{23}^{(\delta)}$ will both be zero. Hence equation (2.2.11) becomes:

$$\begin{pmatrix} Z_1 \\ Z_2 \\ Z_3 \\ 0 \\ 0 \\ \phi(v_1, v_2) \end{pmatrix} = L \begin{pmatrix} 0 \\ 0 \\ 0 \\ D_N \\ E_N \\ F_N \end{pmatrix} \qquad (2.2.12)$$

where ϕ is the Fourier transform of the loading function. We can rearrange (2.2.12) by collecting all of the unknowns into the one vector. This yields:

$$\begin{pmatrix} 0 \\ 0 \\ 0 \\ 0 \\ 0 \\ \phi(v_1, v_2) \end{pmatrix} = \begin{bmatrix} -1 & 0 & 0 & l_{14} & l_{15} & l_{16} \\ 0 & -1 & 0 & l_{24} & l_{25} & l_{26} \\ 0 & 0 & -1 & l_{34} & l_{35} & l_{36} \\ 0 & 0 & 0 & l_{44} & l_{45} & l_{46} \\ 0 & 0 & 0 & l_{54} & l_{55} & l_{56} \\ 0 & 0 & 0 & l_{64} & l_{65} & l_{66} \end{bmatrix} \begin{pmatrix} Z_1 \\ Z_2 \\ Z_3 \\ D_N \\ E_N \\ F_N \end{pmatrix}$$

$$= K u \qquad (2.2.13)$$

The problem has now been reduced to solving this set of simultaneous linear equations. In order to evaluate the entries of the vector u for particular values of v_1 and v_2 we need to first evaluate ϕ and the entries of K at this point, substitute these values into (2.2.13) and then solve. The resulting values of D_n, E_n, and F_n can then be used along with equations (2.2.10) and (2.2.11) to determine the components of stress and displacement at any depth within the body.

For a uniform load of magnitude p applied over the rectangular area S defined to be the set of points (x_1, x_2, x_3) such that $-a \le x_1 \le a$; $-b \le x_2 \le b$; $x_3 = 0$, the Fourier transform, ϕ, of the loading function may be found in any table of Fourier transforms (see for example Spiegel 1968) and is given by:

$$\phi(v_1, v_2) = \frac{4 p \sin(a v_1) \sin(b v_2)}{v_1 v_2} \qquad (2.2.14)$$

In practice it will be necessary to solve (2.2.13) over a grid of values of v_1 and v_2 and then invert the results using a numerical technique (see for example Press *et. al.* 1986) to give the desired function values over a corresponding grid in the space domain. This being the case it is more appropriate to use a numerically derived value for the Fourier transform of the loading function than the theoretical value given in (2.2.14).

§2.2.4 Discussion

The procedure outlined above has several distinct advantages. One of its most attractive features is that it is relatively uncomplicated theoretically, which makes it convenient to implement numerically. Also, the formulation of the problem is one that makes it relatively easy to calculate the stress and displacement at depth, a desirable property when interpreting the rheological implications of a given loading history.

It also however has several shortcomings. One of the most significant of which is that the entries of the matrices M_n in equation (2.2.10a) include both exponentially growing and decaying terms making matrix manipulation numerically unstable at large depths. Also of some concern is the fact that the propagation procedure involves numerically calculating the inverses of a series of matrices (or at least solving the associated linear systems at each layer boundary) which makes the technique computationally expensive and particularly prone to numerical instability given the large variation in the magnitude of the entries at depth. A detailed review of the numerical performance of this procedure and discussion of its limitations will be given in section 2.5.

2.3 Conventional Propagator Matrix Analysis

In the previous section we derived an explicit analytical form for the solution of the governing differential equations within each layer. The coefficients of the solutions were then chosen inside each layer so as to guarantee agreement with the boundary conditions of the system.

In the conventional propagator matrix technique we apply exactly the same boundary condition in the bottom-most layer as we did in the last procedure . Having obtained an explicit form for the solution at this point, we propagate it using a technique from the theory of differential equations (see for example Braun 1983). In practice this technique requires significantly more analytical effort than the basic procedure outlined above but in return it avoids excessive matrix manipulations and provides increased numerical stability. We will discuss the theoretical foundations of this procedure in some detail as it also forms the basis for the wave propagation technique we derive in the next section.

Applying Fourier transforms to the quantities in (2.1.1), and using the identities given in (2.2.1) we may immediately see that:

$$\frac{\partial Z_1}{\partial x_3} = v_1 Z_3 + \frac{T_{13}}{\mu} \qquad\qquad \frac{\partial Z_2}{\partial x_3} = v_2 Z_3 + \frac{T_{23}}{\mu}$$

$$\frac{\partial Z_3}{\partial x_3} = \frac{1}{\lambda + 2\mu}\left(T_{33} - \lambda\left(v_1 Z_1 + v_2 Z_2\right)\right)$$

$$(2.3.1)$$

Taking the derivative with respect to x_3 of equations (2.3.1) and then substituting (2.2.4) into the resulting expressions yields:

$$\frac{\partial T_{13}}{\partial x_3} = \frac{1}{\lambda + \mu}\left(\mu Z_1\left(4(\lambda + \mu) v_1^2 + (\lambda + 2\mu) v_2^2\right) + \mu v_1 v_2 Z_2 \left(3\lambda + 2\mu\right) + \lambda v_1 T_{33}\right)$$

$$\frac{\partial T_{23}}{\partial x_3} = \frac{1}{\lambda + \mu}\left(\mu v_1 v_2 Z_1 \left(3\lambda + 2\mu\right) + \mu Z_2\left((\lambda + 2\mu) v_1^2 + 4(\lambda + \mu) v_2^2\right) + \lambda v_2 T_{33}\right)$$

$$\frac{\partial T_{33}}{\partial x_3} = -\left(v_1 T_{13} + v_2 T_{23}\right) \qquad\qquad (2.3.2)$$

It should be noted here that we are once again assuming that there are no body forces acting within the body. Equations (2.3.1) and (2.3.2) constitute a system of 6 simultaneous first order differential equations. The governing equation of this system may be written:

$$\frac{\partial w}{\partial x_3} = A w \tag{2.3.3}$$

where the entries of A may be found from (2.3.1) and (2.3.2) and w is correspondingly defined to be the vector whose entries are the modified transforms of the various components of stress and deformation $\left(i.e.\ w = \left(Z_1, Z_2, Z_3, T_{13}, T_{23}, T_{33}\right)^T\right)$.

It should be noted that the coefficients in equations (2.3.1) and (2.3.2) (the entries of the matrix A) are dependent only on λ, μ, v_1, and v_2, and not on x_3 except insofar as λ and μ are depth dependent.

Defining k_1 so that $k_1 = \left(\lambda + 2\mu\right)^{-1}$, A may be written explicitly:

$$A = \begin{bmatrix} 0 & 0 & v_1 & \dfrac{1}{\mu} & 0 & 0 \\ 0 & 0 & v_2 & 0 & \dfrac{1}{\mu} & 0 \\ -k_1\lambda v_1 & -k_1\lambda v_2 & 0 & 0 & 0 & k_1 \\ \mu\left(4\,k_1\left(\lambda + \mu\right)v_1^2 + v_2^2\right) & k_1\mu\left(3\lambda + 2\mu\right)v_1 v_2 & 0 & 0 & 0 & k_1\lambda v_1 \\ k_1\mu\left(3\lambda + 2\mu\right)v_1 v_2 & \mu\left(v_1^2 + 4\,k_1\left(\lambda + \mu\right)v_2^2\right) & 0 & 0 & 0 & k_1\lambda v_2 \\ 0 & 0 & 0 & -v_1 & -v_2 & 0 \end{bmatrix}$$

$$\tag{2.3.4}$$

From the general theory of differential equations (again see Braun 1983) we see that if we have a scalar function w that satisfies the equation:

$$\frac{\partial w}{\partial x} = f(x)\,w \tag{2.3.5}$$

for some function f, then w has the form:

$$w = w_0\, e^{\int_{x_0}^{x} f(x')\,dx'} \tag{2.3.6}$$

where $w_0 = w(x_0)$. Assuming we are in a region of the halfspace where the Lamé parameters do not vary with depth (i.e. where the matrix A is constant with respect to x_3) then using (2.3.6) we see that analogously, the solution to (2.3.3) is:

$$w(x_3) = \exp\left(\int_{x_3^0}^{x_3} A(x_3')dx_3'\right) = e^{A[x_3 - x_3^0]}w_0 \qquad (2.3.7)$$

§2.3.1 Calculating the Exponential of a Matrix

We may extend the definition of the exponential of a scalar to the case of an arbitrary $m \times m$ matrix A using the Taylor series expansion of the exponential function:

$$e^A = \sum_{n=0}^{\infty} \frac{A^n}{n!} = I + A + \frac{A^2}{2} + \dots \qquad (2.3.8)$$

where I is once again the Kronecker identity matrix. This definition is valid for both scalar values of A (corresponding to the case where $m = 1$) and the case where A is a square matrix. In the latter instance however, equation (2.3.8) is not a particularly convenient expression to evaluate directly for $m \geq 2$. Instead it is usually more appropriate to apply a standard technique from linear algebra (see for example Strang 1980).

Consider an $m \times m$ matrix A with m linearly independent eigenvectors, $b_1, b_2, \dots b_m$, each with corresponding eigenvalues $\alpha_1, \alpha_2, \dots \alpha_m$. We then define the diagonalising matrix of A to be the matrix, D that satisfies the equation:

$$D^{-1}AD = \Lambda \qquad (2.3.9)$$

where $\Lambda = \text{diag}\left(\alpha_1, \alpha_2, \dots \alpha_m\right)$ is the matrix whose diagonal entries are the eigenvalues of A and whose non-diagonal entries are zero.

Pre-multiplying both sides of equation (2.3.9) by D it is clear that the columns of D are the eigenvectors $b_1, b_2, \dots b_m$. Post-multiplying both sides by D^{-1} similarly shows that the rows of D^{-1} are the left-eigenvectors of A, $y_1^T, y_2^T, \dots y_m^T$ (the solutions to the equation $y_i^T A = \alpha_i y_i^T$).

Rearranging equation (2.3.9) and substituting back into equation (2.3.8) gives:

$$e^A = I + DAD^{-1} + \frac{\left(DAD^{-1}\right)\left(DAD^{-1}\right)}{2} + \frac{\left(DAD^{-1}\right)\left(DAD^{-1}\right)\left(DAD^{-1}\right)}{6} + \dots$$

$$= I + DAD^{-1} + \frac{DA\left(DD^{-1}\right)AD^{-1}}{2} + \frac{DA\left(DD^{-1}\right)A\left(DD^{-1}\right)AD^{-1}}{6} + \dots$$

$$= I + DAD^{-1} + \frac{DA^2D^{-1}}{2} + \frac{DA^3D^{-1}}{6} + \dots$$

$$= De^A D^{-1} \tag{2.3.10}$$

but $e^A = \operatorname{diag}\left(e^{\alpha_1}, e^{\alpha_2}, \dots e^{\alpha_m}\right)$, so that once D is known we may easily calculate e^A.

In the case where A is an $m \times m$ matrix but has only k linearly independent eigenvectors, $b_1, b_2, \dots b_k$, with corresponding eigenvalues, $\alpha_1, \alpha_2, \dots \alpha_k$, and $k < m$, we may still evaluate e^A using a generalisation of the diagonalisation technique outlined above.

It may be shown (see for example Strang 1980) that for the matrix A there exists a matrix D such that:

$$D^{-1}AD = \Lambda = \begin{pmatrix} \Lambda_1 & 0 & 0 & \cdots & 0 \\ 0 & \Lambda_2 & 0 & \cdots & 0 \\ 0 & 0 & \Lambda_3 & \cdots & 0 \\ \vdots & \vdots & \vdots & \ddots & \vdots \\ 0 & 0 & 0 & \cdots & \Lambda_l \end{pmatrix} \tag{2.3.11}$$

where Λ is a block diagonal matrix whose non-diagonal entries are all zero and whose diagonal entries, Λ_i, are block matrices of the form:

$$\Lambda_i = \begin{pmatrix} \alpha_i & 1 & 0 & \cdots & 0 \\ 0 & \alpha_i & 1 & \cdots & 0 \\ 0 & 0 & \alpha_i & & \vdots \\ \vdots & \vdots & & \ddots & 1 \\ 0 & 0 & \cdots & 0 & \alpha_i \end{pmatrix} \tag{2.3.12}$$

So that the diagonal entries of $\boldsymbol{\Lambda}_i$ are simply α_i and the only other non-zero entries are 1's in the superior diagonal immediately adjacent to the main diagonal. $\boldsymbol{\Lambda}$ is called the Jordan form of $\boldsymbol{A}$.

In the case where $\boldsymbol{A}$ has m distinct eigenvectors the $\boldsymbol{\Lambda}_i$ are simply scalar entries, $\boldsymbol{\Lambda}$ is identical to the diagonal matrix in (2.3.9), and $\boldsymbol{D}$ may be constructed from the eigenvectors of $\boldsymbol{A}$. The current case however is slightly more complicated.

From (2.3.9) we have that $\boldsymbol{AD} = \boldsymbol{D\Lambda}$, so that if $\boldsymbol{\Lambda}_i$ is an $n_i \times n_i$ matrix then there will be a corresponding set of n_i adjacent columns of $\boldsymbol{D}$, $\boldsymbol{d}_1^i, \boldsymbol{d}_2^i, \dots \boldsymbol{d}_{n_i}^i$, such that:

$$\boldsymbol{Ad}_1^i = \alpha_i \boldsymbol{d}_1^i$$

$$\boldsymbol{Ad}_j^i = \alpha_i \boldsymbol{d}_j^i + \boldsymbol{d}_{j-1}^i \qquad j = 2, 3, \dots n_i$$

(2.3.13)

It can immediately be seen that $\boldsymbol{d}_1^i = \boldsymbol{b}_1$, the eigenvector corresponding to the eigenvalue α_i, the other $\boldsymbol{d}_j^i$ are called the generalised eigenvectors of $\boldsymbol{A}$. This generalisation applies also to the left-eigenvectors, although because of the change in the direction of multiplication the ordering is reversed, so that $\left(\bar{\boldsymbol{d}}_{n_i}^i\right)^{\mathrm{T}} \boldsymbol{A} = \alpha_i \bar{\boldsymbol{d}}_{n_i}^i$ and $\left(\bar{\boldsymbol{d}}_j^i\right)^{\mathrm{T}} \boldsymbol{A} = \alpha_i \bar{\boldsymbol{d}}_j^i + \bar{\boldsymbol{d}}_{j+1}^i$.

Once we have constructed $\boldsymbol{\Lambda}$ and $\boldsymbol{D}$ we may calculate $e^{\boldsymbol{A}}$ using (2.3.10) which still applies, though evaluating $e^{\boldsymbol{A}}$ is not as simple in this case.

From substituting (2.3.11) back into (2.3.8) it is clear that the off-diagonal zero entries in $\boldsymbol{\Lambda}$ suppress any cross multiplication of the $\boldsymbol{\Lambda}_i$ terms so that:

$$e^{\boldsymbol{\Lambda}} = \begin{pmatrix} e^{\boldsymbol{\Lambda}_1} & \boldsymbol{0} & \boldsymbol{0} & \cdots & \boldsymbol{0} \\ \boldsymbol{0} & e^{\boldsymbol{\Lambda}_2} & \boldsymbol{0} & \cdots & \boldsymbol{0} \\ \boldsymbol{0} & \boldsymbol{0} & e^{\boldsymbol{\Lambda}_3} & \cdots & \boldsymbol{0} \\ \vdots & \vdots & \vdots & \ddots & \vdots \\ \boldsymbol{0} & \boldsymbol{0} & \boldsymbol{0} & \cdots & e^{\boldsymbol{\Lambda}_l} \end{pmatrix}$$

(2.3.14)

We now need to develop a technique for conveniently calculating the exponential of a non-diagonal matrix of the form of $\boldsymbol{\Lambda}_i$.

Given an $m \times m$ matrix $\boldsymbol{A}$ with m distinct eigenvalues, $\alpha_1, \alpha_2, \dots \alpha_m$ (and thus m linearly independent eigenvectors) there exists a matrix $\boldsymbol{D}$ such that (2.3.9) holds. Given an arbitrary function f then $f(\boldsymbol{A})$ may be evaluated using a Taylor series expansion for f:

$$f(A) = \sum_{n=0}^{\infty} \frac{f_n A^n}{n!} = \sum_{n=0}^{\infty} \frac{f_n \left(D \Lambda D^{-1}\right)^n}{n!} = D \left(\sum_{n=0}^{\infty} \frac{f_n \Lambda^n}{n!} \right) D^{-1} = D f(\Lambda) D^{-1} \qquad (2.3.15)$$

where the f_n are the Taylor series coefficients for f. Again applying the Taylor series formulation for f and noting that all of the off-diagonal entries of Λ are zero, it is clear that the i–th diagonal element of $f(\Lambda)$ is $f(\alpha_i)$ and that the off-diagonal elements are zero i.e. $f(\Lambda) = \mathrm{diag}\left(f(\alpha_1), f(\alpha_2), \dots f(\alpha_m) \right)$.

We now define M^i to be the $m \times m$ matrix whose only non-zero entry is $M_{ii}^i = \alpha_i$ and note that:

$$M^i = \alpha_i \prod_{\substack{j=1 \\ j \neq i}}^{m} \left(\frac{\Lambda - \alpha_j I}{\alpha_i - \alpha_j} \right)$$

$$(2.3.16)$$

$$\Lambda = \sum_{i=1}^{m} M^i$$

Substituting back into (2.3.15) and again using the fact the off-diagonal entries of Λ and M^i are zero yields:

$$f(A) = D f \left(\sum_{i=1}^{m} M^i \right) D^{-1} = D \left[\sum_{i=1}^{m} f(M^i) \right] D^{-1} = \sum_{i=1}^{m} \left(D f(M^i) D^{-1} \right)$$

$$= \sum_{i=1}^{m} \left[D f \left(\alpha_i \prod_{\substack{j=1 \\ j \neq i}}^{m} \left(\frac{\Lambda - \alpha_j I}{\alpha_i - \alpha_j} \right) \right) D^{-1} \right] = \sum_{i=1}^{m} f(\alpha_i) D \left[\prod_{\substack{j=1 \\ j \neq i}}^{m} \left(\frac{\Lambda - \alpha_j I}{\alpha_i - \alpha_j} \right) \right] D^{-1}$$

$$= \sum_{i=1}^{m} f(\alpha_i) \left[\prod_{\substack{j=1 \\ j \neq i}}^{m} \left(\frac{A - \alpha_j I}{\alpha_i - \alpha_j} \right) \right] \qquad (2.3.17)$$

which is the standard form for this type of expression (see for example Gantmacher 1960). The case where two of the eigenvalues are equal (i.e. $\alpha_i = \alpha_j$ for some i and j) may be considered by letting $\alpha_j = \alpha_i + \varepsilon$ in (2.3.17) and letting ε approach zero. Doing so yields:

$$f(A) = \sum_{n=1}^{m} \left(\left[f(\alpha_i) \left(1 - \sum_{\substack{l=1 \\ l \neq i,j}}^{m} \left(\frac{1}{\alpha_i - \alpha_l} \right) \right) + f'(\alpha_i) \right] \left(\prod_{\substack{k=1 \\ k \neq i,j}}^{m} \frac{A - \alpha_k I}{\alpha_i - \alpha_k} \right) + \sum_{\substack{k=1 \\ k \neq i,j}}^{m} f(\alpha_k) \left[\prod_{\substack{l=1 \\ l \neq k}}^{m} \left(\frac{A - \alpha_l I}{\alpha_k - \alpha_l} \right) \right] \right)$$

$$(2.3.18)$$

which is the same result as that given by Gantmacher (1960).

We may obviously use (2.3.18) to calculate e^A directly except that taking the limit as ε approaches zero becomes prohibitively complicated when the matrix A has more than two identical eigenvalues. In the case of the matrix A given in (2.3.4) however, (2.3.18) may be used in conjunction with the Jordan form approach to give an explicit form for e^A. In this case we are interested in calculating the exponential of a 2 x 2 matrix, Ω, of the form:

$$\Omega = \begin{pmatrix} \omega z & z \\ 0 & \omega z \end{pmatrix} \qquad (2.3.19)$$

which may be substituted back into (2.3.18) to yield:

$$e^{\Omega} = \begin{pmatrix} e^{\omega z} & z e^{\omega z} \\ 0 & e^{\omega z} \end{pmatrix} \qquad (2.3.20)$$

§2.3.2 Application to the Problem of an Elastic Medium

The characteristic equation of the matrix A given in (2.3.4) is:

$$\det\left(A - \alpha_i I\right) = \left(\alpha_i^2 - \alpha^2\right)^3 = 0 \qquad (2.3.21)$$

where α is as defined for equation (2.2.8). Equation (2.3.21) has two solutions, both of order 3, $\alpha_{1,2,3} = \alpha$ and $\alpha_{4,5,6} = -\alpha$. These eigenvalues each have two corresponding linearly independent eigenvectors of the form:

$$d_{1,4} = \beta_1 \begin{pmatrix} v_2 \\ -v_1 \\ 0 \\ \mu v_2 \alpha_{1,4} \\ -\mu v_1 \alpha_{1,4} \\ 0 \end{pmatrix} \qquad d_{2,5} = \beta_2 \begin{pmatrix} v_1 \\ v_2 \\ -\alpha_{2,5} \\ 2\mu v_1 \alpha_{2,5} \\ 2\mu v_2 \alpha_{2,5} \\ -2\mu \alpha^2 \end{pmatrix} \qquad (2.3.22)$$

where β_1 and β_2 are constant scaling factors to guarantee orthonormality of the system.

For both $i = 1, 4$ the equation $(A - \alpha_i I)x = d_i$ has no solution so that the generalised eigenvectors of A (as defined in equation (2.3.13)) are the solutions to this equation for $i = 2, 5$ and may be written:

$$d_{3,6} = \beta_2 \begin{pmatrix} \dfrac{k_2 v_1}{\alpha_{3,6}} \\ \dfrac{k_2 v_2}{\alpha_{3,6}} \\ k_2 \\ \mu v_1 \\ \mu v_2 \\ \mu \alpha_{3,6} \end{pmatrix} \qquad (2.3.23)$$

where we have defined a new quantity k_2 so that

$$k_2 = \frac{\lambda + 3\mu}{2(\lambda + \mu)} \qquad (2.3.24)$$

These vectors d_i form the columns of the matrix D that gives the Jordan form of the matrix A given in equation (2.3.4). Solving the equations for the left-eigenvectors of A gives corresponding solutions:

$$y_{1,4} = \widehat{\beta}_{1,4} \begin{pmatrix} \mu v_2 \alpha_{1,4} \\ -\mu v_1 \alpha_{1,4} \\ 0 \\ v_2 \\ -v_1 \\ 0 \end{pmatrix} \qquad y_{3,6} = \beta_2 \begin{pmatrix} 2\mu v_1 \alpha_{3,6} \\ 2\mu v_2 \alpha_{3,6} \\ 2\mu \alpha^2 \\ v_1 \\ v_2 \\ \alpha_{3,6} \end{pmatrix} \qquad (2.3.25a)$$

The generalised left-eigenvectors of A take the form:

$$y_{2,5} = \beta_2 \begin{pmatrix} \mu v_1 \\ \mu v_2 \\ -\mu \alpha_{2,5} \\ k_2 v_1 \\ \alpha_{2,5} \\ \frac{k_2 v_2}{\alpha_{2,5}} \\ -k_2 \end{pmatrix} \tag{2.3.25b}$$

Setting $\beta_1 \bar{\beta}_{1,4} = 2\mu \alpha^2 \alpha_{1,4}$, and $\bar{\beta}_2^{\,2} = 4\mu \left(\dfrac{\lambda + 2\mu}{\lambda + \mu} \right) \alpha^2$ in the above expressions gives:

$$y_i \cdot d_j = 0 \quad if \ i \neq j \qquad y_1 \cdot d_1 = y_4 \cdot d_4 = 2\mu \alpha^2 \alpha_{1,4} \beta_1 \bar{\beta}_{1,4} = 1$$

$$y_2 \cdot d_2 = y_3 \cdot d_3 = y_5 \cdot d_5 = y_6 \cdot d_6 = 4\mu \left(\dfrac{\lambda + 2\mu}{\lambda + \mu} \right) \alpha^2 \beta_2^2 = 1 \tag{2.3.26}$$

where it is usual to choose $\beta_1 = \bar{\beta}_1 = -\bar{\beta}_4$. With these relations holding it is clear that D^{-1} is the matrix whose rows are y_i^{T}.

When combined these results yield a convenient form for the matrices D and D^{-1} such that (2.3.11) holds for the matrix A given in (2.3.4). It remains only to calculate the matrix $e^{\Lambda z}$ where $z = x_3 - x_3^0$ and Λ, the Jordan form of A, can be calculated from (2.3.11) and (2.3.12):

$$\Lambda = \begin{bmatrix} \alpha & 0 & 0 & 0 & 0 & 0 \\ 0 & \alpha & 1 & 0 & 0 & 0 \\ 0 & 0 & \alpha & 0 & 0 & 0 \\ 0 & 0 & 0 & -\alpha & 0 & 0 \\ 0 & 0 & 0 & 0 & -\alpha & 1 \\ 0 & 0 & 0 & 0 & 0 & -\alpha \end{bmatrix} \tag{2.3.27}$$

Using (2.3.15) and (2.3.21) gives:

$$e^{\Lambda z} = \begin{bmatrix} e^{\alpha z} & 0 & 0 & 0 & 0 & 0 \\ 0 & e^{\alpha z} & z e^{\alpha z} & 0 & 0 & 0 \\ 0 & 0 & e^{\alpha z} & 0 & 0 & 0 \\ 0 & 0 & 0 & e^{-\alpha z} & 0 & 0 \\ 0 & 0 & 0 & 0 & e^{-\alpha z} & z e^{-\alpha z} \\ 0 & 0 & 0 & 0 & 0 & e^{-\alpha z} \end{bmatrix} \tag{2.3.28}$$

Combining equations (2.3.22), (2.3.23), (2.3.25) (2.3.26), and (2.3.28) we have an explicit expression for $e^{Az} = D e^{Az} D^{-1}$ which we may substitute into (2.3.7). The entries of the matrix e^{Az} are given explicitly in section A.2. If we set v_2 equal to zero throughout A.2 and recall that z is negative then our expression for e^{Az} corresponds to that given by Wolf (1985a). It should again be noted that A, D, Λ, and D^{-1} are not dependent on x_3 except insofar as λ and μ are depth dependent.

§2.3.3 Application to a Stratified Body

Taking the same stratification as that given in section 2.2.2 we see that if $x_3 = d$ for some depth d such that $h_{n-1} \leq d \leq h_n$ then:

$$\left. \frac{\partial w}{\partial x_3} \right|_{x_3 = d} = A_n w(d) \tag{2.3.29}$$

where the entries of A_n are obtained by substituting λ_n and μ_n into (2.3.4). Using (2.3.7) we see that (2.3.29) has solution:

$$w(d) = e^{A_n[d - d_0]} w(d_0) \tag{2.3.30}$$

for some d_0 such that $h_{n-1} \leq d_0 \leq h_n$. In particular if we define $z_n = h_{n-1} - h_n$ then:

$$w(h_{n-1}) = e^{A_n[h_{n-1} - h_n]} w(h_n) = e^{A_n z_n} w(h_n) \tag{2.3.31}$$

where $e^{A_n z_n}$ may be calculated by substituting z_n for z in the equations in appendix A.

Continuity of the stress-displacement vector across the boundaries between layers may again be used recursively to yield:

$$w(0) = e^{A_1 z_1} e^{A_2 z_2} \cdots e^{A_{N-1} z_{N-1}} w(h_{N-1}) = \left[\prod_{n=1}^{N} e^{A_n z_n} \right] w(h_{N-1}) \tag{2.3.32}$$

§2.3.4 Boundary Conditions

Once again we apply the condition of continuity of the stress-displacement vector across the boundaries between layers, apply our load at the surface of the half-space where the horizontal components of stress are taken to be zero, and require that the various components of stress and displacement vanish as distance from the centre of the load increases.

This last boundary condition may be introduced by noting that from section 2.2.2 we have:

$$w\left(h_{N-1}\right) = M_N\left(h_{N-1}\right) y_N \tag{2.3.33}$$

using the same definitions for M_n and y_n as were given in equation (2.2.10a). Substituting back into (2.3.33) and applying the layer boundary conditions yields:

$$w(0) = \left[\prod_{n=1}^{N} e^{A_n z_n}\right] M_N\left(h_{N-1}\right) y_N \tag{2.3.34}$$

which may be re-written:

$$\begin{pmatrix} X_1 \\ X_2 \\ X_3 \\ 0 \\ 0 \\ \phi\left(v_1, v_1\right) \end{pmatrix} = G \begin{pmatrix} 0 \\ 0 \\ 0 \\ D_N \\ E_N \\ F_N \end{pmatrix} \tag{2.3.35}$$

We may again collect all the unknowns onto the one side of the equation as we did in section 2.2.3 and so reduce the problem to solving the equation:

$$\begin{pmatrix} 0 \\ 0 \\ 0 \\ 0 \\ 0 \\ \phi\left(v_1, v_1\right) \end{pmatrix} = \begin{pmatrix} -1 & 0 & 0 & g_{14} & g_{15} & g_{16} \\ 0 & -1 & 0 & g_{24} & g_{25} & g_{26} \\ 0 & 0 & -1 & g_{34} & g_{35} & g_{36} \\ 0 & 0 & 0 & g_{44} & g_{45} & g_{46} \\ 0 & 0 & 0 & g_{54} & g_{55} & g_{56} \\ 0 & 0 & 0 & g_{64} & g_{65} & g_{66} \end{pmatrix} \begin{pmatrix} Z_1 \\ Z_2 \\ Z_3 \\ D_N \\ E_N \\ F_N \end{pmatrix} \tag{2.3.36}$$

$$= Ju$$

where ϕ is the loading function discussed in section 2.2.3, and the entries of J may be calculated from (2.3.34), A.1, and A.2.

As in McConnell's analysis we calculate the matrix J and solve (2.3.36) over a grid of values for v_1 and v_2, and then invert from the Fourier domain to get the solution in real space.

§2.3.5 Discussion

Like the basic propagator matrix technique the advantages of this procedure are its relative theoretical simplicity (particularly when applied to the two dimensional problem) and the ease with which it may be adapted to calculate the stress-deformation vector at depth. The slightly more complex theoretical development has however eliminated the need to calculate the inverse matrices used by the basic technique which should make this procedure somewhat more robust numerically.

Directly solving the equations of motion in the bottom-most layer however retains the problem of significant variation in the magnitude of the matrix entries at large depths. Also of some concern is the fact that the entries of the matrices $e^{A_n z_n}$ consist largely of cosh and sinh functions. At large depths a computer with finite accuracy will be unable to distinguish between these functions which will render the system prone to numerical error in the solving routines. These issues will be discussed in greater detail in section 2.5.

2.4 Wave Propagation Analysis

This technique was originally developed to model the propagation of waves through an elastic half-space. It is designed to achieve increased numerical stability by completely analytically decoupling exponentially increasing and decreasing components of deformation and stress (the up-going and down-going components of the stress-displacement field). It does so in such a fashion that only exponentially decreasing components need be considered during the computational phase, greatly enhancing stability but at the cost of significantly increased analytical complexity.

We start by introducing some new notation, for convenience the more important quantities introduced in this section and the last will be presented in the table below. Much of the new notation is devoted to the projection of standard quantities (the stress-displacement vector, propagator matrix, etc.) into the eigenspace of A. This change of basis plays an important part in the mathematical development of the technique.

Quantity	Description	Equation
A	Governing matrix of the stress-displacement system	2.3.4
D	Matrix that gives the Jordan form of A	2.3.11
$w(x_3)$	Stress-displacement vector at depth x_3	2.3.7
$B(x_3)$	Fundamental matrix solution of 2.3.4	2.4.32
$P(x_3, x_3^0)$	Propagator matrix for w from depth x_3^0 to x_3	2.4.1
$v(x_3)$	Field vector - projection of $w(x_3)$ into eigenspace of A	2.4.2
$Q(x_3, x_3^0)$	Field propagator - propagates v from depth x_3^0 to x_3	2.4.3
$F(x_3, x_3^0)$	Transform propagator - propagates from $v(x_3^0)$ to $w(x_3)$	2.4.46
R, T	Reflection and Transmission matrices	2.4.8
E, E'	Sub-partitions of Q for a uniform layer	2.4.5
n, m	Sub-partitions of D_1	2.4.49
$\phi_{U,D}$	Up- and down-going components of v	2.4.6
g	Stress-displacement vector for the source of deformation	2.4.31
Ψ	Discontinuity in w due to g	2.4.38
Σ	Discontinuity in v due to g	2.4.58
S	Surface vector - projection of Ψ to the surface	2.4.39

Table 2.1: List of important mathematical quantities in the development of
the wave propagator technique

The original formulation of this procedure (Kennett 1981) was intended to model the propagation of waves through an elastic body. In his derivation Kennett keeps the acceleration term in equation (1.1.1), and introduces frequency explicitly into the form for his governing matrix. The development we will give will therefore correspond to the zero frequency case of Kennett. This does not affect the validity of the formalism which is still applicable to the case of static deformations.

We know from the analysis of the previous section that the solution to (2.3.3), the stress-displacement vector, $w(x_3)$, satisfies the relation $w(x_3) = P(x_3, x_3^0) w(x_3^0)$, where from the general form of (2.3.6) we see that the propagator matrix $P(x_3, x_3^0)$ is given:

$$P(x_3, x_3^0) = \exp\left(\int_{x_3^0}^{x_3} A(x'_3)dx'_3\right) \tag{2.4.1}$$

where exp is the exponential function. From this definition it immediately follows that $P(x_3^2, x_3^0) = P(x_3^2, x_3^1) P(x_3^1, x_3^0)$.

Now if we choose a matrix D and a corresponding field vector v so that they satisfy the relation, $w(x_3) = D(x_3) v(x_3)$, then from (2.3.3) and (2.3.7) we have that:

$$\frac{\partial(Dv)}{\partial x_3} = A(Dv) \tag{2.4.2}$$

and

$$v(x_3^0) = \left[D(x_3^0)^{-1} P(x_3^0, x_3) D(x_3)\right] v(x_3) = Q(x_3^0, x_3) v(x_3) \tag{2.4.3}$$

which may be taken as a definition of the field propagator matrix, Q. From this definition and the properties of the original propagator matrix, P, we have that:

$$Q(x_3^2, x_3^0) = Q(x_3^2, x_3^1) Q(x_3^1, x_3^0) \tag{2.4.4}$$

Given the form of Q in (2.4.3) it is usually convenient to choose D to be the matrix that gives the Jordan form of A.

It is important to note that this change of basis into the eigenspace of A is purely a mathematical formalism and does not correspond to a physical process. Performing this transformation does however make the mathematical representation of some physical effects more intuitive, as we shall see later in this section.

We follow Kennett by defining two classes of contribution to the stress-displacement vector and the field vector, the up-going and down-going components. We define an up-going vector quantity to be any vector function whose magnitude increases as depth increases and a down-going vector quantity to be any vector function whose magnitude decreases as depth increases. These definitions coming from the fact that physically, waves decay as they travel further from from their source.

Letting $z = x_3 - x_3^0$ and defining matrices $E(z)$ and $E'(z)$ so that:

$$E(z) = \begin{bmatrix} e^{\alpha z} & 0 & 0 \\ 0 & e^{\alpha z} & ze^{\alpha z} \\ 0 & 0 & e^{\alpha z} \end{bmatrix} \qquad E'(z) = \begin{bmatrix} e^{\alpha z} & 0 & 0 \\ 0 & e^{\alpha z} & -ze^{\alpha z} \\ 0 & 0 & e^{\alpha z} \end{bmatrix} \qquad (2.4.5)$$

then from (2.4.3) and (2.3.28) it is clear that in a region of the halfspace with uniform elastic properties we may choose D to be the matrix defined in (2.3.22), (2.3.23), and (2.3.24) that gives the Jordan form of A. Then substituting the Jordan form from equation (2.3.11) into the definition of the field propagator matrix yields:

$$v(x_3) = \begin{pmatrix} \phi_U \\ \phi_D \end{pmatrix} = \begin{bmatrix} e^{\alpha z} & 0 & 0 & 0 & 0 & 0 \\ 0 & e^{\alpha z} & ze^{\alpha z} & 0 & 0 & 0 \\ 0 & 0 & e^{\alpha z} & 0 & 0 & 0 \\ 0 & 0 & 0 & e^{-\alpha z} & 0 & 0 \\ 0 & 0 & 0 & 0 & e^{-\alpha z} & ze^{-\alpha z} \\ 0 & 0 & 0 & 0 & 0 & e^{-\alpha z} \end{bmatrix} v(x_3^0)$$

$$= \begin{bmatrix} E(z) & 0 \\ 0 & E'(-z) \end{bmatrix} v(x_3^0)$$

$$= Q(x_3, x_3^0) v(x_3^0) \qquad (2.4.6)$$

Thus at any point inside a stratified halfspace the field vector v has both an up-going component, represented by the vector ϕ_U, and a down-going component, represented by the vector ϕ_D.

§2.4.1 Reflection and Transmission of Deformation Fields

The notation and terminology of this procedure were developed for a dynamic case and it is not immediately obvious that the same concepts extend meaningfully to the static case (though the mathematical formalism is certainly still valid). The concepts of up- and down-going fields and their behaviour might be best illustrated by an example.

Consider a flat semi-infinite, elastic half-space with constant Lamé parameters λ_0 and μ_0 throughout. If we place a source of deformation at some depth x_3^s within the body then there will be a resulting stress-displacement field throughout the body represented by the vertical displacement $u_3^0(x_3)$ which will take its maximum value at x_3^s, as illustrated schematically in Figure 2.2a.

In contrast, consider the case where we have a semi-infinite elastic body with constant Lamé parameters λ_0 and μ_0 in the region $x_3 \leq x_3^0$ (with $x_3^0 > x_3^s$) and constant Lamé parameters λ_1 and μ_1 in the region $x_3 \geq x_3^0$ (we will assume for this example that the bottom layer is significantly weaker than the upper, with half the rigidity and bulk modulus). Given the same source of deformation, this second body will have a different distribution of vertical displacement $u_3^1(x_3)$.

Inserting a layer below the level of the source of displacement will have an effect on the displacement field in the upper layer. In the case of an elastic wave this effect would
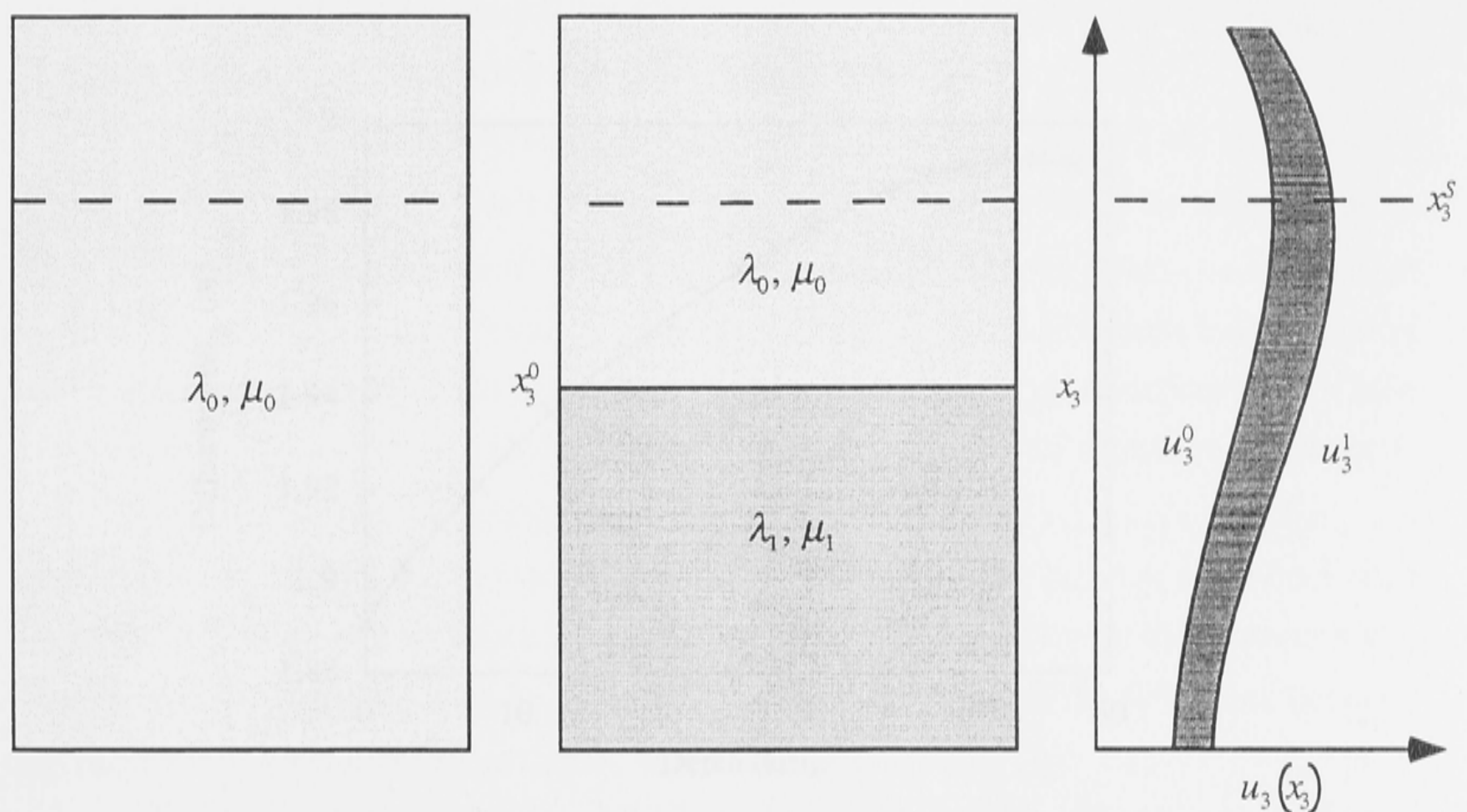

Figure 2.2a: Schematic comparison of the difference in displacement fields produced by insertion of a layer boundary. The source of deformation is the same for both bodies, the two displacement curves are compared in the graph on the right-hand side of the figure.
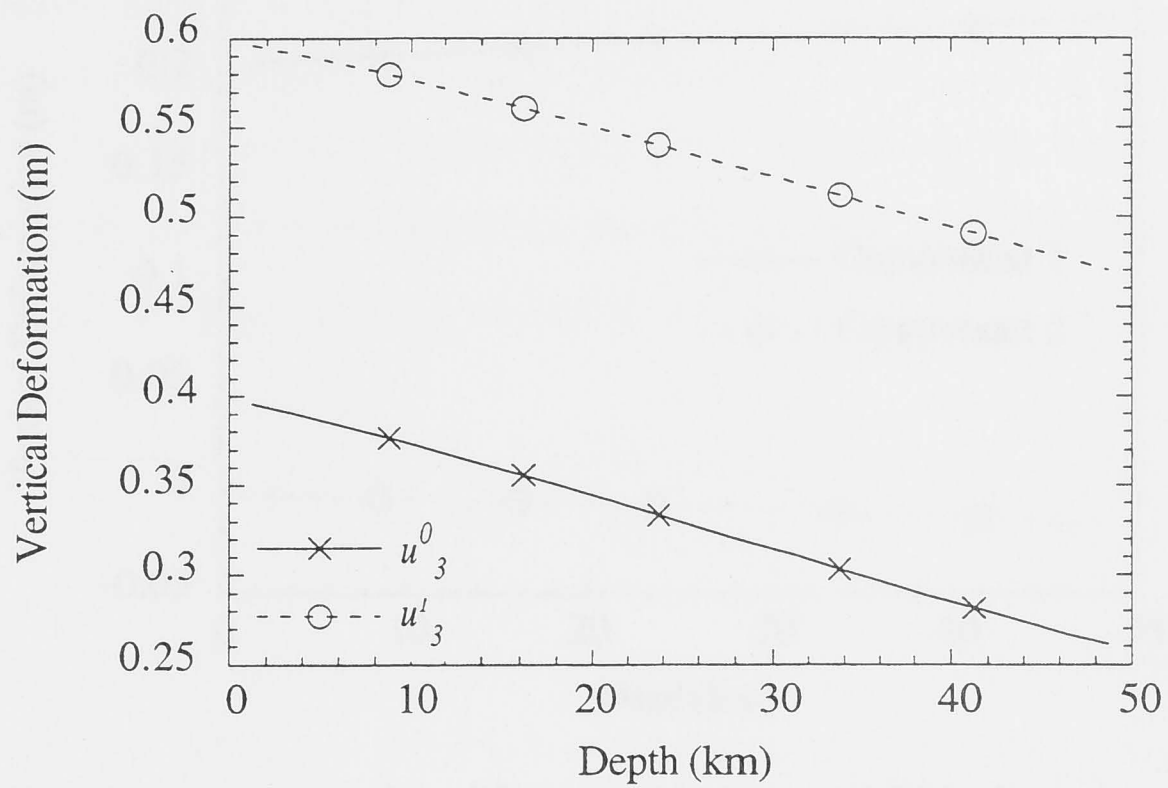
Figure 2.2b: The displacement curves $u_3^0(x_3)$ and $u_3^1(x_3)$ due to a surface load at the origin ($x_3^S = 0$), plotted against depth, x_3. $u_3^0(x_3)$ was calculated for a uniform elastic body of rigidity 3.6×10^{10} Pa, and bulk modulus 6.5×10^{10} Pa. $u_3^1(x_3)$ was calculated for an half-space identical to that used for $u_3^0(x_3)$ except for a layer boundary at 50 km below which the rigidity and bulk modulus were both halved.

Figure 2.2c: Difference between displacement fields, $\Delta u_3(x_3) = u_3^1(x_3) - u_3^0(x_3)$, plotted against depth.

Figure 2.2d: Up-going components of the difference in displacement fields $\Delta u_3(x_3) = u_3^1(x_3) - u_3^0(x_3)$. The residual down-going component is of the order of 10^{-3} m and is not shown in the figure.

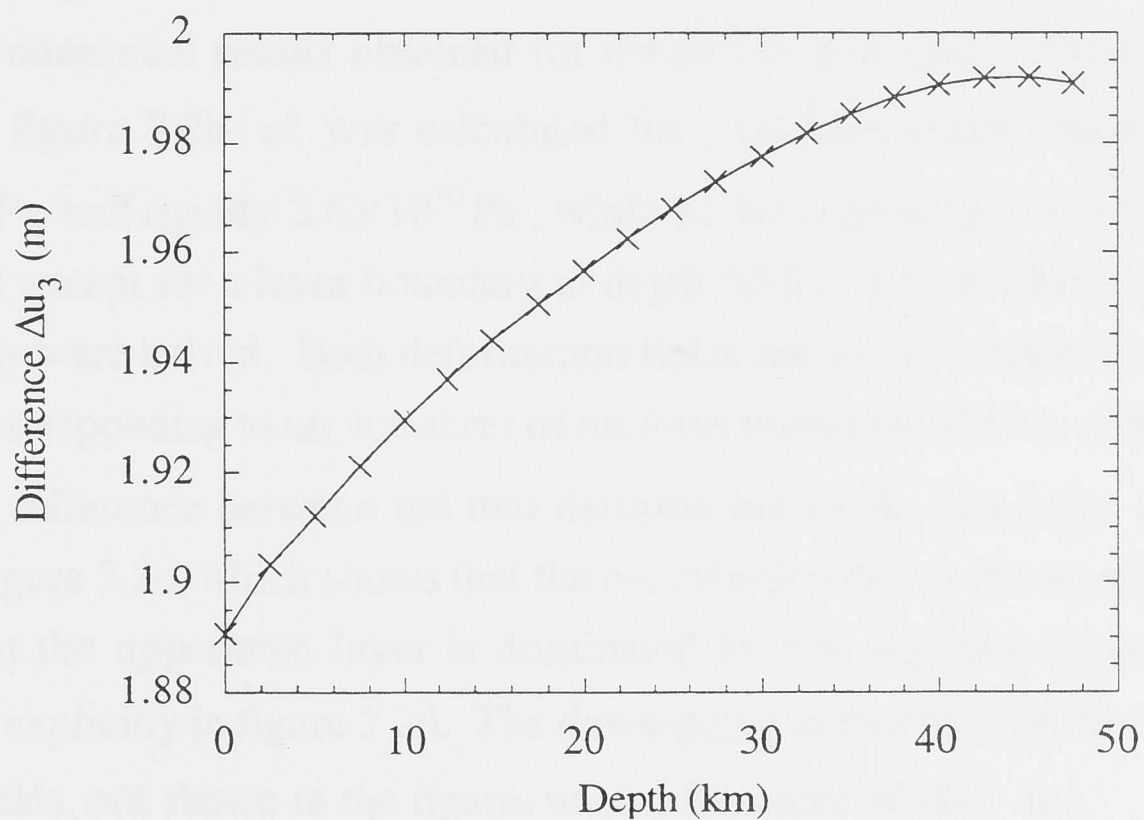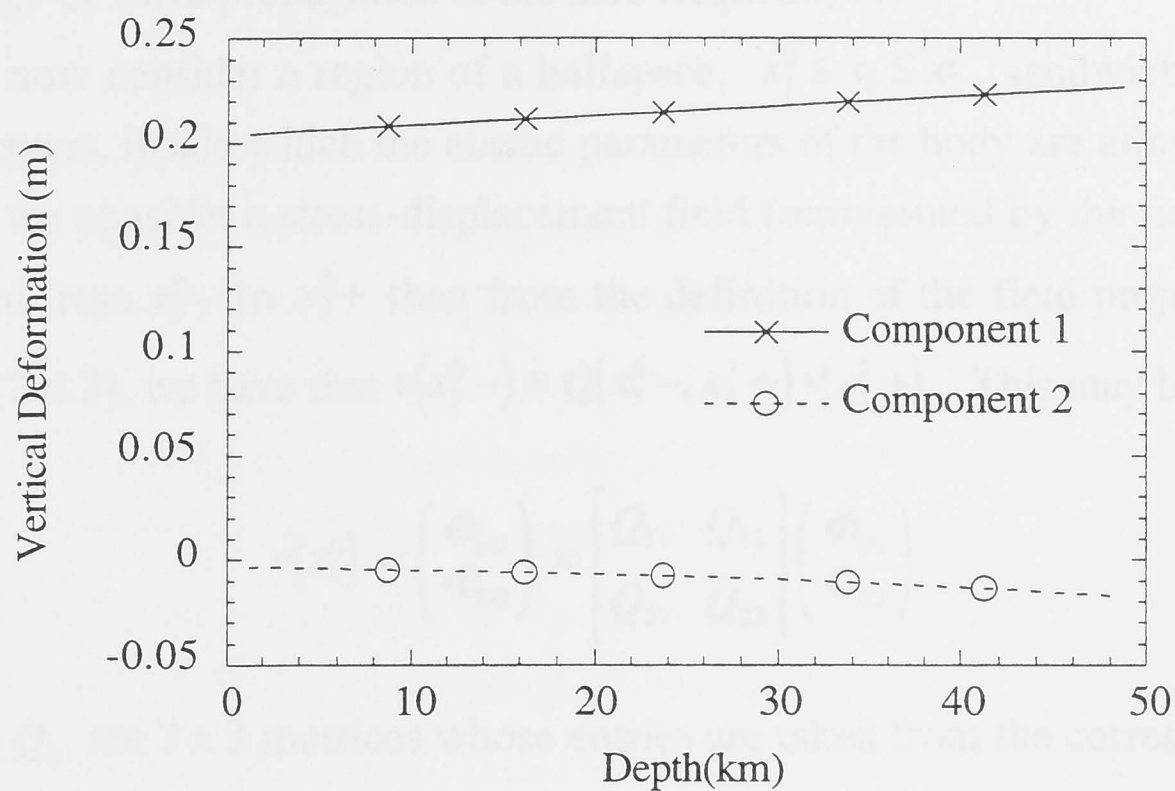include internal reflections and reverberations between the surface and the layer boundary. Analogously, we would therefore expect the difference between the two distributions in the static case to include both an up-going component (corresponding to reflection off the layer boundary) and a significantly smaller down-going component (corresponding to the up-going component in turn being reflected off the surface layer).

The numerical results obtained for the two displacement curves, u_3^0 and u_3^1, are shown in figure 2.2b. u_3^0 was calculated for a uniform elastic body of bulk modulus 6.5×10^{10} Pa and rigidity 3.6×10^{10} Pa, while u_3^1 was calculated for a half-space identical to the first except for a layer boundary at depth 50 km, below which both bulk modulus and rigidity were halved. Both deformation fields are due to a square surface load of side 100 km corresponding to an ice sheet of uniform thickness, 400 m, centred on the origin.

The difference between the two deformation fields, $\Delta u_3(x_3) = u_3^1(x_3) - u_3^0(x_3)$, is given in figure 2.2c, which shows that the contribution due to the inserted layer boundary throughout the uppermost layer is dominated by two separate up-going components, illustrated explicitly in figure 2.2d. The down-going component of the difference between the two fields, not shown in the figure, was of the order of 10^{-3} m.

In the dynamic case reflection off a layer boundary may be defined as the effect of that boundary on the stress-displacement vector in the region above it. This example demonstrates that a completely analogous effect occurs even in the static case. It is

therefore mathematically and conceptually appropriate to retain both the notation and terminology of wave-propagation in the zero frequency case.

We now consider a region of a halfspace, $x_3^0 \leq x_3 \leq x_3^2$, sandwiched between two uniform layers, inside which the elastic parameters of the body are allowed to vary with depth. If we consider a stress-displacement field (represented by the field vector) being propagated from x_3^0- to x_3^2+ then from the definition of the field propagator matrix in equation (2.4.3), we have that $v(x_3^0-) = Q(x_3^0-, x_3^2+) v(x_3^2+)$. This may be re-written:

$$v(x_3^0) = \begin{pmatrix} \Phi_{U0} \\ \Phi_{D0} \end{pmatrix} = \begin{bmatrix} Q_{11} & Q_{12} \\ Q_{21} & Q_{22} \end{bmatrix} \begin{pmatrix} \Phi_{U2} \\ \Phi_{D2} \end{pmatrix} \tag{2.4.7}$$

where the Q_{ij} are 3 x 3 matrices whose entries are taken from the corresponding parts of the matrix Q, and the $\Phi_{U,Dk}$ are 3 x 1 vectors representing the corresponding up-going and down-going entries of the field vector $v(x_3^k)$. We know from (2.4.6) that $v(x_3^0-)$ and $v(x_3^2+)$ may be written in this form inside a uniform region of the halfspace and from continuity must therefore also have this form at the upper and lower boundaries of the region we are considering. We may now define the transmission and reflection matrices for the up and down-going components of the field vector.

Consider a source of deformation at depth $x_3^S < x_3^0$ that produces only a down-going component of deformation and assume that there are no other sources of deformation within the body. Then the down-going component of the field vector at x_3^2+ will be the portion of the down-going deformation at x_3^0- that has been transmitted from x_3^0- to x_3^2+. We are not yet considering the effect of any layer boundaries below $x_3 = x_3^2$ so that there will be no up-going component of deformation at this level due to the source at x_3^0, and the up-going component of the stress-displacement field at x_3^0- will be the reflected portion of the initial down-going displacement field. Defining reflection and transmission matrices R_D^{02} and T_D^{02} for down-going field components such that:

$$\Phi_{D2} = T_D^{02} \Phi_{D0} \qquad\qquad \Phi_{U0} = R_D^{02} \Phi_{D0} \tag{2.4.8}$$

then substituting into (2.4.7) yields:

$$\begin{pmatrix} \Phi_{U0} \\ \Phi_{D0} \end{pmatrix} = \begin{bmatrix} Q_{11} & Q_{12} \\ Q_{21} & Q_{22} \end{bmatrix} \begin{pmatrix} 0 \\ \Phi_{D2} \end{pmatrix} \tag{2.4.9}$$

from which it is clear that:

$$T_D^{02} = Q_{22}^{-1} \qquad\qquad R_D^{02} = Q_{12}(Q_{22})^{-1} \qquad\qquad (2.4.10)$$

Similarly, if we consider a source of deformation at depth $x_3^s > x_3^2$ that produces only an up-going component of deformation and assume that there are no other sources of deformation within the body, then the up-going component of the field vector at x_3^0- will be the portion of the up-going deformation at x_3^2+ that has been transmitted from x_3^2+ to x_3^0-. We are not yet considering the effect of any layer boundaries above depth $x_3 = x_3^0$ so that there will be no down-going component of deformation due to the source at x_3^2, and the down-going component of the stress-displacement field at x_3^2+ will be the reflected portion of the initial up-going displacement field. If we define reflection and transmission matrices R_U^{02} and T_U^{02} for up-going field components such that:

$$\Phi_{U0} = T_U^{02}\Phi_{U2} \qquad\qquad \Phi_{D2} = R_U^{02}\Phi_{U2} \qquad\qquad (2.4.11)$$

then substituting back into (2.4.7) yields:

$$\begin{pmatrix} \Phi_{U0} \\ 0 \end{pmatrix} = \begin{bmatrix} Q_{11} & Q_{12} \\ Q_{21} & Q_{22} \end{bmatrix} \begin{pmatrix} \Phi_{U2} \\ \Phi_{D2} \end{pmatrix} \qquad\qquad (2.4.12)$$

from which it is clear that:

$$T_U^{02} = Q_{11} - Q_{12}(Q_{22})^{-1}Q_{21} \qquad\qquad R_U^{02} = (Q_{22})^{-1}Q_{21} \qquad\qquad (2.4.13)$$

We may use the forms for the reflection and transmission matrices given in equations (2.4.10) and (2.4.13) to rewrite the field propagator matrix Q. Doing so yields one of the fundamental relations in the formalism of the wave propagation procedure, the partition equation:

$$Q\left(x_3^0-, x_3^2+\right) = \begin{bmatrix} T_U^{02} - R_D^{02}\left(T_D^{02}\right)^{-1}R_U^{02} & R_D^{02}\left(T_D^{02}\right)^{-1} \\ -\left(T_D^{02}\right)^{-1}R_U^{02} & \left(T_D^{02}\right)^{-1} \end{bmatrix} \qquad\qquad (2.4.14)$$

which relates the reflection and transmission matrices to the field propagator matrix.

§2.4.2 Composite Reflection and Transmission matrices

Consider the case of two adjacent regions of the halfspace wedged between two uniform layers as illustrated in Figure 2.3 below.

$$
\begin{array}{c}
\textit{Uniform Layer 1} \\
x_3 = x_3^0 \quad \rule{6cm}{0.4pt} \\
\textit{Region 1} \\
x_3 = x_3^1 \quad \rule{6cm}{0.4pt} \\
\textit{Region 2} \\
x_3 = x_3^2 \quad \rule{6cm}{0.4pt} \\
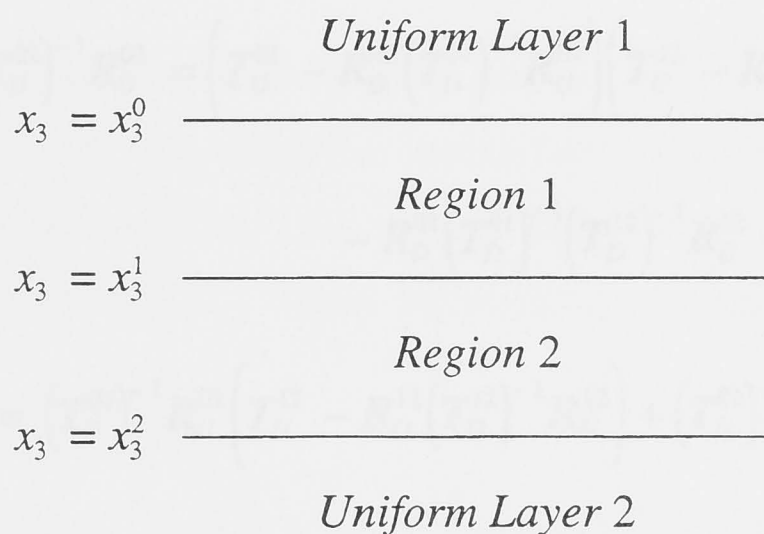\textit{Uniform Layer 2}
\end{array}
$$

Figure 2.3: Side on view of two adjacent regions of the half-space

wedged between two uniform layers.

Each region having its own elastic properties which may vary with depth, and corresponding transmission and reflection matrices. We would like to calculate the overall transmission and reflection matrices for the two regions considered as a whole.

The chain rule for the field propagator matrix Q is given in equation (2.4.4), substituting the general form of the partition equation (equation (2.4.14)) back into this expression yields:

$$
Q\!\left(x_3^0, x_3^2\right) = \begin{bmatrix} T_U^{02} - R_D^{02}\!\left(T_D^{02}\right)^{-1}R_U^{02} & R_D^{02}\!\left(T_D^{02}\right)^{-1} \\[2mm] -\!\left(T_D^{02}\right)^{-1}R_U^{02} & \left(T_D^{02}\right)^{-1} \end{bmatrix}
$$

$$
= \begin{bmatrix} T_U^{01} - R_D^{01}\!\left(T_D^{01}\right)^{-1}R_U^{01} & R_D^{01}\!\left(T_D^{01}\right)^{-1} \\[2mm] -\!\left(T_D^{01}\right)^{-1}R_U^{01} & \left(T_D^{01}\right)^{-1} \end{bmatrix} \times \begin{bmatrix} T_U^{12} - R_D^{12}\!\left(T_D^{12}\right)^{-1}R_U^{12} & R_D^{12}\!\left(T_D^{12}\right)^{-1} \\[2mm] -\!\left(T_D^{12}\right)^{-1}R_U^{12} & \left(T_D^{12}\right)^{-1} \end{bmatrix}
$$

$$
= Q\!\left(x_3^0, x_3^1\right) Q\!\left(x_3^1, x_3^2\right) \tag{2.4.18}
$$

By identifying the corresponding matrix entries we may immediately see that:

$$\left(T_D^{02}\right)^{-1} = \left(T_D^{01}\right)^{-1}\left(I - R_U^{01}R_D^{12}\right)\left(T_D^{12}\right)^{-1}$$

$$R_D^{02}\left(T_D^{02}\right)^{-1} = \left(T_U^{01} - R_D^{01}\left(T_D^{01}\right)^{-1}R_U^{01}\right)R_D^{12}\left(T_D^{12}\right)^{-1} + R_D^{01}\left(T_D^{01}\right)^{-1}\left(T_D^{12}\right)^{-1}$$

$$T_U^{02} - R_D^{02}\left(T_D^{02}\right)^{-1}R_U^{02} = \left(T_U^{01} - R_D^{01}\left(T_D^{01}\right)^{-1}R_U^{01}\right)\left(T_U^{12} - R_D^{12}\left(T_D^{12}\right)^{-1}R_U^{12}\right)$$

$$\phantom{T_U^{02} - R_D^{02}\left(T_D^{02}\right)^{-1}R_U^{02} =} - R_D^{01}\left(T_D^{01}\right)^{-1}\left(T_D^{12}\right)^{-1}R_U^{12}$$

(2.4.19)

$$\left(T_D^{02}\right)^{-1}R_U^{02} = \left(T_D^{01}\right)^{-1}R_U^{01}\left(T_U^{12} - R_D^{12}\left(T_D^{12}\right)^{-1}R_U^{12}\right) + \left(T_D^{01}\right)^{-1}\left(T_D^{12}\right)^{-1}R_U^{12}$$

from which we may obtain explicit forms for the combined reflection and transmission matrices:

$$R_D^{02} = R_D^{01} + T_U^{01}R_D^{12}\left(I - R_U^{01}R_D^{12}\right)^{-1}T_D^{01} \qquad T_D^{02} = T_D^{12}\left(I - R_U^{01}R_D^{12}\right)^{-1}T_D^{01}$$

(2.4.20)

$$R_U^{02} = R_U^{12} + T_D^{12}R_U^{01}\left(I - R_D^{12}R_U^{01}\right)^{-1}T_U^{12} \qquad T_U^{02} = T_U^{01}\left(I - R_D^{12}R_U^{01}\right)^{-1}T_U^{12}$$

Kennett discusses the physical interpretation and validity of these expressions when applied to elastic waves, they include the effect of all internal reverberations as well as direct transmission and reflection.

It should be noted that if there is a discontinuity in elastic parameters at any of the regional boundaries, $x_3 = x_3^0$, $x_3 = x_3^1$, or $x_3 = x_3^2$ then instead of propagating our solution from x_3^0 to x_3^2 via x_3^1, we propagate our solution from x_3^0- to x_3^2+ via $x_3^1\pm$. It is not important which side of x_3^1 we choose to put the discontinuity as long as we are consistent throughout. In effect, rather than using the normal propagator matrices, $Q\left(x_3^0, x_3^1\right)$ and $Q\left(x_3^1, x_3^2\right)$, throughout our analysis we use $Q\left(x_3^0-, x_3^1\pm\right)$ and $Q\left(x_3^1\pm, x_3^2+\right)$ instead.

§2.4.3 Application to a Stratified Body

If we consider the case of a stratified body as discussed in section 2.2.2 then we may use the forms for the composite reflection and transmission matrices given in equation (2.4.20) to construct reflection and transmission matrices for the halfspace as a whole.

In the case where both x_3 and x_3^0 lie inside the n-th layer of the halfspace we may choose $\boldsymbol{D}_n$ to be the matrix that yields the Jordan form of $\boldsymbol{A}_n$ (i.e. the matrix that satisfies equation (2.3.11)). From section 2.3.3 we see that if λ_n and μ_n do not vary with depth then neither do the entries of $\boldsymbol{D}_n$. Upon substituting $\boldsymbol{D}_n$ for $\boldsymbol{D}$, equations (2.4.2) and (2.4.3) become:

$$\frac{\partial v}{\partial x_3} = \left[\left(\boldsymbol{D}_n\right)^{-1}\boldsymbol{A}_n\boldsymbol{D}_n\right]v = \left[\left(\boldsymbol{D}_n\right)^{-1}\left(\boldsymbol{D}_n\boldsymbol{\Lambda}_n\left(\boldsymbol{D}_n\right)^{-1}\right)\boldsymbol{D}_n\right]v = \boldsymbol{\Lambda}_n v \qquad (2.4.21)$$

$$v\left(x_3^0\right) = \left[\left(\boldsymbol{D}_n\right)^{-1}e^{\boldsymbol{\Lambda}_n\left[x_3^0 - x_3\right]}\boldsymbol{D}_n\right]v\left(x_3\right) = \left[\left(\boldsymbol{D}_n\right)^{-1}\left(\boldsymbol{D}_n\,e^{-\boldsymbol{\Lambda}_n z}\left(\boldsymbol{D}_n\right)^{-1}\right)\boldsymbol{D}_n\right]v\left(x_3\right) = e^{-\boldsymbol{\Lambda}_n z}v\left(x_3\right) \qquad (2.4.22)$$

The form for the eigenvalues in this case is completely independent of depth (from equation (2.3.21)), so the entries of the matrix $\boldsymbol{\Lambda}_n$ are independent of the layer number, n. This is not the case once pre-stress advection or internal buoyancy are included however, as we shall see in chapter 4, so it is useful to retain this notation.

Within each layer of the halfspace the forms for the field propagator matrix given in equations (2.4.6) and (2.4.22) hold. Noting that

$$v\left(x_3^0\right) = \boldsymbol{Q}\left(x_3^0, x_3\right)v\left(x_3\right) = \boldsymbol{Q}\left(x_3^0, x_3\right)\boldsymbol{Q}\left(x_3, x_3^0\right)v\left(x_3^0\right) \qquad (2.4.23)$$

gives the relation:

$$\boldsymbol{Q}\left(x_3, x_3^0\right) = \left[\boldsymbol{Q}\left(x_3^0, x_3\right)\right]^{-1} \qquad (2.4.24)$$

Applying this result to the field propagator matrix of a uniform layer (given in equation (2.4.6)) yields:

$$\boldsymbol{Q}\left(x_3^0, x_3\right) = \begin{bmatrix} E(z)^{-1} & 0 \\ 0 & E'(-z)^{-1} \end{bmatrix} = \begin{bmatrix} E(-z) & 0 \\ 0 & E'(z) \end{bmatrix} \qquad (2.4.25)$$

Which may also be obtained by substituting $-z$ for z in (2.4.6). This result may be compared with the the partition equation, (2.4.14), to give explicit forms for the reflection and transmission matrices of a uniform layer of thickness z_n, lying between $x_3 = h_{n-1}$ and $x_3 = h_n$:

$$T_D^n = E'(z_n) \qquad T_U^n = E(z_n) \qquad R_U^n = 0 \qquad R_D^n = 0 \qquad (2.4.26)$$

using the same definition for z_n as was given in section 2.3.3 (i.e. $z_n = h_{n-1} - h_n$).

The situation at the boundary between two layers at depth $x_3 = h_n$ is illustrated in Figure 2.4 below.

$$\textit{Layer n:} \quad \frac{\partial w}{\partial x_3} = A_n w = \left[D_n \Lambda (D_n)^{-1} \right] w$$

$$x_3 = h_n \quad \rule{8cm}{0.4pt}$$

$$\textit{Layer n +1:} \quad \frac{\partial w}{\partial x_3} = A_{n+1} w = \left[D_{n+1} \Lambda (D_{n+1})^{-1} \right] w$$

Figure 2.4: Side-on view of the boundary between two layers and the equations that hold either side of the boundary.

From continuity of the stress-displacement vector across the boundaries between layers we have:

$$v(h_n -) = \left[(D_{n-1})^{-1} D_n \right] v(h_n +) = Q(h_n -, h_n +) \, v(h_n +) \qquad (2.4.27)$$

We may then apply the partition equation, (2.4.14), to this result to obtain the reflection and transmission matrices for the boundary. We may also use equation (2.4.26) to obtain the reflection and transmission matrices for a uniform layer. Once both sets of matrices have been determined they may be combined by applying the form for composite reflection and transmission matrices given in equation (2.4.20). Repeated applications of these results allows us to evaluate the field propagator matrix, Q, throughout the entire half-space, starting from the bottom-most layer and working upwards to the surface.

To illustrate our recursive procedure consider Figure 2.5 below. Starting from $h_N +$ we may apply equation (2.4.27) to calculate the reflection and transmission matrices for the boundary $x_3 = h_N$. Then at any boundary layer h_n we assume we have been able to

calculate the reflection and transmission matrices for the region $\left[h_{n+1}-, h_N+\right]$ (using equation (2.4.27) will yield the reflection and transmission matrices for the bottom-most layer boundary $\left[h_N-, h_N+\right]$ so that our procedure has a starting point).

Substituting the forms for the transmission and reflection matrices given in equations (2.4.26) and (2.4.27) into the recursion relation (2.4.20) allows us to calculate the reflection and transmission matrices for the region $\left[h_n-, h_{n+1}-\right]$. Applying the recursion relation (2.4.20) again then allows us to combine our results for both regions and obtain reflection and transmission matrices for the region $\left[h_n-, h_N+\right]$. We may then move on to the next layer in the body.

$$
\begin{array}{ll}
x_3 = h_n & \dfrac{h_n-}{h_n+} \\[3ex]
x_3 = h_{n+1} & \rule{6cm}{0.4pt} \\[1ex]
 & \vdots \\[1ex]
x_3 = h_{N-1} & \rule{6cm}{0.4pt} \\[1ex]
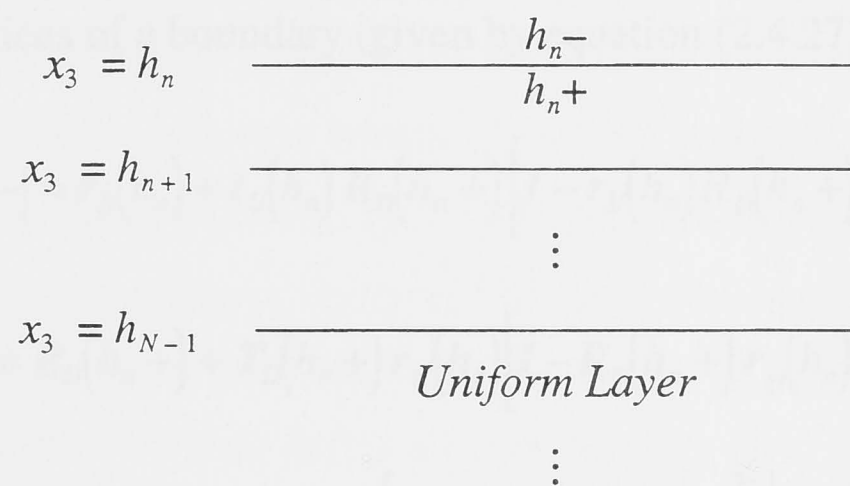 & \textit{Uniform Layer} \\[1ex]
 & \vdots
\end{array}
$$

Figure 2.4 Application of recursive procedure upwards from the bottom layer.

We may derive explicit expressions for the transmission and reflection matrices during each step in our recursive procedure. For ease of notation we make the following definitions:

$$
\begin{aligned}
R_{U,D}(x_3) &= R_{U,D}(x_3, h_N+) & T_{U,D}(x_3) &= T_{U,D}(x_3, h_N+) \\
r_{U,D}(x_3) &= R_{U,D}(x_3-, x_3+) & t_{U,D}(x_3) &= T_{U,D}(x_3-, x_3+)
\end{aligned}
\tag{2.4.28}
$$

Using these definitions, the recursion relation (2.4.20), and the form for the transmission and reflection matrices of a uniform layer (given in equation (2.4.26)) yields the identities given in equation (2.4.29) below.

$$R_D(h_n +) = T_U(h_n +, h_{n+1} -) R_D(h_{n+1} -) T_D(h_n +, h_{n+1} -)$$

$$= E(z_{n+1}) R_D(h_{n+1} -) E'(z_{n+1})$$

$$T_D(h_n +) = T_D(h_{n+1} -) T_D(h_n +, h_{n+1} -) = T_D(h_{n+1} -) E'(z_{n+1})$$

$$T_U(h_n +) = T_U(h_n +, h_{n+1} -) T_U(h_{n+1} -) = E(z_{n+1}) T_U(h_{n+1} -)$$

$$R_U(h_n +) = R_U(h_{n+1} -)$$

(2.4.29)

Now using the recursion relation, (2.4.20), to combine this result with the reflection and transmission matrices of a boundary (given by equation (2.4.27)) yields:

$$R_D(h_n -) = r_D(h_n) + t_U(h_n) R_D(h_n +) \left[I - r_U(h_n) R_D(h_n +) \right]^{-1} t_D(h_n)$$

$$R_U(h_n -) = R_U(h_n +) + T_D(h_n +) r_U(h_n) \left[I - R_D(h_n +) r_U(h_n) \right]^{-1} T_U(h_n +)$$

$$T_D(h_n -) = T_D(h_n +) \left[I - r_U(h_n) R_D(h_n +) \right]^{-1} t_D(h_n)$$

(2.4.30)

$$T_U(h_n -) = t_U(h_n) \left[I - R_D(h_n +) r_U(h_n) \right]^{-1} T_U(h_n +)$$

It is worth noting again that we are effectively considering the zero frequency case and our waves are not actually travelling through the body but are static deformations. So there is in fact no transmission or reflection due to the internal layer boundaries in the normal sense, but as discussed earlier there is behaviour analogous to transmission and reflection. The transmission and reflection matrix notation also provides a convenient formalism for analysing the zero frequency problem and the similarity in the governing equations of the static and dynamic regimes means that the same relations hold in both settings.

§2.4.4 Introducing the Source of Deformation

We wish to consider the case of a body that has been deformed from its equilibrium state by some force applied within it, in particular the case where this force takes the form of a vertical stress applied at the surface of the body. It is standard in this procedure to consider such a surface load as the limiting case of an internal source of deformation restricted to a small region that is allowed to approach the surface. We start therefore, by considering a general stress applied somewhere within the body, and developing a technique for calculating the value of the stress-displacement vector due to this stress at any other point within the body below the level of the source, and then allow first the source of deformation and then the receiver to approach the surface.

We consider then a stratified half-space as discussed in section 2.2.2 with a zero stress condition applying at the surface and some source of deformation, represented by the stress-displacement vector $\boldsymbol{\gamma}$, applied within the body. In each layer of the halfspace we define a fundamental solution matrix $\boldsymbol{B}_n$ whose columns are linearly independent solutions of the governing equation, (2.3.3), (where we have substituted A_n for A), so that for some constant coefficient vector $\boldsymbol{c}_n$, we have that $w(x_3) = \boldsymbol{B}_n(x_3)\boldsymbol{c}_n$. The existence of such a set of solutions is guaranteed by the theory of differential equations (see for example Braun 1983). We also define a corresponding field matrix V_n such that at any depth within the body $\boldsymbol{B}_n(x_3) = \boldsymbol{D}_n V_n(x_3)$ (analogous to the field vector v defined earlier).

From (2.1.3) we see that the forcing term $\boldsymbol{\gamma}$ must be introduced into the field equations. Restricting our attention to the n-th layer of a stratified halfspace equation (2.3.3) becomes:

$$\partial_{x_3} w(x_3) = A_n w(x_3) + \gamma(x_3)$$

$$(2.4.31)$$

where ∂_{x_3} represents the linear differential operator $\dfrac{\partial}{\partial x_3}$.

We once again follow the analysis of Kennett (1981) and note from the definitions of the propagator matrix, P , defined in equation (2.4.1), and the fundamental solution matrix, $\boldsymbol{B}_n$, defined above, that since the columns of $\boldsymbol{B}_n$ are solutions of (2.3.3), $\boldsymbol{B}_n(x_3) = \boldsymbol{P}(x_3, x_3^0) \boldsymbol{B}_n(x_3^0)$, so that where both x_3 and x_3^0 lie inside the n-th layer of the stratification we have:

$$\boldsymbol{P}(x_3, x_3^0) = \boldsymbol{B}_n(x_3)\left(\boldsymbol{B}_n(x_3^0)\right)^{-1}$$

$$(2.4.32)$$

which may be combined with the governing equation, (2.3.3), to show that:

$$\partial_{x_3}\left[P(x_3, x_3^0)^{-1}\right] = \partial_{x_3}\left[B_n(x_3^0)B_n(x_3)^{-1}\right] = B_n(x_3^0)\partial_{x_3}\left[B_n(x_3)^{-1}\right]$$

$$= -B_n(x_3^0)B_n(x_3)^{-1}\partial_{x_3}\left[B_n(x_3)\right]B_n(x_3)^{-1} \tag{2.4.33}$$

$$= -\left[B_n(x_3^0)B_n(x_3)^{-1}\right]A_n B_n(x_3)B_n(x_3)^{-1} = -P(x_3, x_3^0)^{-1}A_n$$

where we have used the general identity $0 = \partial_x\left(BB^{-1}\right) = B\left(\partial_x B^{-1}\right) + \left(\partial_x B\right)B^{-1}$.

Premultiplying (2.4.31) by $P(x_3, x_3^0)^{-1}$ and rearranging yields:

$$P(x_3, x_3^0)^{-1}\gamma(x_3) = P(x_3^0, x_3)\gamma(x_3) = P(x_3, x_3^0)^{-1}\left[\partial_{x_3}w(x_3)\right] - P(x_3, x_3^0)^{-1}A_n w(x_3)$$

$$\tag{2.4.34}$$

$$= \partial_{x_3}\left[P(x_3, x_3^0)^{-1}w(x_3)\right]$$

which may be integrated and then rearranged to yield:

$$w(x_3) = P(x_3, x_3^0)w(x_3^0) + \int_{x_3^0}^{x_3} P(x_3, \zeta)\gamma(\zeta)\,d\zeta \tag{2.4.35}$$

We wish to consider the case where our source of deformation is confined to the plane $x_3 = x_3^s$, so that γ has the form:

$$\gamma(x_3) = \gamma_1\,\delta(x_3 - x_3^s) + \gamma_2\,\delta'(x_3 - x_3^s) \tag{2.4.36}$$

where δ in this case is the Dirac delta function and δ' its derivative with respect to x_3. We will assume that the source lies within the $n-$th layer of the stratification $\left(\text{i.e. } h_{n-1} < x_3^s < h_n\right)$. The form of equation (2.4.36) covers a large class of sources of deformation, and in particular the case of a force applied only across the boundary $x_3 = 0$. Substituting this term back into equation (2.4.35) gives the integral the form:

$$\int_{x_3^0}^{x_3} P(x_3, \zeta)\gamma(\zeta)\,d\zeta = H(x_3 - x_3^s)\,P(x_3, x_3^s)\left[\gamma_1 + \gamma_2 A_n\right]$$

$$\tag{2.4.37}$$

$$= H(x_3 - x_3^s)\,P(x_3, x_3^s)\,\Psi$$

where H is the Heaviside step function. Equation (2.4.37) therefore defines a discontinuity in the stress-displacement vector w :

$$w\left(x_3^S +\right) - w\left(x_3^S -\right) = \Psi \tag{2.4.38}$$

From equation (2.4.36) we see that for this class of body forces the governing equation (2.4.31) has the same form as equation (2.3.3) for all $x_3 \neq x_3^S$. All of the relations we have derived so far are therefore still valid in these regions, we need simply to include the effect of the stress-displacement discontinuity Ψ at $x_3 = x_3^S$.

§2.4.5 Boundary Conditions for a Buried Source of Deformation

At the surface, we can see immediately from the definition of the propagator matrix P that the surface vector, S, due to the stress-displacement discontinuity Ψ at depth $x_3 = x_3^S$ is given by:

$$S = \begin{pmatrix} S_W \\ S_T \end{pmatrix} = P\left(0, x_3^S\right) \Psi \tag{2.4.39}$$

where S_W is the 3 x 1 vector whose entries are the various components of displacement and S_T is the 3 x 1 vector whose entries are the various components of stress. That S may be written in this form is a direct consequence of the definition of the stress-displacement vector w.

The total stress displacement vector at the surface must satisfy the zero stress boundary condition and may therefore be written:

$$w(0) = \begin{pmatrix} w_0 \\ 0 \end{pmatrix} \tag{2.4.40}$$

The stress-displacement vector at a depth just below the source of deformation may be related to the stress-displacement field in the bottom-most layer using the propagator matrix P :

$$w\left(x_3^S +\right) = P\left(x_3^S, h_{N-1}\right) w\left(h_{N-1}\right) \tag{2.4.41}$$

We may then use (2.4.38) to calculate the stress-displacement vector at a depth just above the source of deformation:

$$w\left(x_3^s -\right) = P\left(x_3^s, h_{N-1}\right) w\left(h_{N-1}\right) - \Psi \tag{2.4.42}$$

which may in turn be propagated to the surface using the propagator matrix P :

$$w(0) = P\left(0, x_3^s\right) w\left(x_3^s -\right) = P\left(0, h_{N-1}\right) w\left(h_{N-1}\right) - P\left(0, x_3^s\right) \Psi$$

$$= P\left(0, h_{N-1}\right) w\left(h_{N-1}\right) - S \tag{2.4.43}$$

We now consider the boundary condition in the bottom-most layer where we require that displacement must be a down-going quantity (i.e. that it must decrease as depth increases). From the form of the field propagator matrix for a uniform layer given in equation (2.4.6), it is clear that within any such layer the solution of the governing equation (2.3.3) may be written as a linear combination of three down-going and three up-going vector functions, we may therefore take these up-going and down-going vectors to be the basis functions for our solution space. In the bottom-most layer of the stratification we may take the fundamental solution matrix, B_n, to be the matrix whose columns are the up-going and down-going basis vectors of our solution space. Without loss of generality we may take the first three columns of B_n to be the up-going basis vectors and the last three columns to be the down-going basis vectors. Our solution vector will then be a linear combination of the last three columns of B_n and may be written:

$$w\left(h_{N-1}\right) = B_N\left(h_{N-1}\right) \begin{pmatrix} 0 \\ C_N \end{pmatrix} \tag{2.4.44}$$

Where C_n is a 3 x 1 constant vector whose entries will be determined by the boundary conditions applied at the surface of the body.

We are still free however to specify the initial values for our solution space basis vectors (i.e. we are free to choose a value for the field matrix $V_n\left(x_3^0\right)$ at some point, x_3^0, within the layer). In this case we choose $V_n\left(h_{n-1}\right) = I$, which, from the definition of V_n, yields:

$$B_N\left(h_{N-1}+\right) = D_N\left(h_{N-1}+\right) \tag{2.4.45}$$

Substituting this result into the form for the solution vector in the bottom-most layer given in equation (2.4.44), and the resulting expression into equation (2.4.43) yields a form for the stress-displacement vector at the surface:

$$w(0) = \left[P(0, h_{N-1}) D_N \right] \begin{pmatrix} 0 \\ C_N \end{pmatrix} - S = F(0, h_{N-1} +) \begin{pmatrix} 0 \\ C_N \end{pmatrix} - S \qquad (2.4.46)$$

which may be taken as a definition of the transform propagator matrix, F.

From the definition of the field propagator matrix Q (equation (2.4.3)) we have:

$$Q(0+, h_{N-1}+) = D(0+)^{-1} P(0, h_{N-1}) D(h_{N-1}+) \qquad (2.4.47)$$

which may be combined with the definition of the transform propagator matrix to give:

$$F(0, h_{N-1}+) = D(0+) Q(0+, h_{N-1}+) = D_1 Q(0+, h_{N-1}+) \qquad (2.4.48)$$

If we partition the matrix D_1 into 3 x 3 sub-matrices:

$$D_1 = \begin{pmatrix} m_U & m_D \\ n_U & n_D \end{pmatrix} \qquad (2.4.49)$$

and adopt the following notation for the reflection and transmission matrices of the half-space as a whole:

$$R_{U,D}^{ON} = R_{U,D}(0+, h_{N-1}+) \qquad T_{U,D}^{ON} = T_{U,D}(0+, h_{N-1}+) \qquad (2.4.50)$$

then upon substituting the partition equation and these last two results into equation (2.4.48) we may re-write the transform propagator in terms of the sub-partitions of D_1 and the reflection and transmission matrices of the half-space as a whole:

$$F(0, h_{N-1}+) = \begin{pmatrix} F_{11} & F_{12} \\ F_{21} & F_{22} \end{pmatrix}$$

$$= \begin{pmatrix} m_U & m_D \\ n_U & n_D \end{pmatrix} \begin{bmatrix} T_U^{ON} - R_D^{ON}(T_D^{ON})^{-1} R_U^{ON} & R_D^{ON}(T_D^{ON})^{-1} \\ -(T_D^{ON})^{-1} R_U^{ON} & (T_D^{ON})^{-1} \end{bmatrix} \qquad (2.4.51)$$

where the F_{ij} are 3 x 3 sub-matrices of F.

Now substituting this result, the definition of the surface vector, (2.4.39), and the surface boundary condition, (2.4.40), into the form given in equation (2.4.46) for the stress-displacement vector at the surface yields:

$$\begin{pmatrix} w_0 \\ 0 \end{pmatrix} = \begin{pmatrix} F_{11} & F_{12} \\ F_{21} & F_{22} \end{pmatrix} \begin{pmatrix} 0 \\ C_N \end{pmatrix} - \begin{pmatrix} S_W \\ S_T \end{pmatrix} \tag{2.4.52}$$

from which we immediately see that:

$$C_N = F_{22}^{-1} S_T \tag{2.4.53}$$

which may in turn be used to show that:

$$w_0 = \left(F_{12} F_{22}^{-1} \right) S_T - S_W \tag{2.4.54}$$

We may then use (2.4.51) to derive explicit formulae for the matrices F_{12} and F_{22}:

$$F_{12} = \left(m_D + m_U R_D^{ON} \right) \left(T_D^{ON} \right)^{-1} \qquad F_{22} = \left(n_D + n_U R_D^{ON} \right) \left(T_D^{ON} \right)^{-1} \tag{2.4.55}$$

which may be substituted into (2.4.54) to yield:

$$w_0 = \left(m_D + m_U R_D^{ON} \right) \left(n_D + n_U R_D^{ON} \right)^{-1} S_T - S_W$$

$$= \left(m_D + m_U R_D^{ON} \right) \left(I - \tilde{R} R_D^{ON} \right)^{-1} \left(n_D \right)^{-1} S_T - S_W \tag{2.4.56}$$

where $\tilde{R} = - n_D^{-1} n_U$.

We may use this expression to calculate the surface displacement in the case we are considering (where we may take $S_W = 0$ and the only non-zero entry in the vector S_T is the vertical component of stress which is given by the loading function ϕ). But we will first develop a technique for calculating the stress-displacement vector at any point within the body.

§2.4.6 Buried Sources and Receivers

At any depth x_3 within the body we may write the field vector $v(x_3)$ in terms of its up-going and down-going components:

$$v(x_3) = \begin{pmatrix} v_U(x_3) \\ v_D(x_3) \end{pmatrix} \qquad (2.4.57)$$

Now at the level of the source there is a discontinuity in the field vector v, corresponding to the discontinuity in the stress-displacement vector w. From the definition of the field vector we see that this discontinuity, Σ, is given by:

$$\left[v(x_3^S) \right]_-^+ = \Sigma(x_3^S) = \begin{pmatrix} \Sigma_U^S \\ \Sigma_D^S \end{pmatrix} = D(x_3^S)^{-1} \Psi \qquad (2.4.58)$$

then from this result and the definition of the field vector in equation (2.4.3) we see that:

$$v(x_3^S -) = v(x_3^S +) - \Sigma(x_3^S) = Q(x_3^S +, h_{N-1}) v(h_{N-1} +) - \Sigma(x_3^S) \qquad (2.4.59)$$

For notational convenience we define:

$$R_D^{SN} = R_D(x_3^S +, h_{N-1} +) \qquad\qquad R_U^{OS} = R_U(0, x_3^S -) \qquad (2.4.60)$$

with similar notation for the other transmission and reflection matrices for these regions.

We take the receiver (the point at which we wish to calculate the stress-displacement vector) to be at depth x_3^R inside the body.

Consider the case where the receiver lies below the the source of deformation (i.e. where $x_3^S < x_3^R < h_{N-1}$) then since there are no sources below the receiver the up-going component of the field vector at this point is simply the total reflected portion of the down-going component. This may be written:

$$v_U(x_3^R) = R_D(x_3^R, h_{N-1}) v_D(x_3^R) \qquad (2.4.61)$$

Similarly, if our receiver lies above the source of deformation we have that:

$$v_D(x_3^R) = R_U(0, x_3^R) v_U(x_3^R) \qquad (2.4.62)$$

From the regularity condition in the bottom-most layer we know that there is no up-going component of the field vector in this region (i.e. $v_U(h_{N-1}+) = 0$). Using the notation of (2.4.60) we may apply this last expression, equation (2.4.61), and the partition equation, (2.4.14) to equation (2.4.59) to yield:

$$
\begin{pmatrix} v_U(x_3^S -) \\ R_U^{OS} v_U(x_3^S -) \end{pmatrix} = \begin{pmatrix} T_U^{SN} - R_D^{SN}(T_D^{SN})^{-1} R_U^{SN} & R_D^{SN}(T_D^{SN})^{-1} \\ -(T_D^{SN})^{-1} R_U^{SN} & (T_D^{SN})^{-1} \end{pmatrix} \begin{pmatrix} 0 \\ v_D(h_{N-1}+) \end{pmatrix} - \begin{pmatrix} \Sigma_U^S \\ \Sigma_D^S \end{pmatrix}
\tag{2.4.63}
$$

We may eliminate $v_D(h_{N-1}+)$ from this expression to show that:

$$
v_U(x_3^S -) = R_D^{SN} \left[R_U^{OS} v_U(x_3^S -) + \Sigma_D^S \right] - \Sigma_U^S
\tag{2.4.64}
$$

So that from (2.4.62) and (2.4.64) we may derive expressions for both components of the field vector just above the source of deformation:

$$
v_U(x_3^S -) = \left[I - R_D^{SN} R_U^{OS} \right]^{-1} \left(R_D^{SN} \Sigma_D^S - \Sigma_U^S \right)
$$
$$
v_D(x_3^S -) = R_U^{OS} v_U(x_3^S -)
\tag{2.4.65}
$$

Using (2.4.58), (2.4.59), (2.4.61), (2.4.65), and the fact that for any two square matrices A and B for which the relevant inverses exist we have the relations $A(I-A)^{-1} = (I-A)^{-1} - I$ and $A(I-BA)^{-1} = (I-AB)^{-1}A$ we may similarly derive expressions for the up-going and down-going components of the field vector just below the source of deformation. Doing so yields:

$$
v_D(x_3^S +) = \left[I - R_U^{OS} R_D^{SN} \right]^{-1} \left(\Sigma_D^S - R_U^{OS} \Sigma_D^S \right)
$$
$$
v_U(x_3^S +) = R_D^{SN} v_D(x_3^S +)
\tag{2.4.66}
$$

Given that we are only interested in displacements due to surface loads we need only consider the case where the receiver lies below the source of deformation.

In this case we may use the definition of the field propagator matrix and its inverse in equations (2.4.3) and (2.4.24) to show that:

$$v\left(x_3^R\right) = Q\left(x_3^R,\ x_3^S +\right)v\left(x_3^S +\right) = Q\left(x_3^S +,\ x_3^R\right)^{-1}v\left(x_3^S +\right) \tag{2.4.67}$$

From (2.4.14) we then see that:

$$\left(Q\left(x_3^S +,\ x_3^R\right)\right)^{-1} = \begin{bmatrix} \left(T_U^{SR}\right)^{-1} & -\left(T_U^{SR}\right)^{-1}R_D^{SR} \\ R_U^{SR}\left(T_U^{SR}\right)^{-1} & T_D^{SR} - R_U^{SR}\left(T_U^{SR}\right)^{-1}R_D^{SR} \end{bmatrix} \tag{2.4.68}$$

which may be substituted back into (2.4.67) to yield:

$$v_D\left(x_3^R\right) = \left[T_D^{SR} - R_U^{SR}\left(T_U^{SR}\right)^{-1}\left(R_D^{SR} - R_D^{SN}\right)\right]v_D\left(x_3^S +\right) \tag{2.4.69}$$

$$v_U\left(x_3^R\right) = -\left(T_U^{SR}\right)^{-1}\left(R_D^{SR} - R_D^{SN}\right)v_D\left(x_3^S +\right)$$

Using the recursion relation in equation (2.4.20) we may write R_D^{SN} in terms of $T_U^{SR}, T_D^{SR}, R_D^{SR}, R_U^{SR}$ and R_D^{RN}. Substituting the resulting expression for the reflection matrix into (2.4.69) and applying the matrix identities we used to derive (2.4.66) yields:

$$v_D\left(x_3^R\right) = \left[I - R_U^{SR}R_D^{RN}\right]^{-1}T_D^{SR}v_D\left(x_3^S +\right) \tag{2.4.70}$$

We may then extend (2.4.49) to $D\left(x_3^R\right)$, and use equation (2.4.70), the definition of the field vector, v, and the relations between its up- and down-going components given in equations (2.4.61) and (2.4.66) to derive the displacement vector at x_3^R:

$$w_R = \left[m_D^R + m_U^R R_D^{RN}\right]\left[I - R_U^{SR}R_D^{RN}\right]^{-1}T_D^{SR}\left[I - R_U^{OS}R_D^{SN}\right]^{-1}\left(\Sigma_D^S - R_U^{OS}\Sigma_U^S\right) \tag{2.4.71}$$

which allows us to calculate the deformation at any point inside the body.

§2.4.7 Surface Loads and Receivers

If we consider a point x_3 that lies above the source then from the general form of the surface stress-displacement vector given in equation (2.4.46), and the surface boundary condition given in equation (2.4.52) we have that:

$$\begin{pmatrix} w_0 \\ 0 \end{pmatrix} = F(0, x_3) v(x_3) = \begin{pmatrix} F_{11}(x_3) & F_{12}(x_3) \\ F_{21}(x_3) & F_{22}(x_3) \end{pmatrix} \begin{pmatrix} v_U(x_3) \\ v_D(x_3) \end{pmatrix} \qquad (2.4.72)$$

We may now use (2.4.65) and (2.4.72) to show:

$$v_D(x_3) = R_U(0, x_3) v_U(x_3) = \left(F_{22}(x_3) \right)^{-1} F_{21}(x_3) v_U(x_3) \qquad (2.4.73)$$

Now as x_3 approaches zero and we enter the upper-most layer of the stratification, we have that $F(0, x_3) = D(x_3) = D_1$, which may be combined with the partitioning of D_1 (equation (2.4.49)), the form for the stress-displacement vector at the surface given in equation (2.4.56), and the above result, to show that:

$$R_U(0, 0+) = \left(F_{22}(0+) \right)^{-1} F_{21}(0+) = -n_D^{-1} n_U = \tilde{R} \qquad (2.4.74)$$

We may immediately apply this result to find the displacement vector just below the surface. Using (2.4.74) and noting that there are no layer boundaries and negligible attenuation of the stress-displacement vector between the source and the receiver since $x_3^R - x_3^S \approx 0$ (so that $R_U^{SR} = 0$ and $T_D^{SR} = I$) we have that $R_U^{OS} = \tilde{R}$. This in turn yields:

$$w_{0+} = \left[m_D + m_U R_D^{ON} \right] \left[I - \tilde{R} R_D^{ON} \right]^{-1} \left(\Sigma_D^0 - \tilde{R} \Sigma_U^0 \right)$$

$$= \left[m_D + m_U R_D^{ON} \right] \left[n_D + n_U R_D^{ON} \right]^{-1} \left(n_D \Sigma_D^0 + n_U \Sigma_U^0 \right) \qquad (2.4.75)$$

Noting that $\Psi(0) = \left(S_w \quad S_T \right)^T = D_1 \Sigma(0)$ we see that $S_T = \left(n_D \Sigma_D^0 + n_U \Sigma_U^0 \right)$ so that (2.4.75) may be rewritten:

$$w_{0+} = \left[m_D + m_U R_D^{ON} \right] \left[n_D + n_U R_D^{ON} \right]^{-1} S_T \qquad (2.4.76)$$

which we could have obtained from (2.4.56) by setting $S_w = 0$.

This total surface deformation is all we are in fact interested in, the case we are considering does not require us to allow non-zero values of the discontinuity in displacement, S_w, in our form for the source of deformation. We instead specify the vertical stress at the surface through the stress vector S_T and calculate the total resulting surface deformation.

Although we could have used (2.4.56) to yield the form for the surface deformation, the formalism of sections 2.4.6 and 2.4.7 is necessary if we want to calculate deformation or stress throughout the body. While we could propagate from a surface vector into the body, doing so without the proper methodology re-introduces exponentially growing terms and undermines the central strength of the procedure. Maintaining complete decoupling of exponentially increasing and decreasing terms is strictly necessary.

As in the previous two procedures we use this technique to obtain the deformation over a grid of values in the transform domain and then numerically transform to get the stress-displacement field in the spatial domain.

§2.4.8 Discussion

This procedure is significantly more theoretically complicated than either of the procedures discussed previously. Despite this it is still reasonably simple to implement numerically though it is less conveniently adapted to determining the stress-displacement vector at depth.

The principle advantage of this technique is that the reflection matrix R_D^{ON} is calculated recursively using (2.4.27), (2.4.29), and (2.4.30) which contain no exponentially growing terms (E' and E containing positive exponentials of z_n which are defined to be negative), as compared with the propagator matrix techniques developed in sections 2.2 and 2.3. This substantially reduces the variation in magnitude of the matrix entries, making the procedure correspondingly more robust numerically.

The inverse matrices we are required to calculate are all of the form $\left[A + B\right]^{-1}$ where B may be a matrix with exponentially decaying entries but A has no depth-dependence at all (A is usually either a sub-matrix of some D_n or the identity matrix as in (2.4.75) or (2.4.71)) so that the sum of the matrices approaches A as the entries of B get smaller. This has the effect of keeping variation in the magnitude of the matrix entries to an acceptable level, so that they are not particularly prone to computational inaccuracies during numerical matrix manipulation. A second consequence of this property is that the inverted matrices do not contain any exponentially increasing terms.

2.5 Numerical Stability of Propagator Matrix Techniques

§2.5.1 Surface Deformation due to a Square Load: Analytical Techniques

While any two numerical techniques may be consistent, absolute accuracy can only be determined by direct comparison with analytical results. In small-scale engineering problems it is standard (see for example Timoshenko & Goodier 1970, Love 1927) to neglect internal buoyancy and pre-stress advection. This simplification often makes analytical solutions possible and in the particular case of a unit load over a square of side a on the surface of a uniform elastic half-space, the deformation at the centre of the load is given by (Timoshenko & Goodier 1970):

$$u_3(0) = \tfrac{2}{\pi} \ln\left(1 + \sqrt{2}\right) a \frac{(\lambda + 2\mu)}{\mu(\lambda + \mu)} \approx 0.56\, a \frac{(\lambda + 2\mu)}{\mu(\lambda + \mu)} \tag{2.5.1}$$

where λ and μ are the Lamé parameters of the body. A similar form may also be obtained for the average deformation over the area of the load:

$$u_3^{av} \approx 0.475\, a \frac{(\lambda + 2\mu)}{\mu(\lambda + \mu)} \tag{2.5.2}$$

Both forms agree very well with the analysis by Love (1929) in which he derives the form for the deformation due to a rectangular surface load on a flat semi-infinite half-space. It is worth considering Love's formulation in a little detail as it illustrates some of the difficulties of the engineering approximation.

Given an arbitrary point in the body $x = \left(x_1, x_2, x_3\right)^T$ and a point on the surface of the body $x' = \left(x_1', x_2', 0\right)^T$, we define the distance function between the two:

$$r(x, x') = \left((x_1 - x_1')^2 + (x_2 - x_2')^2 + x_3^2\right)^{1/2} \tag{2.5.3}$$

We then define the logarithmic and Newtonian potentials:

$$\Gamma(x) = \iint_S \ln\left(x_3 + r(x, x')\right) dx_1'\, dx_2' \tag{2.5.4}$$

$$V(x) = \iint_S r(x, x')^{-1} dx_1'\, dx_2' \tag{2.5.5}$$

where S is the region over which the load is applied. Both integrands become singular at points inside the region S which raises the issue of analyticity. In his analysis Love constructs a region, Σ, of radius ε around each singularity and allows ε to approach zero. An explicit analytical form is found by changing to polar coordinates inside Σ and considering the limit. Failure to carefully consider the issue of analytical behaviour can lead to analytical expressions with hidden singularities (see for example Sneddon 1951).

In the absence of external forces, solutions to equation (2.1.3) can be written in terms of the the logarithmic and Newtonian potentials (Love 1929). The vertical component of surface deformation, for example, is given by

$$u_3 = \frac{1}{4\pi\mu}\left(\frac{\lambda+2\mu}{\lambda+\mu}\frac{\partial\Gamma}{\partial x_3} - x_3\frac{\partial V}{\partial x_3}\right) \tag{2.5.6}$$

Defining the quantity $A(x)$ to be 0.25, 0.5, or 1, depending on whether x lies on a corner, an edge, or wholly within S, the form for the derivatives in this expression is:

$$\frac{\partial\Gamma}{\partial x_3} = \iint_{S-\Sigma} r(x,x')^{-1}\,dx_1'\,dx_2' + A(x)\pi\varepsilon \tag{2.5.7}$$

$$\frac{\partial V}{\partial x_3} = -\iint_{S-\Sigma} x_3\,r(x,x')^{-3}\,dx_1'\,dx_2' - A(x)\pi \tag{2.5.8}$$

which guarantees that our analytical solution is well behaved throughout the body, in particular directly under the load, and makes an ideal comparison for our numerical results.

§2.5.2 Numerical Stability of the Propagator Matrix Techniques

Figure 2.6 illustrates a comparison of the numerical procedures developed in the previous sections and the analytical technique developed by Love. The results shown are for a 400 m thick ice sheet with a side of 100 km and centred on the origin. The body was taken to be uniform with a bulk modulus of 6.5×10^{10} Pa and a rigidity of 3.6×10^{10} Pa, and the calculation was performed over a grid of 1024×1024 data points, uniformly spaced at a distance of 2 km. The cross-section shown in the figure
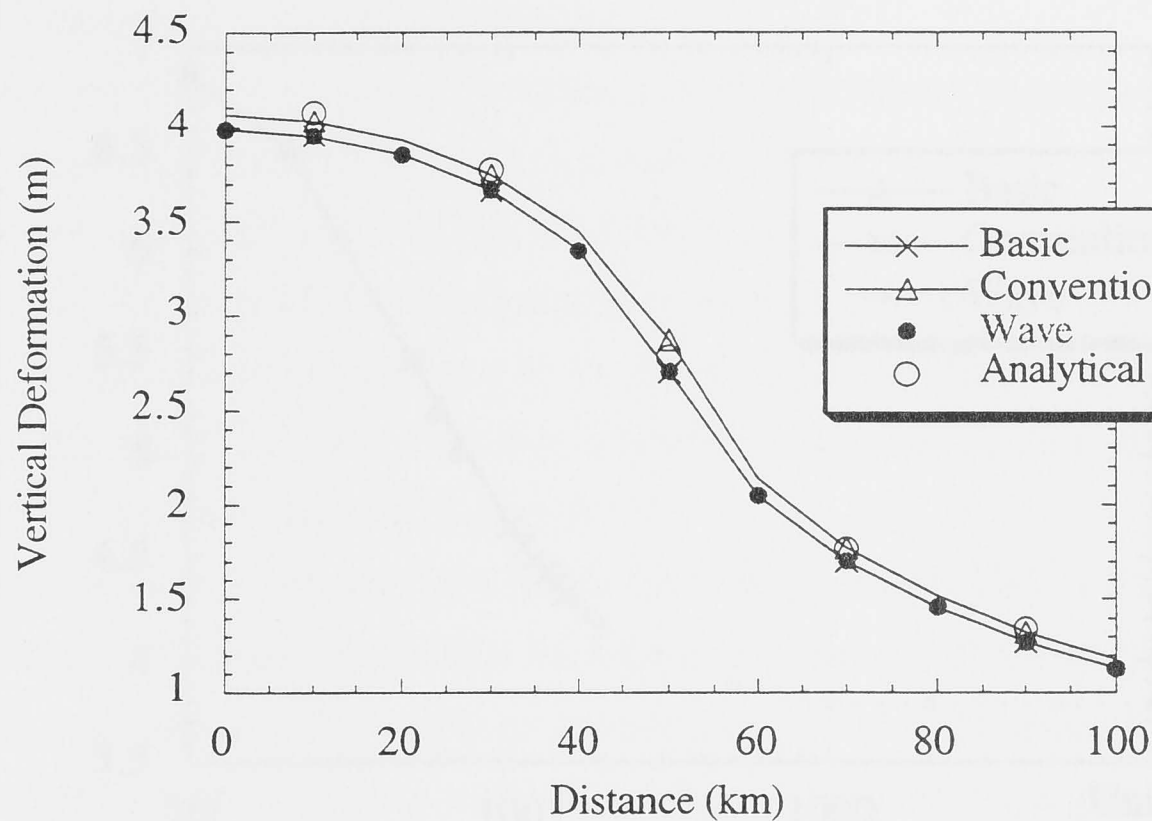
Figure 2.6: Comparison of results for the basic, conventional and wave propagator matrix techniques of McConnell (1965), Wolf (1985a) and Kennett (1981) against the analytical procedure of Love (1929)

was taken along the x_1-axis though the fit is uniformly good over the surface of the half-space, all of the techniques considered giving agreement to the analytical solution within 2.5 percent and according very well with the expressions given by Timoshenko in equations (2.5.1) and (2.5.2).

Having determined that our numerical solutions agree with the analytical solutions we can compare the numerical stability of the three techniques with depth.

One simple test is to determine the surface deformation of a two layer elastic body, and in a series of increments move the internal boundary deeper and deeper into the body. Then as the depth of the layer boundary increases, the deformation at the surface should asymptotically approach that expected for a uniform half-space with the physical properties of the upper layer.

To maximise numerical stability, a scaling factor was introduced into the conventional propagator matrix technique. The entries of the propagator matrix being uniformly scaled by a factor of $e^{-\alpha h_{N-1}}$ which was removed in the final stages of the calculation. The results of a series of tests are given in figure 2.7.

The results shown in the figure were calculated for a 400 m thick ice sheet of side 100 km for a body in which the bottom layer has half the rigidity and bulk modulus of
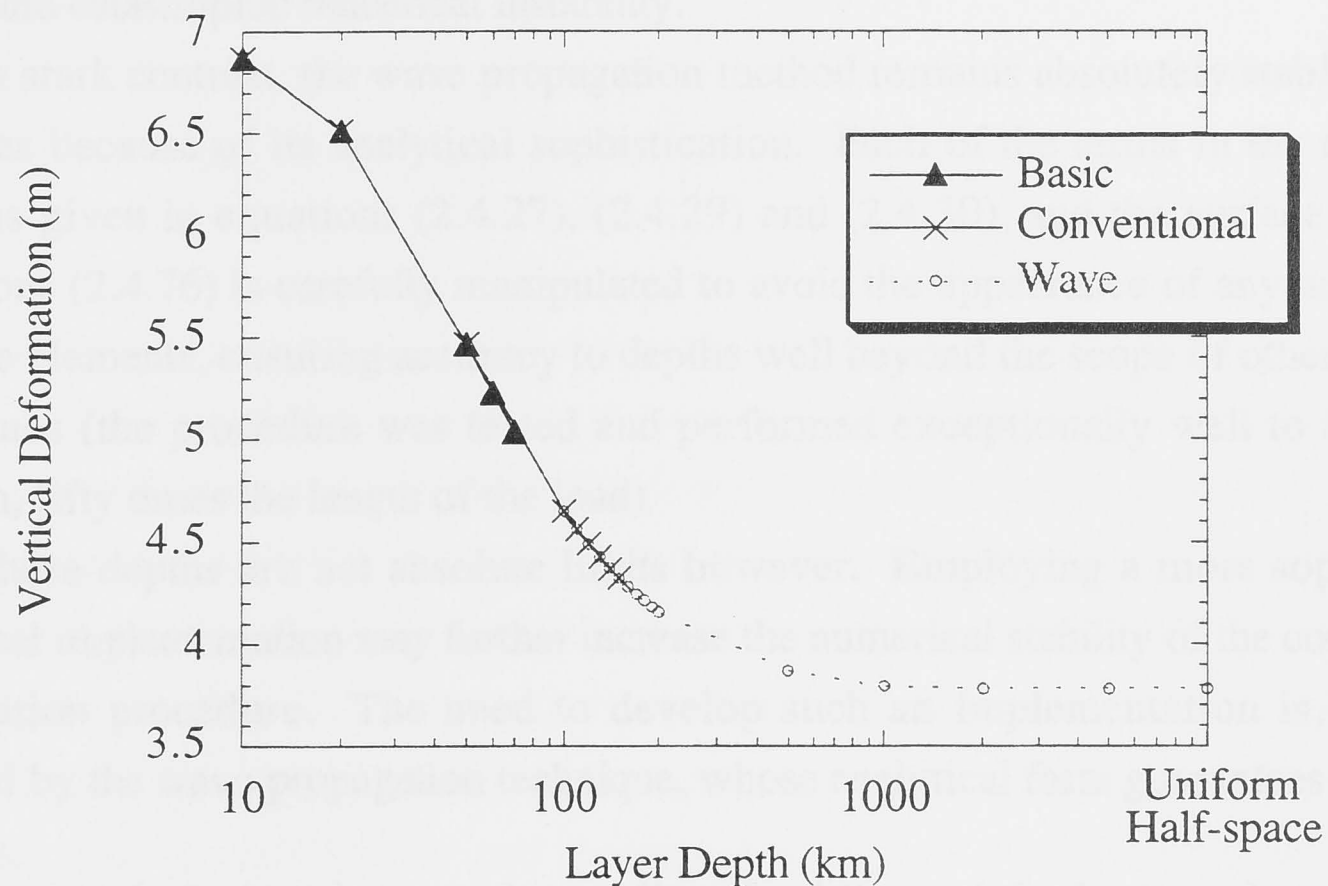
Figure 2.7: Results for surface deformation under the centre of a square load of side 100 km over a two-layered half-space. Results are plotted against the depth of the layer boundary which is moved steadily deeper into the body.

the upper-most (in the upper layer the bulk modulus and rigidity take values of 6.5×10^{10} Pa and 3.6×10^{10} Pa respectively). We see from the figure that, as predicted, as the depth of the layer boundary increases the surface deformation under the centre of the load approaches that expected for a uniform half space, calculations for a stratified half-space were only performed to a depth of 5 000 km and compared with the result for a uniform body. We can also see that the basic propagator matrix suffers catastrophic numerical errors when the layer depth is between 70 and 80 km and the conventional technique breaks down between 150 and 160 km.

Scaling the entries of the various component matrices increases the robustness of the conventional technique without at all affecting the stability of the basic propagator matrix procedure. In both techniques the source of the numerical instability is the opposing signs of the exponential terms. Taking the conventional technique as an example, as depth increases there quickly ceases to be any significant difference between the cosh and sinh terms in the propagator matrix and it becomes degenerate, scaling removes any problems with the absolute magnitude of the matrix entries themselves but cannot combat the degeneracy of the matrix at depth. This effect is magnified in the basic

propagator matrix technique where the matrix entries are often simple positive or negative exponentials, resulting in vast differences in magnitude in the entries of the propagator matrix and catastrophic numerical instability.

In stark contrast, the wave propagation method remains absolutely stable as depth increases because of its analytical sophistication. Each of the terms in the recurrence relations given in equations (2.4.27), (2.4.29) and (2.4.30), and the surface boundary conditions (2.4.76) is carefully manipulated to avoid the appearance of any numerically unstable elements, ensuring accuracy to depths well beyond the scope of other flat-earth techniques (the procedure was tested and performed exceptionally well to a depth of 5000km, fifty times the length of the load).

These depths are not absolute limits however. Employing a more sophisticated numerical implementation may further increase the numerical stability of the conventional propagation procedure. The need to develop such an implementation is, however, obviated by the wave propagation technique, whose analytical form guarantees numerical stability.

A more important issue understanding the failure of the basic and conventional propagator matrix procedures is the nature of the numerical implementation. There are several factors influencing the numerical accuracy of our calculation. One such factor is the resolution of the load, a load defined by only a few grid points can only be modelled with limited accuracy. Another, as we shall see next chapter, is the size of the grid over which the stress-displacement vector is calculated. We are forced to assume that the displacement due to the load is zero at the edge of the grid, if the grid is not large enough for this approximation to be valid, inaccuracies will result.

The effect of these two factors is significant. Given a square load of side $2a$, the symmetry of the problem allows us to restrict our attention to the first quadrant. Our results will be given over a grid of $N_x \times N_x$ points, uniformly spaced δx units apart, where we are free to choose N_x and δx. These quantities must be chosen so the resolution of the load (represented in this case by $N_a = a/\delta x$) is sufficiently high, and the distance, $N_x \delta x$, from the centre of the load to the edge of the grid is large enough that the zero condition at the edge is valid.

In the implementation itself we may consider integer wave numbers by re-scaling the units of distance so the interval $[0, N_x \delta x]$ becomes $[0, \pi]$. Working in these units and using the form given in equation (2.3.21) for the eigenvectors of the governing matrix in equation (2.3.4), we see that α takes a maximum value of $\left(2N_x^2\right)^{1/2} = \sqrt{2}\, N_x$ (in

these dimensions the component wave numbers take integer values between 0 and N_x). This gives us the following result for the maximum value of the exponential term, $e^{\alpha z}$, in the units of our numerical formulation:

$$\max\left(e^{\alpha z}\right) = \exp\left(\frac{\sqrt{2}\,\pi N_x z}{N_x \delta x}\right) = \exp\left(\frac{\sqrt{2}\,\pi z}{\delta x}\right) \tag{2.5.9}$$

The form for equation (2.5.9) shows that it is not the actual depth that limits the numerical stability of the conventional technique but rather the dimensionless depth, normalised in terms of grid-spacing. Having restricted our attention to relatively small loads we need a fine grid spacing to keep the resolution of the load high, which limits the depth to which the basic and conventional techniques remain stable.

Equation (2.5.9) demonstrates that any increase in δx will proportionately increase the depth to which the standard propagator matrix procedures are valid. The results for figure 2.7 were obtained for a grid spacing of 1 km and may therefore be viewed as illustrating behaviour with dimensionless depth.

2.6   Discussion

The basic and conventional flat earth propagator matrix techniques developed in this chapter have been shown to suffer significant numerical limitations. These limitations do not affect their suitability to the problems to which they have so far been applied. The scales in these problems have been large enough that the exponential terms in the propagator matrices do not get small enough to cause rounding errors to be significant.

The implementation of either a direct inverse procedure or forward modelling application that relies on superposition of the deformation due to small unit loads requires a numerical technique that provides stability at depths significantly larger than the width of the load. For such an application the wave propagation technique is ideal, its analytical complexity is more than justified by its stability and flexibility. The three dimensional Cartesian formulation given here allows loads of any geometry to be modelled accurately at any depth.

The major limitation of the wave propagator technique to this point is the failure to include either pre-stress advection or internal buoyancy. The deformation due to seismic sources is not large enough that either of these terms is significant but pre-stress cannot be neglected when modelling rebound problems. The formulation given here forms the basis of a flexible and powerful flat earth technique for modelling rebound problems, however, the effects of both pre-stress and internal buoyancy must be considered before it may be meaningfully applied to a physical rebound problem. The inclusion of these terms does not require significant modification of the procedure itself and will be discussed in chapter 4, while the extension to a Maxwell visco-elastic body and the details of the numerical implementation will be developed in greater detail in the next chapter.

Chapter 3

NUMERICAL IMPLEMENTATION OF INTEGRAL TRANSFORM TECHNIQUES

3.0 Introduction

Glacial rebound data preserved in the sea level record and changes in the geoid can be used to constrain both the constitutive behaviour of the earth to changes in surface loading on this time scale (c. 10 000-20 0000 years for the Holocene and latest Pleistocene ice sheets) and the melting history of the ice sheets involved. An accurately detailed spatial and temporal model of the deglaciation event in turn provides important climatological constraints for the epoch being considered and also helps us to more accurately determine the earth's response parameters.

Direct inverse procedures rely on the fact that forward modelling (direct computation of the data that needs to be fitted to the observations, in this case the deformation due to an ice sheet) is not particularly expensive numerically. This is not the case for the spherical harmonic techniques discussed in chapter 1, especially if we want to develop a high resolution model. As we discussed in chapter 2, one alternative is to restrict our attention to ice sheets whose lateral extent is such that the curvature of the earth may be neglected and it may be treated as a flat semi-infinite half-space.

The techniques developed in the previous chapter rely implicitly on the use of the Fourier transform, while their extension to the visco-elastic case via the correspondence principle is based on the the Laplace transform, as discussed in section 1.3. Despite their undeniable analytical usefulness, the use of integral transform techniques poses serious computational challenges that must be considered carefully if the accuracy of our flat earth procedures is to be maintained.

Use of the Fourier transform in the classical and wave propagator matrix procedures is complicated by degeneracy at the origin in the Fourier domain, the governing matrix of equation (2.3.3) develops a degenerate set of six identical eigenvalues, all equal to zero, rendering the analysis of sections 2.3 and 2.4 invalid. This indeterminacy results in a uniform shifting of the resulting function values, which must be compensated for. The need for high spatial resolution also places some rather rigorous demands on our numerical implementation since our grid cannot be too coarse in comparison with the lateral extent of the load. When combined these two constraints place serious limitations on any numerical implementation of flat earth techniques. We will open this chapter by considering the requirements and consequences of the Fast Fourier Transform (FFT) technique and sources of error common to its use, particularly origin shift, definition of the load and the phenomenon of function aliasing. We will discuss in detail how to

minimise these errors when applying the technique to the propagator matrix procedures of Chapter 2.

The Laplace transform is particularly unwieldy to invert numerically (see for example Krylov & Skoblya 1977, Davies & Martin 1979) and the conditions under which any given numerical inversion scheme might give inaccurate results need to be carefully considered. The second section of this chapter will be devoted to the development of several numerical techniques for the inverse Laplace transform and the results for each technique will be compared for Love number calculations for an incompressible and compressible body using the methodology of chapter 1.

The purpose of this discussion is simply understanding and minimising possible sources of numerical error and selection of a suitably convenient and accurate inversion procedure. Detailed theoretical discussion of the physical validity of these techniques and the stability of the Love number problem for a Maxwell Earth is not within the scope of the current work (see for example Fang & Hager 1994, Vermeersen, Sabadini, & Spada 1996b for a more detailed discussion)

3.1   The Fast Fourier Transform

The Fourier transform and its inverse defined in section 1.3.3 take a slightly simpler form in the case of a symmetric function such as the vertical displacement of an elastic half-space by a symmetric load. If we let $u_3^p(x)$ be the vertical displacement of an elastic half-space due to a surface load distribution $p(x)$ that is symmetric about $x = 0$ then $u_3^p(x)$ will also be symmetric about the origin and the Fourier transform takes the form:

$$\mathcal{F}\left(u_3^p(x)\right) = \hat{u}_3^p(v) = \int_{-\infty}^{\infty} u_3^p(x) e^{-ivx}\, dx = \int_{-\infty}^{\infty} u_3^p(x)\Big(\cos(vx) - i\sin(vx)\Big)\, dx$$

$$= \int_0^{\infty} u_3^p(x)\cos(vx)\, dx + \int_{-\infty}^{0} u_3^p(x)\cos(vx)\, dx$$

$$- i\left(\int_0^{\infty} u_3^p(x)\sin(vx)\, dx + \int_{-\infty}^{0} u_3^p(x)\sin(vx)\, dx\right)$$

$$= \int_0^{\infty} u_3^p(x)\cos(vx)\, dx + \int_0^{\infty} u_3^p(-x)\cos(-vx)\, dx$$

$$- i\left(\int_0^{\infty} u_3^p(x)\sin(vx)\, dx + \int_0^{\infty} u_3^p(-x)\sin(-vx)\, dx\right)$$

$$= 2\int_0^{\infty} u_3^p(x)\cos(vx)\, dx \tag{3.1.1}$$

similarly, the inverse integral takes the form:

$$\mathcal{F}^{-1}\left(\hat{u}_3^p(v)\right) = \frac{1}{\pi}\int_0^{\infty} \hat{u}_3^p(v)\cos(vx)\, dv = u_3^p(x) \tag{3.1.2}$$

The horizontal components of displacement are anti-symmetric (i.e. they satisfy the relation $u_3^p(-x) = -u_3^p(x)$ rather than $u_3^p(-x) = u_3^p(x)$), so that when substituted into the above definitions the results are Fourier sine transforms rather than cosine transforms. the analytical and numerical properties of both are very similar however and without loss of generality we will restrict our attention to the particular case of cosine transforms.

Both the transform and the inverse transform involve infinite integrals. This is something of a problem when evaluating them numerically, unless the function being transformed only has finite support (i.e. there is only a finite region in which the function is non-zero) or asymptotically approaches zero as x becomes large, and does so quickly enough to allow the integral to converge (which is true of the particular case of the deformation of an elastic halfspace under a finite surface load). In either case we can

approximate the actual transform by considering larger and larger finite regions of integration, using the identity:

$$\lim_{a \to \infty} \int_a^\infty u_3^p(x) \cos(vx) dx = 0 \qquad (3.1.3)$$

so that for sufficiently large values of a we have:

$$\int_0^a u_3^p(x) \cos(vx) dx \approx \hat{u}_3^p(v) \qquad (3.1.4)$$

The equality would be exact if $[0, a]$ included the entire support of $u_3^p(x)$.

Numerically, we are faced with the problem of approximating the Fourier transform of a function from its value at a set of discrete points. The calculation required to perform the inverse transform is almost identical and need not be considered as a separate case. The most efficient technique for calculating the necessary integral is the Fast Fourier Transform or FFT (see for example Press et. al. 1986). This technique implicitly assumes the function being transformed has finite support, normally taken to lie within $[0, \pi]$, though by scaling appropriately it may be applied over any region. In its normal numerical implementation, it also assumes that the function values are evenly spaced throughout this region and that the total number of points at which the function is being sampled is a power of 2 (for optimal computational efficiency).

This last property allows no other technique for increasing the number of sampling points than doubling them, which effects the cost of actually performing the transform (which is an $O(N \log_2 N)$ operation where N is the number of data points for which the transform is being calculated), and can be a severe limitation in cases where obtaining the function values requires a great deal of computational effort (such as for example an application of the wave propagation technique).

Still letting $u_3^p(x)$ be the deformation at the point x due to a point load at the origin, then the deformation due to a load distribution $p(x)$ has the form:

$$u_3^p(x) = \int_{-\infty}^\infty u_3^\delta(x - x_o) p(x_o) dx_o \qquad (3.1.5)$$

Applying Fourier transforms and invoking the Convolution Theorem (see for example Spiegel 1968) yields:

$$\hat{u}_3^p(v) = \hat{u}_3^\delta(v) \hat{p}(v) \qquad (3.1.6)$$

This allows us to restrict our attention to the deformation due to a point load at the origin, where we have $\hat{p}(v) = 1$. Once we have calculated the response of a given half-space to a point load in the transform domain we multiply it by the transform of the loading function and invert to get the deformation in the spatial domain.

If we perform our analysis for a function in the region $\left[0, N \delta x\right]$ for a fixed integer N , then the sample spacing, δx , between consecutive data points limits the accuracy with which we can model features in the spatial domain . If our data points are widely spaced then we will lose much of our power to resolve high frequency features. The Nyquist critical frequency $\left(v_c = \frac{1}{2} \delta x\right)$ is the largest frequency for which we can numerically calculate the Fourier transform, any power in the transform function at higher frequencies will be aliased back into the interval $\left[0, v_c\right]$.

In this particular application we start our analysis in the frequency domain, our data spacing there will be $\frac{1}{\delta x}$ and we will lose any contributions from frequencies smaller than this or larger than the Nyquist critical frequency. Our accuracy at these shorter and longer wavelengths is therefore adversely affected by aliasing. Figure 3.1 shows the effect of sample-spacing on evaluation of the sine function in the Fourier transform domain, the larger the spacing between data points compared with the frequency of sine curve, the poorer the fit of the transform function until the high frequency features of the original function are lost. Care should be taken to ensure that the sample spacing and the number of data points are chosen so that the correct range of frequencies are considered in our numerical scheme and the behaviour of the deformation function is modelled with adequate resolution.
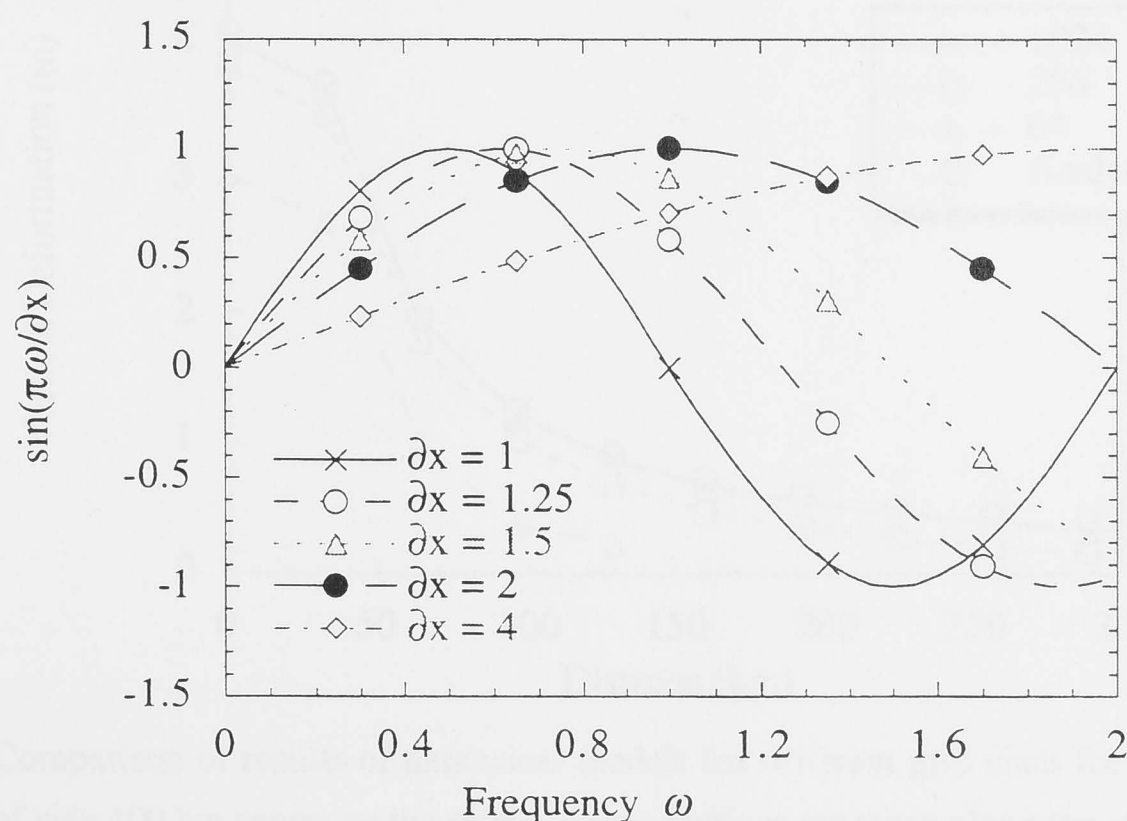

Figure 3.1: Plot of sine function in the transform domain for different sample-spacings.

A more significant risk of numerical error is posed by the analytical properties of propagator matrix procedures however. Examining the governing matrix of equation (2.3.4) we see that our flat earth techniques break down at the origin in the frequency domain ($v_1 = 0$, $v_2 = 0$), where the eigensystems become completely degenerate. The origin corresponds to a load of infinite lateral extent so that after applying the inverse transform, this indeterminacy results in a constant offset in the resulting function values from their true values as the transform routine is unable to correctly locate the origin. However, since we know that the function we are modelling, $u_3^p(x)$, approaches zero as x becomes large, we can assume that the value our inverse transform yields at the far corner of the grid from the origin in the space domain is in fact zero and translate all the other values accordingly. The accuracy of this approximation is dependent on the lateral extent of our grid and the rate at which the deformation approaches zero.

Figure 3.2 illustrates the effect of this assumption. The results were obtained for a uniform elastic body with a bulk modulus of 6.5×10^{10} Pa and a rigidity of 3.6×10^{10} Pa. Test runs were performed over a series of grids, ranging in size from 64×64 to 1024×1024 data points with constant data spacing of 2 km. The results were compared with those for the analytical technique of Love (1929) for an ice sheet 400 m thick and side 100 km centred on the origin, the cross-sections shown were taken along the x_1-axis though the resulting trends were consistent across the surface of the half-space.

The qualitative behaviour of the numerical models was good for all grid sizes though agreement with the analytical solution was unsatisfactory until the lateral extent of
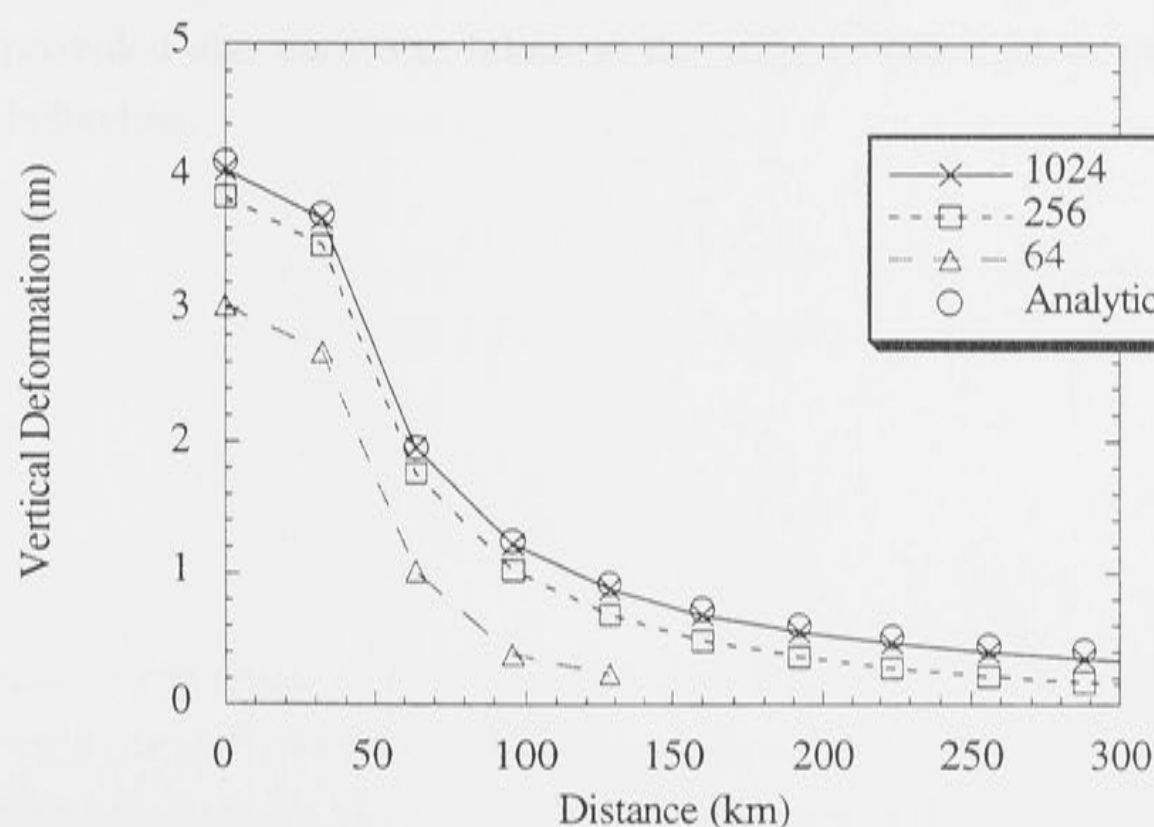

Figure 3.2: Comparison of results of numerical models for different grid sizes for deformation due to a square load of side 100 km centre on the origin. Cross-sections are taken along the x_1-axis.

the grid was approximately ten times that of the load, when the difference fell below 5 percent. The error fell to less the 2.5 percent when the grid was 20 times the size of the load (that is, for a grid of 512×512 data points since we only have to model the deformation throughout the first quadrant where the load has a side of 50 km, results for the rest of the body may be obtained by symmetry relations), and less than one percent for the maximum grid size considered. The results for small grid sizes provide accurate results for spatial gradients and trends, but the larger grids are well within the capacity of available computing technology and should be used where possible.

A second series of runs were performed in which the grid size was kept constant at 1024×1024 data points and the grid spacing was varied from 1 km up to 5 km or between two and ten percent of the width of the load. Within this range the choice of spacing was found not to have a significant effect on the accuracy of the modelling procedure with accuracy improving slightly as the grid became coarser (in other words, as the grid became larger with respect to the load being modelled). One significant feature of the Fourier transform approximation for a square load is that in order to achieve best fit, the value of the data points at the edge of the load should be halved so as to avoid oscillations.

Using Fourier transforms as part of any numerical implementation requires that care be taken when choosing both grid size and spacing so as to guarantee adequate representation of the data and to minimise errors due to data aliasing and translation of the origin. For elastic rebound problems on a flat half-space, the lateral extent of the grid over which the calculations are to be performed should be at least ten times as large as the feature being modelled, and preferably between twenty and forty times the width of the load. A grid-spacing of ten percent the width of the load was generally found to be adequate, provided due care was taken at the edge of the load to avoid introducing oscillatory behaviour.

3.2   The Laplace Transform: Numerical Evaluation of the Mellin Integral

As defined in section 1.3.3, and as with the Fourier transform above, the Laplace transform and its inverse both involve integrals over regions of infinite extent, but in any numerical formulation we will only be able to evaluate the function over a discrete set of points. The inversion of the Laplace transform therefore also involves calculating an infinite integral from function values given for a finite number of data points. The problem in this case is significantly more difficult however, as we shall discuss below.

From the form for the inverse Laplace transform (otherwise known as the Mellin integral) given in equation (1.3.7) and the Residue Theorem (see for example Kreyszig 1983) we see that the inverse transform of an almost everywhere regular function may be calculated by summing the residues of the transform function throughout the entire complex plane. Numerically locating the transform function's poles and evaluating their residues is computationally very expensive unless there is some way of limiting the search to a particular region in the complex plane. Even if the nature and distribution of the poles is somehow restricted it is still very difficult to guarantee that all the poles of the function will be found unless there is some further constraint on the number of poles the transform function will have. The chance of missing a pole can however be minimised by using a rigorous enough search over the region of interest but only at commensurate increase in the numerical cost, and for the problem of Love number calculations the complexity of the functions involved is often prohibitive.

For an impulse function in the time domain, $\delta(t)$, the visco-elastic deformation at a given point through time will, assuming regularity, consist of the elastic deformation at time zero (the elastic deformation, assumed to be instantaneous) followed by a gradual relaxation to the undeformed state. This may be expressed mathematically:

$$u_3(t) = u_3^E \, \delta(t) + \sum_{k=1}^{N} r_k e^{-s_k t} \qquad (3.2.1)$$

where the r_k are the residues and the $-s_k$ the poles of the Laplace transform of the deformation. The transform of the deformation function then takes the form:

$$\tilde{u}_3(s) - u_3^E = \sum_{k=1}^{N} r_k \left(s + s_k\right)^{-1} \qquad (3.2.2)$$

The deformation for loads with a more complex dependence on time is again a simple implementation of the Convolution Theorem. In practice the deformation is in fact broken up into components that are easier to calculate numerically (Love numbers for a spherical model or functions of wave numbers in the case of a flat earth) but each of these

components has the form of (3.2.1) so that on re-combining, the total deformation inherits the same form.

As discussed above, determining the location of all of the poles of a given complex function is a very difficult numerical exercise, especially if the number and location of the poles is not constrained in some way. This approach however forms the basis of the normal mode technique developed by Wu (1978) and Peltier (1985). We may consider as an illustrative example the expression for surface deformation given in equation 2.4.76:

$$w_{0+} = \left[m_D + m_U R_D^{ON} \right] \left[n_D + n_U R_D^{ON} \right]^{-1} S_T \tag{3.2.3}$$

Considering this quantity as a function of the transform variable s we see that the poles of $w_{0+}(s)$ will be those values of s for which the secular determinant of $n_D + n_U R_D^{ON}$ is zero. This is because the general form for the inverse of a matrix A is given by $A^{-1} = A^* (\det A)^{-1}$ where A^* denotes the adjugate matrix of the system, its elements being the corresponding cofactors of the matrix A (see for example Strang 1980). If the elements of A are all finite then the elements of the adjugate matrix must also be finite, so that the only possibility for the expression to become singular is for the determinant to approach zero. An inversion of (3.2.3) may therefore be performed by searching for a complete set of zeroes of the determinant of $n_D + n_U R_D^{ON}$, and calculating the residues of the entries of the adjugate matrix at each of the poles.

This approach is particularly numerically intensive, requiring an iterative routine to determine the location of the zeroes of the determinant, each iteration requiring recalculation of the matrix to be inverted and its determinant, and the procedure ending with a calculation of the residues of the cofactors.

Algebraic and physical considerations may be used to constrain the total number of poles the system has (see, for example, Wu & Ni 1996, Vermeersen, Sabadini, & Spada 1996a). Numerical instability may however become a serious concern if the iteration procedure is not confined to an appropriate region of the complex plane.

In the calculation of glacial rebound, a less numerically intensive inversion technique is often employed. Of these perhaps the most notable is the pure collocation technique proposed by Schapery (1962) (see also Mitrovica & Peltier 1992) where a set of exact poles is replaced by a set of hopefully similar values of the transform variable chosen *a priori*.

In the collocation approach we approximate the deformation given in equation (3.2.1) by the function:

$$u_3^*(t) = u_3^E \delta(t) + \sum_{k=1}^{N} R_k e^{-s_k^* t} \tag{3.2.4}$$

where the s_k^* are chosen *a priori* to coincide as closely as possible with the values that might reasonably be expected for the exact modes of relaxation. The coefficients R_k are then chosen to give the best fit of $\tilde{u}_3^*$ to the transform function, $\tilde{u}_3$, so that they satisfy the equation:

$$\tilde{u}_3\left(s_j^*\right) - u_3^E = \sum_{k=1}^{N} \left(s_j^* + s_k^*\right)^{-1} R_k = \sum_{k=1}^{N} \zeta_{jk} R_k \tag{3.2.5}$$

This technique is however prone to a number of numerical instabilities. If the number of collocation points, N, is too large, or the spacing between them is too small instability in the pivot points of the matrix $\left(\zeta_{jk}\right)$ may result (see for example Mitrovica & Peltier 1992). Numerical instability in the calculation of the quantity $\tilde{u}_3\left(s_j\right)$ may also occur if the sample points chosen are inappropriately small. Johnston (1993) suggests that pivot stability may be addressed by considering instead the associated problem:

$$\tilde{u}_3\left(s_j^*\right) - u_3^E = \sum_{k=1}^{N} s_k^*\left(s_j^* + s_k^*\right)^{-1} \frac{R_k}{s_k^*} = \sum_{k=1}^{N} \zeta_{jk}^* R_k^* \tag{3.2.6}$$

which significantly reduces the condition number of the matrix $\left(\zeta_{ij}\right)$. This adjustment is doubly attractive when considering Heaviside and stepwise linear loading functions where the quantity $R_k^* = {}^{R_k}\!/_{s_k^*}$ is a more useful quantity to calculate. The form for these terms illustrates an important source of numerical error for the collocation technique. Love number calculations are often inaccurate for very small values of the transform variable s (Johnston, personal communication). Even very small errors in this case are magnified by the division by s and can have a significant effect on the final form of the function as we shall see later.

The accuracy of the collocation technique depends also on how closely the parameters s_k^* approximate the body's actual modes of relaxation. The lack of a formal system for selecting these various parameters to give optimal accuracy and the technique's susceptibility to numerical instability makes it rather suspect and the development of a more robust and numerically convenient procedure for inverting from the transform domain is one of the most significant outstanding theoretical problems in the field of visco-elastic loading problems.

Wu & Peltier (1982) employ a mixed collocation technique in which the poles of the transform function are found as for the normal mode analysis scheme and the residues found by solving an equation analogous to (3.2.6) rather than determine them directly though this represents only a marginal numerical saving and is prone to the same limitations as the normal mode technique in the compressible case where the regularity of the transform function is prone to failure.

The collocation procedures are in fact a special case of a larger class of numerical techniques for inverting from the transform domain that centre on approximating the function as a sum of powers of exponentials.

A more direct implementation of this class of technique was first proposed by Erdélyi (1943), (see also Papoulis 1956, Lanczos 1957, Davies & Martin 1979), this method relies on the expansion of $u_3(t)$ in terms of Legendre polynomials of even order:

$$u_3(t) = \sum_{n=0}^{\infty} a_n P_{2n}(e^{-rt}) \qquad (3.2.7)$$

Applying the Laplace transform to (3.2.7), letting $s = (2k+1)r$, using the change of variable $x = e^{-rt}$, consulting standard tables of integrals (see for example Gradshteyn & Ryzhik 1980), and simplifying the resulting expression gives:

$$r\tilde{u}_3((2k+1)r) = r\int_0^{\infty} u_3(t)e^{-(2k+1)rt}\,dt$$

$$= \sum_{n=0}^{\infty} r a_n \int_0^{\infty} P_{2n}(e^{-rt})e^{-(2k+1)rt}\,dt$$

$$= \sum_{n=0}^{\infty} a_n \int_0^1 P_{2n}(x)x^{2k}\,dx$$

$$= \sum_{n=0}^{\infty} \frac{\sqrt{\pi}\,2^{-(2k+1)}(2k)!}{(k-n)!\,\Gamma(k+n+\tfrac{3}{2})}\,a_k$$

$$= \sum_{n=0}^{k} \frac{(k-n+1)_n}{2(k+1/2)_{n+1}}\,a_n \qquad (3.2.8)$$

where we define $(j)_n$:

$$(j)_n = \begin{cases} 1 & for\ n = 0 \\[2mm] \prod_{m=0}^{n-1}(j+m) & aliter \end{cases} \qquad (3.2.9)$$

The system of equations (3.2.9) may be solved recursively to get the coefficients of the Legendre polynomials, a_n, in (3.2.7) to whatever degree of accuracy is required.

In the techniques so far discussed we have chosen an expansion for the deformation, $u_3(t)$, and determined the values of the coefficients of expansion by collocation. It is however often more appropriate to expand for the transform function, although rather than expand in powers of s or e^{-rs}, we use instead inverse powers of

s represented by a new variable *z* based on a bilinear transform: $z = (s+a)/(s+c)$. The quantities *a* and *c* are constants chosen such that $c > a$, the transform mapping the region $\left[-(a+c)/2, \infty\right]$ onto $[-1, 1]$.

Of the various forms of this technique many require evaluation of the transform function at points away from the real axis. In the case of either Love number or propagator matrix calculations we see from (1.3.13) and (1.3.14) that complex values of *s* result in complex values for the Lamé parameters which makes computation possible but cumbersome. A bilinear procedure requiring evaluation of the transform function only along the real axis would ideally suit our needs.

Piessens (1972) proposes a class of such techniques in which he approximates the transform function with a series of Jacobi polynomials of *z*. He focuses particularly on the special case of Chebyshev polynomials and we will follow his example. In this approach we write the transform function in the form:

$$\tilde{u}_3(s) = s^{-(\alpha+1)} \sum_{n=0}^{\infty} a_n T_n\left(1 - bs^{-1}\right) \qquad (3.2.10)$$

where α is a constant chosen so that for the transform function under consideration the following relation holds for large values of *s* :

$$\tilde{u}_3(s) \sim s^{-(\alpha+1)} \qquad (3.2.11)$$

From (3.2.2) and the Convolution Theorem we see that for the particular case of the deformation of an elastic body under a Heaviside or stepwise linear load, $\alpha = 0$ and may be neglected in our treatment.

Inverting (3.2.10) term by term we write:

$$u_3(t) = \sum_{n=0}^{\infty} a_n \Psi_n\left(\frac{bt}{2}\right) \qquad (3.2.12)$$

where the functions Ψ_n can be evaluated in a number of ways. For small values of *n* the inversion can be done term by term:

$$\Psi_0(x) = 1$$

$$\Psi_1(x) = 1 - 2x \qquad (3.2.13)$$

$$\Psi_2(x) = 1 - 8x + 4x^2$$

Then these terms can be used to start one of two recursion schemes. The first uses the recursion relation for Chebyshev polynomials (see for example Spiegel 1968):

$$T_n(z) = 2z T_{n-1}(z) - T_{n-2}(z) \qquad (3.2.14)$$

Substituting for x and inverting yields:

$$\Psi_n(x) = 2\,\Psi_{n-1}(x) - \Psi_{n-2}(x) - 4\int_0^x \Psi_{n-1}(x')\,dx' \qquad (3.2.15)$$

This approach has the advantage of analytical simplicity but makes numerical evaluation rather expensive as the polynomials have to be considered as power series. An alternative formulation is to view the Ψ_n as generalised hypergeometric functions and apply Sister Celine's technique (Rainville 1960) which yields the recursion relation in the form:

$$-\Psi_n(x) = \left(A + Bx\right)\Psi_{n-1}(x) + \left(C + Dx\right)\Psi_{n-2}(x) + E\,\Psi_{n-3}(x) \qquad (3.2.16)$$

for $n \geq 2$. The coefficients in this relation are found to be:

$$A = \frac{(n-1)^2(2n-3)}{n(n-2)} - 2n \qquad\qquad E = \frac{(n-1)(3-n)}{n(n-2)}$$

$$B = 4n^{-1} \qquad\qquad C = -\left(1 + A + E\right) \qquad (3.2.17)$$

$$D = \frac{4(n-1)}{n(n-2)}$$

The coefficients from (3.2.10) are given by a least squares analysis (see for example Spiegel 1968):

$$a_n = \frac{2 - \delta_{0n}}{\pi} \int_{-1}^{1} \Phi(z)\left(1 - z^2\right)^{-\frac{1}{2}} T_n(z)\,dz$$

$$= \frac{2 - \delta_{0n}}{\pi} \int_{-1}^{1} \Phi(z)\left(1 - z^2\right)^{-\frac{1}{2}} \cos\left(n \cos^{-1} z\right)dz$$

$$= \frac{2 - \delta_{0n}}{\pi} \int_{0}^{\pi} \Phi(\cos\varphi)\cos\left(n\,\varphi\right)d\varphi \qquad (3.2.18)$$

which can be approximated numerically:

$$a_n \approx \left(2 - \delta_{0n}\right) \sum_{k=0}^{N} \Phi(\cos\varphi_k)\cos\left(n\,\varphi_k\right) \qquad (3.2.19)$$

where we define:

$$\varphi_k = \left(\frac{2k+1}{N+1}\right)\frac{\pi}{2} \qquad\qquad \Phi(z) = b(1-z)^{-1}\,\tilde{d}\!\left(b(1-z)^{-1}\right) \qquad\qquad (3.2.22)$$

It is standard to choose N in (3.2.19) to be the degree of approximation of the transform function, so that (3.2.10) and (3.2.12) become finite sums to N.

§3.2.1 Comparison of Numerical Techniques for Evaluating the Mellin Integral

Since its development by Schapery (1962) the pure collocation technique has been widely used by investigators of glacial rebound (Peltier 1974, 1976, Nakada & Lambeck 1987) and one of the more popular techniques used in this field for inverting the Laplace transform. It suffers from a number of significant limitations however which have not so far been satisfactorily resolved and have led some workers to avoid it wherever possible. In this section we will compare the performance of the pure collocation technique with the alternative procedures presented above and attempt to develop some criteria for determining the applicability of each.

Inversion of the Laplace transform is most frequently required during Love number calculations, making this problem the most suitable for comparison of the techniques so far discussed. Figure 3.3 shows the results of Love number calculations performed using normal mode analysis, collocation, bilinear transformation, and Legendre polynomial approximation. The results given are for an incompressible body with rigidity and density calculated numerically from the PREM model of Dziewonski & Anderson (1981) and averaged over each region in the body, the lithosphere, low viscosity channel, upper mantle, lower mantle, and core. The lithosphere in this model is taken to be elastic and 70 km thick, the low viscosity channel extends from the base of the lithosphere to the 400 km discontinuity and has a viscosity of 3×10^{20} Pa s, and the remainder of the upper mantle is given a viscosity of 10^{21} Pa s. From the 670 km discontinuity to the core mantle boundary, the viscosity is taken to be 10^{22} Pa s while the core itself is treated as being liquid.

The agreement between the normal mode and bilinear results is initially exact to within machine accuracy but rapidly deteriorates until the bilinear transform is no longer producing reasonable results by approximately 8×10^3 yr years. Increasing the scaling factor b in equation (3.1.16) to try and expand this region of agreement adversely affects the accuracy of the integral in equation (3.1.25). The results given in the figure are typical for values of b ranging between 0.03 and 0.1, with N between 60 and 90.
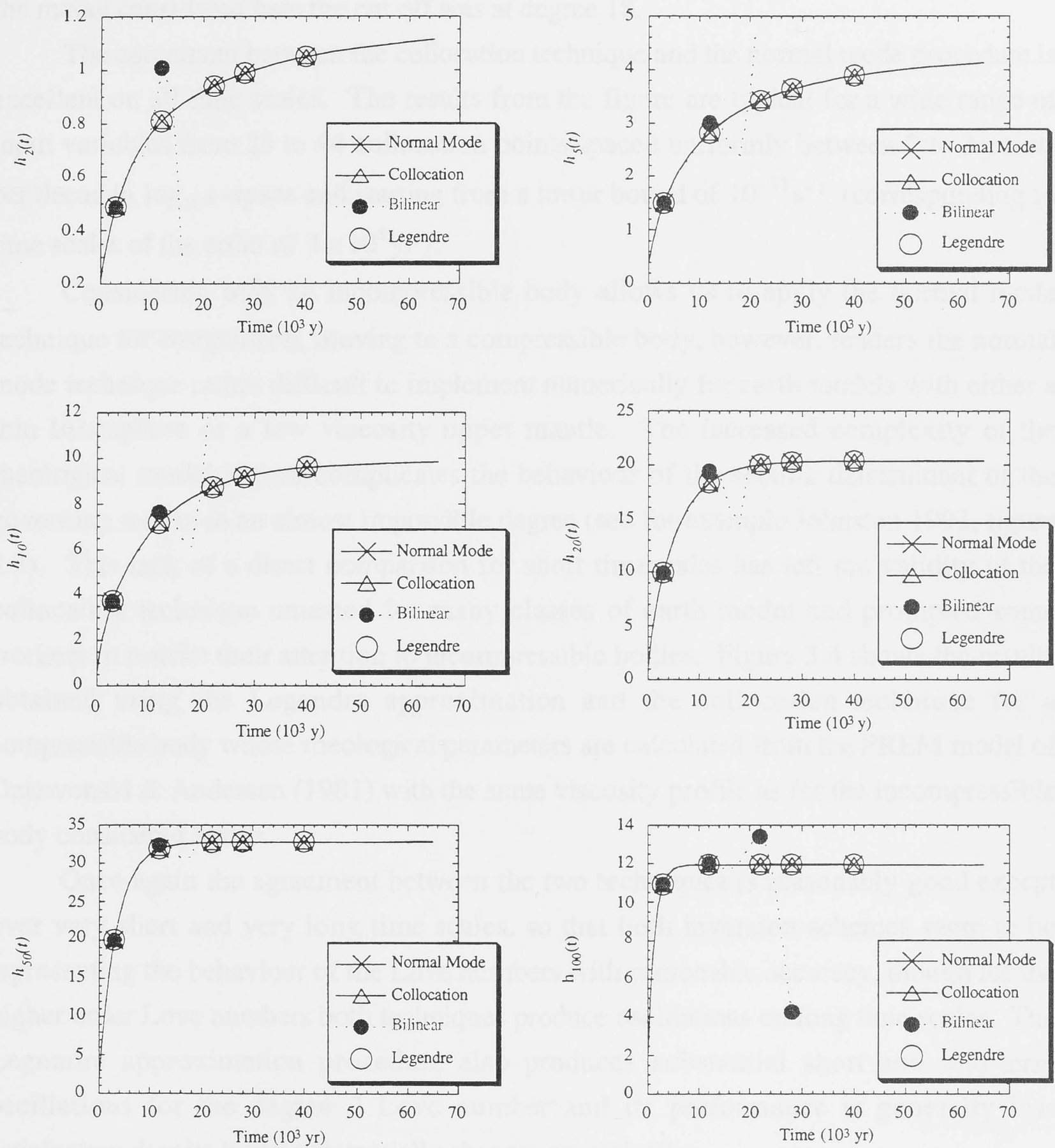
Figure 3.3

Comparison of results for numerical inversion of the Laplace transform for the Love numbers of an incompressible body using normal mode, pure collocation, bilinear, and Legendre approximations.

The agreement between the normal mode technique and the Legendre polynomial approximation is very good except for very short time-scales (less than approximately 2×10^3 yr) on which the Legendre polynomial procedure is not entirely stable. The results in the figure are typical for values of the scaling factor r in equation (3.2.7) ranging between 0.03 and 0.1, with the Legendre polynomial series truncated between degree 10 and 15. Solving the recursive linear system in equation (3.2.8) is prone to numerical error if the maximum degree in the summation is too large. The exact limit

depends on both the earth model and the degree of the Love number being calculated, for the model considered here the cut off was at degree 18.

The agreement between the collocation technique and the normal mode procedure is excellent on all time scales. The results from the figure are typical for a wide range of input variables from 25 to 44 collocation points spaced uniformly between 2 to 3 points per decad in $\log_{10} s$ -space and starting from a lower bound of $10^{-13} s^{-1}$ (corresponding to time scales of the order of 3×10^5 yr).

Considering only an incompressible body allows us to apply the normal mode technique for comparison, moving to a compressible body, however, renders the normal mode technique rather difficult to implement numerically for earth models with either a thin lithosphere or a low viscosity upper mantle. The increased complexity of the rheological model in turn complicates the behaviour of the secular determinant of the governing matrix to an almost impossible degree (see for example Johnston 1993, figure 2.3). This lack of a direct comparison for short timescales has left the validity of the collocation technique untested for many classes of earth model and prompted some workers to restrict their attention to incompressible bodies. Figure 3.4 shows the results obtained using the Legendre approximation and the collocation technique for a compressible body whose rheological parameters are calculated from the PREM model of Dziewonski & Anderson (1981) with the same viscosity profile as for the incompressible body considered above.

Once again the agreement between the two techniques is reasonably good except over very short and very long time scales, so that both inversion schemes seem to be representing the behaviour of the Love numbers with reasonable accuracy, though for the higher order Love numbers both techniques produce oscillations on long time scales. The Legendre approximation procedure also produces substantial short and mid-term oscillations for the degree 2 Love number and its performance is generally less satisfactory despite being substantially cheaper numerically.

The Legendre polynomial technique is far more prone to numerical instability in the compressible case, the maximum degree of summation falling to 10 for low degree Love numbers and 6 for the higher degree calculations. The results in the figure are for a scaling factor of 0.08 and an approximation summed to 10 terms for the degree 2 and 5 Love numbers and 5 terms otherwise. The collocation results are for 25 collocation points uniformly spaced at 3 points per decad in $\log_{10} s$ -space and starting from a lower bound of $10^{-13} s^{-1}$.

One of the most striking deficiencies of the collocation technique when applied to a compressible body is its tendency to introduce oscillatory behaviour on long time scales. That the same feature is found in the results of an independent inversion scheme raises the
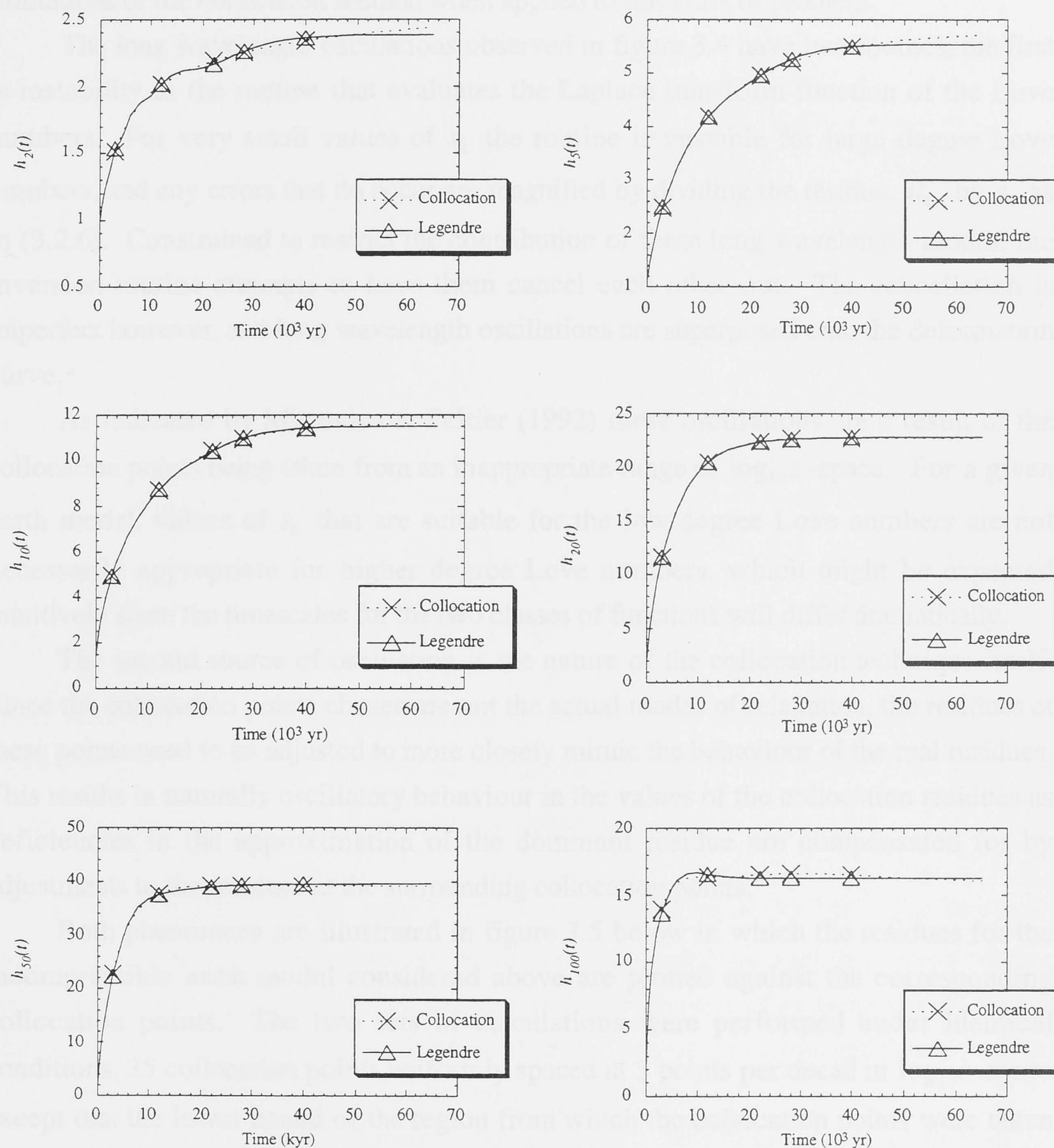
Figure 3.4

Comparison of results for collocation and Legendre approximation procedures for a compressible body.

possibility that they are independent of the inversion scheme used. The nature and effect of these oscillations has only been peripherally investigated by previous workers. Mitrovica & Peltier (1992) showed that oscillatory behaviour occurs in Love number calculations if the region from which the collocation points are chosen is insufficiently broad, they do not consider results for Love numbers of large degree however or beyond about 2×10^5 yr after the application of the load and are able to remove the effect completely with an appropriate choice of parameters.

The behaviour of Love numbers on longer time scales will have an effect on efforts to include previous loading cycles and some effort should be made to understand the limitations of the collocation method when applied to this class of problem.

The long wavelength oscillations observed in figure 3.4 have two sources, the first is instability in the routine that evaluates the Laplace transform function of the Love numbers. For very small values of s_k the routine is unstable for large degree Love numbers, and any errors that do occur are magnified by dividing the residue, R_k, by s_k as in (3.2.6). Constrained to restrict the contribution of these long wavelength modes, the inversion routine attempts to have them cancel each other out. The cancellation is imperfect however, and long wavelength oscillations are superposed onto the deformation curve.

As indicated by Mitrovica & Peltier (1992) these oscillations are a result of the collocation points being taken from an inappropriate range of $\log_{10} s$-space. For a given earth model, values of s_k that are suitable for the low degree Love numbers are not necessarily appropriate for higher degree Love numbers, which might be expected intuitively since the timescales for the two classes of functions will differ dramatically.

The second source of oscillation is the nature of the collocation technique itself. Since the collocation points chosen are not the actual modes of relaxation, the residues at these points need to be adjusted to more closely mimic the behaviour of the real residues. This results in naturally oscillatory behaviour in the values of the collocation residues as deficiencies in the approximation of the dominant residue are compensated for by adjustments to the residues at the surrounding collocation points.

Both phenomena are illustrated in figure 3.5 below in which the residues for the incompressible earth model considered above are plotted against the corresponding collocation points. The two sets of calculations were performed under identical conditions, 25 collocation points uniformly spaced at 3 points per decad in $\log_{10} s$-space except that the lower bound of the region from which the collocation points were taken was allowed to vary from -3 in the first set of calculations to -6 in the second (where our basic unit of time is thousands of years, 10^3 yr). The results show that although there is no significant change for the case of Love numbers of degree 50, there is a dramatic change in the size and position of the dominant modes for the degree 100 calculations. The massive oscillations for very small values of frequency, s, are caused by numerical instability of the Love number calculation routine in this region. The oscillations around the dominant mode are a result of the approximate nature of the inversion scheme itself.

The larger oscillations may be removed by shifting the lower bound of the region from which the collocation points, s_k, are taken. For Love numbers from degree 50 to
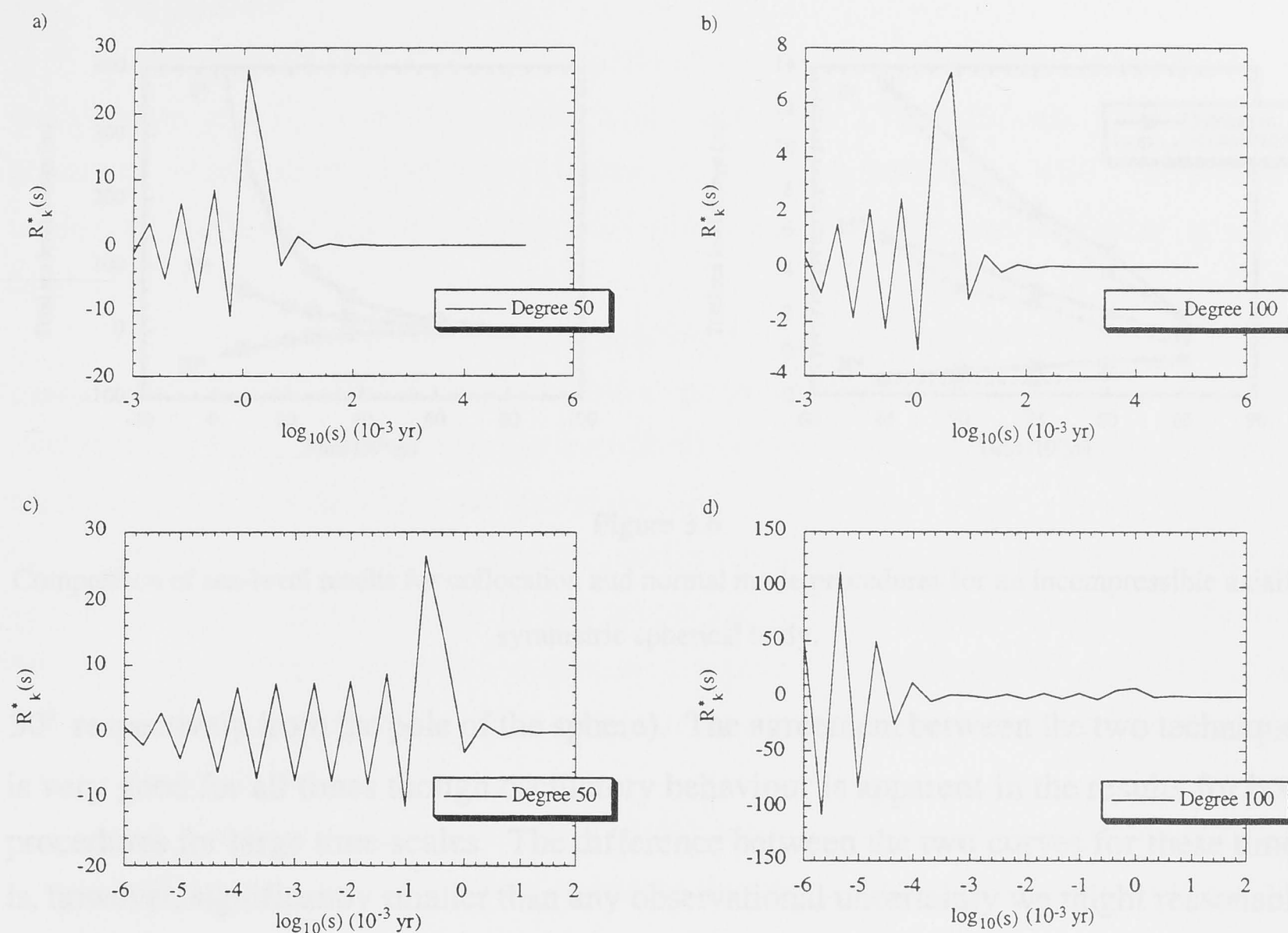
Figure 3.5: Residues of Love numbers of degree 50 and 100 for the incompressible case. Results for figures (a) and (b) were calculated by sampling over the region $[-3, 2]$ in $\log_{10} s$ -space, while the results for figures (c) and (d) were obtained by sampling over the region $[-6, 2]$ in $\log_{10} s$ -space.

128 it was found to be more appropriate to start sampling at $10^{-4} \mathrm{yr}^{-1}$ for the earth models considered. This feature of the collocation technique may become a serious source of error if results are being modelled for Love numbers of extremely high degree, and due care should be taken to ensure that the degree of approximation is not so excessive as to detrimentally affect behaviour through time.

We see from this result that some degree of oscillatory behaviour is intrinsic to the collocation technique, particularly at higher degrees, and the magnitude and nature of this effect should be examined since it will restrict the applicability of the procedure as part of a numerical modelling scheme. Figure 3.6 below shows the total sea level change through time due to an axially symmetric parabolic ice sheet of radius $10°$ with a Heaviside melting history. The load is taken to be applied to a radially symmetric earth model with the same incompressible rheology as was used for figures 3.3 and 3.5, and the resulting sea-level change was calculated using the code developed by Johnston (1993).

The figures compare the results for the collocation and normal mode procedure at the centre of the ice sheet, and two points in the near field (at angular distances $15°$ and
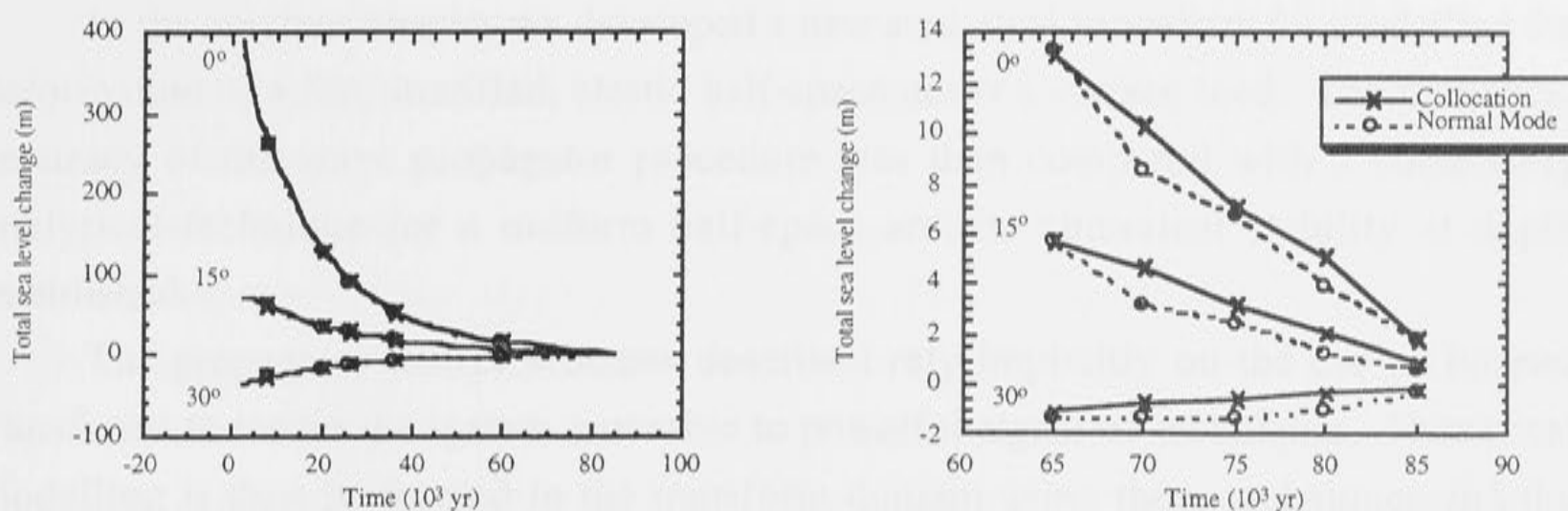
Figure 3.6

Comparison of sea-level results for collocation and normal mode procedures for an incompressible axially symmetric spherical body.

$30°$ respectively from the pole of the sphere). The agreement between the two techniques is very good for all times though oscillatory behaviour is apparent in the results for both procedures for large time-scales. The difference between the two curves for these times is, however, significantly smaller than any observational uncertainty we might reasonably expect.

This result suggests that the collocation technique is very well suited to the problem of calculating sea-level change and modelling glacial loading problems despite its simplistic formulation. Certainly it produces significantly better results for a wider range of earth models than any of the alternative inversion techniques considered here, without undue numerical complexity or cost. As Mitrovica & Peltier (1992) suggest however, care must be taken with its application and where possible comparisons made with analytical solutions such as the inviscid limit or numerical schemes of established reliability.

3.3 Discussion

In the previous chapter we developed a new analytical formalism for modelling the deformation of a flat, stratified, elastic half-space under a surface load. The numerical accuracy of the wave propagator procedure was then compared with a completely analytical technique for a uniform half-space and its numerical stability at depth established.

The propagator matrix schemes described rely implicitly on the use of Fourier transforms to render the system amenable to powerful algebraic techniques. Numerical modelling is then performed in the transform domain using these techniques and the results inverted numerically to the spatial domain.

In practice we wish to model the earth's visco-elastic rather than elastic response and the precision of any given elastic technique is meaningless if it is significantly deteriorated by the extension to a visco-elastic regime, which involves the use of Laplace transforms and a second numerical inversion from the frequency domain is require to give results through time.

Both inverse transformations carry significant risk of numerical error unless care is taken throughout the implementation to ensure that the inversion procedures used and the associated parameters are appropriate to the problem being modelled.

The FFT technique is widely used in numerical modelling applications and its behaviour is generally well understood. The most significant source of error when used with the wave propagator technique is translation of the origin and consequent constant offset of the results. This offset is a product of the degeneracy of the governing matrix of equation (2.3.4) at the origin of the Fourier transform domain and may be removed by imposing a zero boundary condition at the corners of the grid. This zero edge condition is only valid for appropriately large grids however and the spacing and extent of the grid should be chosen so that this assumption is valid.

Resolution of the surface load, as represented by the ratio between grid-spacing and the width of the load, should not be completely neglected but is a less significant issue than the extent of the grid. It is however important to appropriately scale the points at the edge and corners of the load, particularly for component loads of a superposition scheme.

Calculating the Mellin integral numerically is a more complicated issue for which a large number of computational techniques have been developed. In this chapter we considered the Legendre polynomial approximation proposed by Erdélyi (1943), the bilinear transform procedure due to Piessens (1972), the collocation technique of Schapery (1962), and the normal mode scheme employed by Peltier (1985). Despite its analytical sophistication the bilinear transform technique was found to suffer from severe numerical instability after approximately 8×10^3 yr, though its performance immediately after the application of the load was exceptionally good.

The normal mode technique performed well on all time scales for an incompressible body but relies on numerically locating the zeroes of the secular determinant of the propagator matrix for the Love number calculations. The complex behaviour of this quantity in the compressible case, particularly for earth models with either a thin lithosphere or a low upper mantle viscosity, suggests some caution when applying the normal mode procedure to this class of problem. Previously this failure of the normal mode technique made comparisons impossible, so that the accuracy of the collocation technique was untested for earth models where normal mode analysis was impractical.

The Legendre approximation technique exhibits some numerical inaccuracy over very short time scales (before about 2×10^3 yr), but generally performs extremely well when applied to an incompressible body, as does the collocation procedure. Both schemes may be extended to the compressible regime and the agreement between the two is strong enough to suggest the results for both procedures are reasonably accurate. The Legendre technique was subject to oscillatory behaviour in most cases however and exhibited significant numerical instability at some high degrees. Its overall performance in the compressible case was less than satisfactory, especially when compared with the collocation scheme.

The collocation technique was found to be stable over all time scales for both compressible and incompressible earth models, and to agree well with the results for the Legendre approximation and normal mode schemes. As with the normal mode procedure, the results of sea-level calculations on an incompressible earth for the collocation technique are subject to small amplitude oscillations over very long time-scales ($\sim 10^5$ yr). The magnitude of these oscillations was smaller for the collocation technique but in both cases was much less than observational uncertainty. Some degree of oscillatory behaviour at large time-scales is intrinsic to the collocation scheme, but its effect on the accuracy of dependent calculations will be negligible, provided care is taken to avoid inappropriately small values of the Laplace transform variable.

Using the collocation technique to extend the propagator matrix procedures of chapter 2 to the visco-elastic case offers the twin advantages of numerical convenience and stability, the risk of introducing significant numerical error being substantially reduced compared with the other inversion procedures considered here. The error introduced by the numerical inversion of the Fourier transform is also small provided the extent of the grid over which the calculations are performed is sufficiently large.

Calculations in the visco-elastic regime rely crucially on inclusion of the pre-stress term however, the next chapter completes the extension of the elastic techniques developed in chapter 2 to the visco-elastic case by incorporating the pre-stress advection and dilatation terms.

Chapter 4

THE EFFECT OF PRE-STRESS ADVECTION AND INTERNAL BUOYANCY

4.0 Introduction

Modelling the surface deformation due to a large load by superposing the contributions of a number of smaller loads involves accurately calculating deformations at depths much greater than the width of these component loads. We saw in chapter 2 that this requirement can pose significant numerical problems for propagator matrix procedures unless we are careful to analytically decouple exponentially growing and decaying terms.

The theoretical development of the propagator matrix techniques given in chapter 2 was simplified by neglect of the gravitational perturbation, pre-stress advection, and internal buoyancy terms in the equations of motion given in (1.1.6). Neglecting sphericity is inherent to flat earth procedures and Amelung & Wolf (1994) have shown that this is partially offset by neglecting the effect of gravitational perturbation. Pre-stress advection however, must be included in the visco-elastic case if the calculated deformation is to have any physical meaning. The internal buoyancy term is often neglected when modelling the flat earth (Wolf 1985a,b) despite the fact that it is no more analytically complicated to include than pre-stress advection. The validity of neglecting internal buoyancy has yet to be firmly established however and the algebraic complexity of its inclusion has so far prohibited any direct comparison of its effect in the flat earth case.

The conventional propagator matrix and wave propagation techniques rely on deriving an analytical form for the various terms in the Jordan form of the governing matrix in equation (2.3.4), the eigenvalues, diagonalising matrix and its inverse. Both techniques lose a lot of their potency and stability if we are forced to evaluate these quantities numerically rather than rely on the analytical form. Numerical calculation of these terms in each layer, at each point in the Fourier domain, for each point in the Laplace domain is prohibitively expensive computationally and a source of serious numerical error. The basic propagator matrix technique does not suffer from this limitation but, as we showed in chapter 2, is the first of the flat earth propagator matrix procedures to break down as depth increases.

In this chapter we will consider the effect of incorporating pre-stress and internal buoyancy into the wave propagator matrix procedure developed in chapter 2. Both terms remove the need to consider a Jordan form, but significantly complicate the analysis required to diagonalise the governing matrix. Their inclusion also dramatically increases the numerical complexity of the eigensystem of the governing matrix by introducing pairs

of near-degenerate eigenvectors, making a thorough analytical treatment essential to any numerical implementation.

   We will give the analytical results for each case and consider the effect of each term on numerical calculations of deformation for a visco-elastic half-space. An additional complication arises in the case where pre-stress advection and internal buoyancy are both included, the scale of the problem having a dramatic impact on the analytical properties of the technique. In this instance the grid-size and spacing for our numerical implementation must be carefully chosen to avoid imaginary eigenvalues.

   The numerical stability of the wave propagator matrix technique will then be further examined for a visco-elastic body to test its suitability for large superposition problems of the type required in inversion and forward modelling schemes in the field of glacial rebound.

   The numerical instability and analytical complexity of the eigensystems produced by including pre-stress advection and internal buoyancy have prompted some workers (Wolf 1985b, Wu 1992) to circumvent the problem entirely by considering instead an incompressible body, dramatically simplifying the behaviour of the governing matrix and completely removing the need to consider internal buoyancy. We will close the chapter by modifying the propagator matrix procedures for the compressible case to accommodate an incompressible regime for both the case where pre-stress is neglected and where it is included.

4.1 Including Pre-stress & Internal Buoyancy in a Flat-Earth Formulation

The governing equation (2.1.3) neglects pre-stress advection, internal buoyancy and the effect of perturbations of the geoid. Pre-stress advection is normally neglected in the engineering literature (see for example Timoshenko & Goodier 1970 and Sneddon 1951) and though comparison of results that disregard this term provide a useful check of the accuracy of our implementation they do not provide physically meaningful results for modelling glacial rebound. We will demonstrate the need to include pre-stress advection in section 4.1.2. Internal buoyancy has been neglected by several authors in the case of a flat earth (Wolf 1985a,b, McConnell 1965) since inclusion of the pre-stress advection term is already enough to significantly complicate the mathematical development of propagator matrix techniques. It is also standard to neglect the effect of perturbations to the earth's gravitational field though this has been demonstrated (Amelung & Wolf 1994) to partially counter the effect of neglecting sphericity.

To begin this section we will examine the effect of the inclusion of each of these terms on the governing equation of our propagator matrix techniques. In effect each term changes the form of the governing matrix A in (2.3.4) with corresponding changes to its eigenvectors and their eigenvalues.

§4.1.1 Incorporation into the Propagator Matrix Technique

From examination of (1.1.6) we see that the pre-stress advection term takes the form $-\nabla\left(\rho^{(0)}g^{(0)}\cdot u\right)$. In our flat-earth model the gravity field is taken to be uniform and acts directly into the body, while density varies only as a function of depth so that this expression becomes $-g\nabla\left(\rho^{(0)}u_3\right)$, which in vector notation can be written:

$$-g\begin{pmatrix} \rho^{(0)}\dfrac{\partial u_3}{\partial x_1} \\ \rho^{(0)}\dfrac{\partial u_3}{\partial x_2} \\ \dfrac{\partial}{\partial x_3}\left(\rho^{(0)}u_3\right) \end{pmatrix} \tag{4.1.1}$$

Wu & Peltier (1982) and Wolf (1985b) both proposed simplifying the algebra of the system for an incompressible body by considering the local increment of stress, $t_{33}^{(\Delta)}$, related to the material increment of elastic stress perturbation, $t_{33}^{(\delta)}$, by the equality:

$$t_{33}^{(\Delta)} = t_{33}^{(\delta)} + \rho^{(0)}g u_3 \tag{4.1.2}$$

In our standard formulation, density is assumed to be constant within each layer but is allowed to vary between layers so that for discontinuous density profiles the continuity

of $t_{33}^{(\Delta)}$ is not guaranteed across layer boundaries, modifying one of our fundamental boundary conditions. Modelling the local increment of stress provides a very useful comparison for testing more sophisticated implementations in the case of bodies with uniform density profiles however. The same convention could be adopted to include pre-stress in the compressible case but would not simplify the algebra of the eigensystem and would complicate the layer boundary conditions.

Examining the form for the internal buoyancy term given in equation (1.1.9) and noting that $g^{(0)} = g e_3$ (where again e_3 is the unit vector parallel to the x_3 axis) we see that this quantity may be written in the form $g \nabla \cdot \left(\rho^{(0)} u \right) e_3 = g e_3 \left(\rho^{(0)} \Delta + u_3 \partial_{x_3} \rho^{(0)} \right)$. The assumption that density is uniform inside each layer allows us to neglect the $\partial_{x_3} \rho^{(0)}$ term, which will only be non-zero at the layer boundaries where it becomes indeterminate. We accommodate similar discontinuities in other rheological parameters at these boundaries and continuity of stress and displacement across them is still a valid boundary condition.

Neglecting acceleration and the gravitational perturbation term we may cast the inertia equation (1.1.1) in the form:

$$\nabla \cdot t^{(\delta)} + \nabla \left(\rho^{(0)} g^{(0)} \cdot u \right) \delta_1 + \rho^{(\Delta)} g^{(0)} \delta_2 = 0 \qquad (4.1.3)$$

where δ_1 and δ_2 are parameters alternating between 0 and 1 that allow us to control the inclusion or exclusion of the pre-stress advection and internal buoyancy terms respectively.

Incorporating the forms derived for the internal buoyancy and pre-stress advection terms into the governing matrix for this case gives it the form:

$$A = \begin{bmatrix} 0 & 0 & v_1 & \frac{1}{\mu} & 0 & 0 \\ 0 & 0 & v_2 & 0 & \frac{1}{\mu} & 0 \\ -k_1\lambda v_1 & -k_1\lambda v_2 & 0 & 0 & 0 & k_1 \\ \mu\left(4k_1(\lambda+\mu)v_1^2+v_2^2\right) & k_1\mu(3\lambda+2\mu)v_1v_2 & \rho g v_1 \delta_1 & 0 & 0 & k_1\lambda v_1 \\ k_1\mu(3\lambda+2\mu)v_1v_2 & \mu\left(v_1^2+4k_1(\lambda+\mu)v_2^2\right) & \rho g v_2 \delta_1 & 0 & 0 & k_1\lambda v_2 \\ \rho g v_1\left(\delta_2-k_2\lambda\right) & \rho g v_2\left(\delta_2-k_2\lambda\right) & 0 & -v_1 & -v_2 & \rho g k_2 \end{bmatrix} \qquad (4.1.4)$$

where k_1 is as defined for equation (2.3.4), $k_2 = k_1\left(\delta_2 - \delta_1\right)$.

If either δ_1 or δ_2 are non-zero then the governing matrix A will have a complete set of left and right eigenvectors and the need to perform a Jordan form analysis is

obviated. The form for the columns of the diagonalising matrix and the rows of its inverse are very nearly identical through all possible non-zero cases. The eigenvectors may be written:

$$
\boldsymbol{d}_{1,4} = \beta_1 \begin{pmatrix} v_2 \\ -v_1 \\ 0 \\ \mu v_2 \alpha_{1,4} \\ -\mu v_1 \alpha_{1,4} \\ 0 \end{pmatrix}
\qquad
\boldsymbol{d}_i = \beta_{3i} \begin{pmatrix} v_1 \\ v_2 \\ d_{3i} \\ \mu v_1 (\alpha_i - d_{3i}) \\ \mu v_2 (\alpha_i - d_{3i}) \\ k_{3i} d_{3i} + \lambda \alpha^2 \end{pmatrix}
\qquad (4.1.5)
$$

where α is as defined for equation (2.2.8), $k_{3i} = \alpha_i k_1^{-1}$ and $i = 2, 3, 5, 6$. The form of the quantity d_{3i} is dependent on the values of δ_1 and δ_2 and will be given below for each case.

The left eigenvectors, $\boldsymbol{y}_i$, provide the rows for the inverse of the diagonalising matrix $\boldsymbol{D}$ and may be written:

$$
\boldsymbol{y}_{1,4} = \widehat{\beta}_{1,4} \begin{pmatrix} \mu v_2 \alpha_{1,4} \\ -\mu v_1 \alpha_{1,4} \\ 0 \\ v_2 \\ v_1 \\ 0 \end{pmatrix}
\qquad
\boldsymbol{y}_i = \widehat{\beta}_{3i} \begin{pmatrix} \mu v_1 (\alpha_i + y_{i6}) \\ \mu v_2 (\alpha_i + y_{i6}) \\ (k_{3i} + k_4) y_{i6} - \lambda \alpha^2 \\ v_1 \\ v_2 \\ y_{i6} \end{pmatrix}
\qquad (4.1.6)
$$

where $k_4 = (\delta_1 - \delta_2) \rho g$ and, as for equation (4.1.5), the quantity y_{i6} is dependent on the values of δ_1 and δ_2 and will be given below for each case.

As in chapter 2 we choose the scaling factors β and $\widehat{\beta}$ to ensure orthonormality, β_1 and $\widehat{\beta}_{1,4}$ remain unchanged from equation (2.3.26) while β_{3i} and $\widehat{\beta}_{3i}$ are again dependent on the values of δ_1 and δ_2.

We first consider the case $\delta_1 = 1$ and $\delta_2 = 0$, so that the effect of pre-stress advection is included but not internal buoyancy. Under these conditions the characteristic equation of the governing matrix is:

$$
\det\left(\boldsymbol{A}^* - \alpha_i \boldsymbol{I}\right) = \left(\alpha_i^2 - \alpha^2\right)^2 \left(\alpha_i^2 + \rho g k_1 \alpha_i - \alpha^2\right) = 0
\qquad (4.1.7)
$$

Equation (4.1.7) has two double roots and two single roots:

$$\alpha_{1,2} = \alpha \qquad \alpha_{4,5} = -\alpha \qquad \alpha_{3,6} = -k_3 \pm \sqrt{\alpha^2 + k_5^2} \qquad (4.1.8)$$

where $k_5 = \dfrac{\rho g k_1}{2}$. These results correspond to those of Wolf (1985a) for the two dimensional case though he simplifies the form of $\alpha_{3,6}$ for mathematical convenience.

The form of the quantities d_{3i}, y_{i6}, β_{3i} and $\hat{\beta}_{3i}$ in this instance is given below:

$$d_{3\,2,5} = \frac{-(\lambda + \mu)\alpha^2}{\rho g \pm (\lambda + \mu)\alpha} \qquad y_{2,5\,6} = \pm \alpha \qquad \hat{\beta}_{3\,2,5}\beta_{3\,2,5} = \frac{\rho g + (\lambda + \mu)\alpha_{2,5}}{\rho g \, 2\mu\alpha^2 \, \alpha_{2,5}} \quad (4.1.9)$$

$$d_{3\,3,6} = -\alpha_{3,6} \qquad y_{3,6\,6} = \frac{\rho g}{(\lambda + \mu)} + \alpha_{3,6} \qquad \hat{\beta}_{3\,3,6}\beta_{3\,3,6} = \frac{\lambda + \mu}{\rho g \mu \left(\alpha_{3,6}^2 + \alpha^2\right)} \quad (4.1.10)$$

where we take $\hat{\beta}_{3\,2,5} = \beta_{3\,2,5}$ and $\hat{\beta}_{3\,3,6} = -\beta_{3\,3,6}$ to ensure the correct signs.

One notable feature of the inner products of corresponding pairs of left and right eigenvectors is that they are very small in comparison with the vector entries, $\rho g / (\lambda + \mu)$ being very small in comparison to the wave numbers, as discussed by Cathles (1975). To guarantee orthonormality the scaling terms β_{3i} and $\hat{\beta}_{3i}$ must be correspondingly large, as can be seen from their form given above. This reflects the fact that d_2 and d_3 are very nearly identical but are orthonormal to a corresponding pair of nearly identical left eigenvectors y_2 and y_3, the same holding for other vector pairs in the system. This property of near-degeneracy is common to all cases where either δ_1 or δ_2 are non-zero and makes the linear algebra associated with these cases very sensitive to numerical error so that analytical forms should be used wherever possible. Using the Jordan form procedure given in chapter 2 increases the numerical robustness of the technique (at the cost of the physical meaningfulness of our results).

Substituting the expressions given in equations (4.1.9) and (4.1.10) above back into equations (4.1.5) and (4.1.6) allows the diagonalising matrix and its inverse for the governing matrix A to be calculated analytically, and employed in the wave propagation technique developed in chapter 2 to model the case of a compressible body subject to pre-stress but not internal buoyancy.

Turning our attention to the case where $\delta_1 = 0$ and $\delta_2 = 1$, so that the effect of pre-stress advection is neglected but internal buoyancy is included, the characteristic equation for the governing matrix A becomes:

$$\det\left(A^* - \alpha_i I\right) = \left(\alpha_i^2 - \alpha^2\right)^2 \left(\alpha_i^2 - \rho g k_1 \alpha_i - \alpha^2\right) = 0 \qquad (4.1.11)$$

and again has two double roots, $\pm\alpha$, and two single roots:

$$\alpha_{3,6} = k_5 \pm \sqrt{\alpha^2 - k_5^2} \qquad (4.1.12)$$

where k_5 is as defined for equation (4.1.8).

In this case the quantities d_{3i}, y_{i6}, β_{3i} and $\hat{\beta}_{3i}$ take the form:

$$d_{3\,2,5} = -\alpha_{2,5} \qquad y_{2,5\,6} = \frac{(\lambda+\mu)\alpha^2}{\pm(\lambda+\mu)\alpha - \rho g} \qquad \beta_{3\,2,5}\beta_{3\,2,5} = \frac{\rho g - (\lambda+\mu)\alpha_{2,5}}{\rho g\, 2\mu\alpha^2\,\alpha_{2,5}} \qquad (4.1.13)$$

$$d_{3,5\,6} = \frac{\rho g}{(\lambda+\mu)} - \alpha_{3,6} \qquad y_{3,6\,6} = \alpha_{3,6} \qquad \hat{\beta}_{3\,3,6}\,\beta_{3\,3,6} = \frac{\lambda+\mu}{\rho g\mu\left(\alpha_{3,6}^2 + \alpha^2\right)} \qquad (4.1.14)$$

where we take $\hat{\beta}_{3\,2,5} = -\beta_{3\,2,5}$ and $\hat{\beta}_{3\,3,6} = \beta_{3\,3,6}$.

Once again we have obtained completely analytical forms for the eigenvalues of the governing matrix A and its diagonalising system in this instance, allowing the wave propagation technique to be applied to the case of a flat semi-infinite half-space in which internal buoyancy is to be included but pre-stress is not.

Including both internal buoyancy and pre-stress (i.e. setting $\delta_1 = \delta_2 = 1$), the form of the characteristic equation then becomes:

$$\det\left(A - \alpha_i I\right) = \left(\alpha_i^2 - \alpha^2\right)\left(\left(\alpha_i^2 - \alpha^2\right)^2 - \left(\rho g\right)^2 \frac{k_1}{\mu}\alpha^2\right) = 0 \qquad (4.1.15)$$

and A thus has six distinct eigenvalues:

$$\alpha_{1,4} = \pm\alpha \qquad \alpha_{2,3,5,6} = \pm\left(\alpha^2 \pm \rho g\,\alpha\sqrt{k_1/\mu}\right)^{1/2} \qquad (4.1.16)$$

where, for convenience $\alpha_{1,2,3}$, are taken to be positive and $\alpha_{4,5,6}$ take the corresponding negative values. It should be noted that the form of these eigenvalues is such that they become a degenerate system if pre-stress and internal buoyancy are both neglected or the body is incompressible. In this instance d_{3i}, y_{i6}, β_{3i} and $\hat{\beta}_{3i}$ may be written:

$$d_{3i} = \frac{\left(\rho g - (\lambda+\mu)\alpha_i\right)\alpha^2}{(\lambda+2\mu)\alpha_i^2 - \mu\alpha^2} \qquad y_{i6} = \frac{\left(\rho g + (\lambda+\mu)\alpha_i\right)\alpha^2}{(\lambda+2\mu)\alpha_i^2 - \mu\alpha^2}$$

$$(4.1.17)$$

$$\bar{\beta}_{3\,i}\beta_{3\,i} = \frac{(\lambda + 2\mu)\alpha_i^2 - \mu\alpha^2}{4\mu(\lambda + 2\mu)\alpha^2\,\alpha_i(\alpha_i^2 - \alpha^2)}$$

where we take $\bar{\beta}_{3\,2,5} = \beta_{3\,2,5}$ and $\bar{\beta}_{3\,3,6} = -\beta_{3\,3,6}$, corresponding to $\alpha_{2,5}^2 - \alpha^2 > 0$ and $\alpha_{3,6}^2 - \alpha^2 < 0$.

The case where both internal buoyancy and pre-stress is included may therefore also be considered analytically using the wave propagation procedure in chapter 2. The equations for the forms of the vectors and their components given in equations (4.1.5), (4.1.6), (4.1.16) and (4.1.17) above allow the diagonalising system and eigenvalues of the governing matrix to be expressed in forms that are extremely convenient for numerical implementation though they are not without limitations as we shall see in section 4.1.3.

These analytical forms were obtained after significant algebraic effort, the instability of the eigensystem frustrated attempts at numerically calculating any of the terms required, including the normalisation factors, for realistic earth parameters. The algebraic complexity of the system can be reduced by considering instead the two-dimensional case. Moving from a two-dimensional to a three-dimensional formulation has the effect that two new eigenvalues, $\pm\alpha$, are added to the system for the two-dimensional case, with corresponding linearly independent left and right eigenvectors, $d_{1,4}$ and $y_{1,4}$. This result was not expected *a priori* however and the algebraic treatment for the three dimensional case was repeated in each instance.

§4.1.2 The importance of Pre-Stress Advection in the Elastic Case

As discussed in chapter 2 it is standard for both internal buoyancy and pre-stress advection to be neglected in most engineering applications (see for example Sneddon 1951, Timoshenko & Woinowsky-Krieger 1959, and Timoshenko and Goodier 1970), this is understandable to some extent given the comparative size of these terms. If we only wish to calculate an approximate value for surface deformation it may seem reasonable to neglect these effects entirely since they are orders of magnitude smaller than the other terms in the governing equation, and their inclusion may therefore give rise to numerical instability as the ratio between pivots becomes unacceptably large.

As an example of such an approximation let us consider the surface loading of a uniform semi-infinite half-space by a unit load applied over an infinitely long strip. This problem is analogous to that of a uniform half-space under a cylindrical surface load except that instead of Hankel transforms (integral transforms using Bessel functions of the first kind) we use Fourier transforms. Applying the algebraic solution of Sneddon (1951) for the case where pre-stress is neglected we obtain an analytical solution for the vertical displacement in the form:

$$\frac{\lambda + 2\mu}{2(\lambda + \mu)} u_3(x_1, x_3) = \frac{1}{2\pi\mu} \int_0^\infty \cos(v_1 x_1) \sin(v_1 a) e^{-v_1 x_3} v_1^{-2} [\chi + v_1 x_3] dv_1 \qquad (4.1.18)$$

where $\chi = [2k_1(\lambda + \mu)]^{-1}$ with k_1 as defined for (2.3.4), and a is the half-width of the load which is assumed to be uniform and symmetric about the x_2-axis, along which it is taken to be of infinite extent.

Performing the same calculation numerically gives rather unexpected results. Figure 4.1 below shows the results taken along the x_1-axis for vertical displacement under a 100km wide strip over a uniform body of rigidity 3.6×10^{10} Pa and bulk modulus 6.5×10^{10} Pa, for a grid-spacing of 2 km. The load was taken to be a 400 m thick sheet of ice and for a grid size of 128×128 data points, deformation at its centre was found to be roughly 5.0 m. Doubling the size of the grid significantly increased the deformation at the centre of the load to 6.6 m. An increase of this magnitude seems to indicate that the grid used for the calculation is not yet large enough for the zero edge condition discussed in section 3.1 to be valid. Redoubling the grid size to 512×512 data points resulted in a further increase to the deformation at the centre of the load, which had reached 8.2 m, and by this stage the edge of the grid is some 20 times the width of the load. At that distance the deformation due to the load will certainly be at least diminished and this nearly constant contribution prompts us to reconsider the problem.
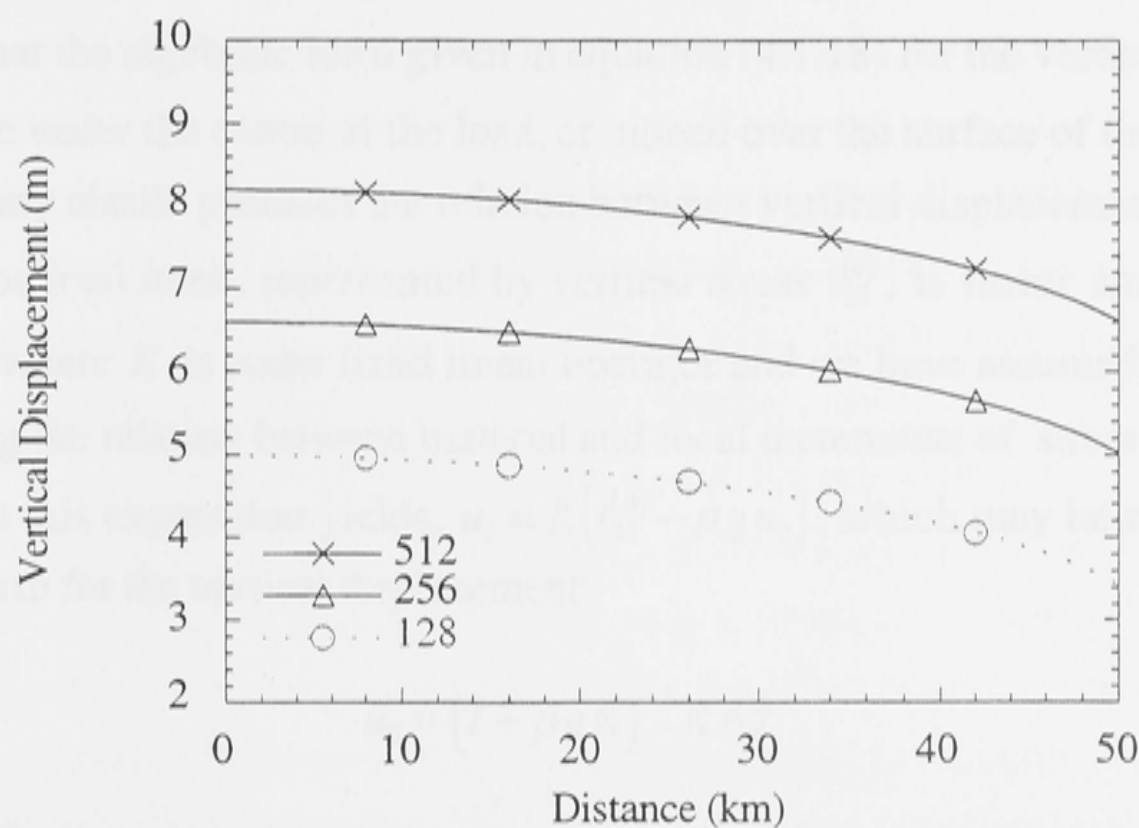

Figure 4.1: Deformation of a flat, uniform elastic half-space under an infinite, uniform strip load along the x_2-axis for different grid-sizes. Calculations were performed for grids of 128×128, 256×256, and 512×512 points with the deformation taken to be zero at the corner of the grid farthest from the origin..

Substituting $x_1 = x_3 = 0$ into equation (4.1.18) yields the analytical form for the deformation at the centre of the load:

$$u_3(0,0) = \frac{\chi}{2\pi\mu} \int_0^\infty \sin(v_1 a) \, v_1^{2} \, dv_1 \tag{4.1.19}$$

which may be expended as a Taylor series to yield:

$$u_3(0,0) = \frac{\chi}{2\pi\mu} \left(\int_0^\infty \frac{a}{v_1} dv_1 + \sum_{n=1}^\infty \frac{(-a)^{n+2}}{(2n+1)!} \int_0^\infty v_1^{2n-1} \, dv_1 \right) \tag{4.1.20}$$

This expression will be dominated by the first of the integrals which yields $\left[a \log(v_1) \right]_0^\infty$ consistent with a linear increase in deformation in response to a geometric increase in the size of grid and indicating that equation (4.1.19) is an algebraic solution but singular at the surface of the body.

Consulting a table of standard integrals (see for example Gradshteyn & Ryzhik 1980) we see that one of the general forms for the integral in equation (4.1.19) is:

$$\int_0^\infty x^{\eta-1} \sin(ax) \cos(bx) \, dx = \frac{1}{2} \sin\left(\frac{\eta}{2}\right) \Gamma(\eta) \left[(a+b)^{-\eta} + |a-b|^{-\eta} \operatorname{sign}(a-b) \right] \tag{4.1.21}$$

This expression becomes singular for $\eta = -1$ however, and is unaffected by setting $b = 0$ so that the algebraic form given in equation (4.1.18) for the vertical displacement is not analytic under the centre of the load, or indeed over the surface of the half-space.

For any elastic problem the relation between vertical displacement due to a surface load and the load itself, represented by vertical stress $t_{33}^{(\delta)}$, is linear and takes the form, $u_3 = K \, t_{33}^{(\delta)}$ where K is some fixed linear operator and we have assumed zero shear-stress. Substituting the relation between material and local increments of stress given in equation (4.1.2) into this expression yields, $u_3 = K \left(t_{33}^{(\Delta)} - \rho g u_3 \right)$, which may be rearranged to give the final form for the vertical displacement:

$$u_3 = \left(I + \rho g K \right)^{-1} K \, t_{33}^{(\Delta)} \tag{4.1.22}$$

If we view K as a scalar multiple then in the limit where K is large we see that pre-stress acts so that the vertical displacement is finite. Conversely, in the limit where K is small in comparison with unity, pre-stress has little or no effect on the vertical displacement.

Singularities are not entirely uncommon in analytical solutions derived in engineering formulations, Timoshenko & Goodier (1970) for example derive an expression for the vertical deformation of a uniform, semi-infinite elastic half-space under a unit point load:

$$u_3(x) = \frac{1}{4\pi(\lambda + \mu)}\left(x_1^2 + x_2^2 + x_3^2\right)^{-1/2}$$

(4.1.23)

and in order to avoid a singularity are forced to invoke a vanishingly small region around the point at which the load is applied in which the bulk modulus is infinite but which deforms plastically with the surrounding material (pp. 404). They are also forced to appeal to the same behaviour to avoid singularities in their treatment of a semi-infinite plate (pp 99, 103). This sort of approach is typical in the mathematical formalism of Boussinesq problems in general where the analytical solution is not taken to be valid until some small distance from the point at which the load is applied (see for example Saada 1974) though Love (1929) is able to remove the singularities in his formalism by isolating the singularities due to the logarithmic potential and noting that the contribution due to the Newtonian potential is zero over the surface of the body.

The singularity in the form of (4.1.8) is not so easy to account for however. In this instance, the infinite extent of the load along the x_2-axis produces an effectively zero wave number which in turn results in an instability in the Fourier expansion of the solution (Jeffreys 1976). This singularity is not a result of a faulty mathematical formulation but is still clearly not physically plausible since we do not observe large deformations under long railway tracks or roads. In this case the singular behaviour of the solution is a result of neglecting pre-stress. The linear operator relating vertical stress and displacement in equation (4.1.22) is particularly useful in guaranteeing analyticity, and though the effect of pre-stress advection is not significant in the elastic case for small loads it becomes significant if the wavelength in either direction becomes large.

As has long been maintained by many workers (Peltier 1974, Wu & Peltier 1982, Nakiboglu & Lambeck 1982, Wolf 1985c,d, 1994) inclusion of pre-stress is critical in visco-elastic rebound problems. The analytical similarity of the results obtained for the internal buoyancy term in section 4.1.1 might seem to indicate that it is of equal significance and in this section we will examine the effect of each term in turn.

If we consider the formalism for propagator matrix procedures developed in chapter 2, neglecting pre-stress advection and internal buoyancy completely removes the density of the body from the mathematical formulation. The mathematical analysis therefore has no way of representing buoyancy forces within the body in the visco-elastic case.

The results of attempts to extend the elastic formalism of chapter 2 directly to a visco-elastic regime are given in figure 4.2. The earth model for these calculations
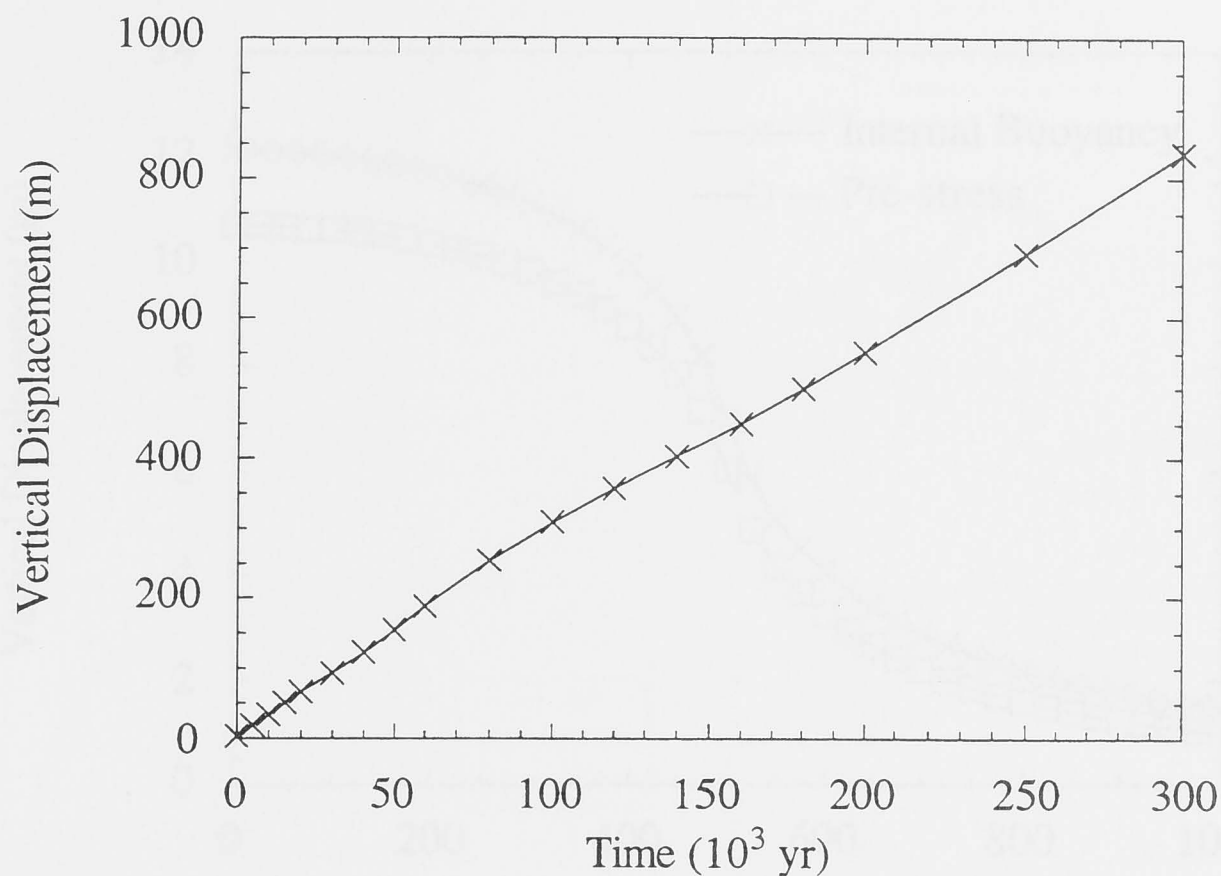
Figure 4.2: Deformation through time at the centre of the load for a Maxwell body with neither pre-stress advection or internal buoyancy included.

consisted of an 80 km lithosphere of viscosity 10^{29} Pa s with a uniform layer of viscosity 10^{21} Pa s beneath, both rigidity and bulk modulus were taken to be constant throughout the half-space at 3.6×10^{10} Pa and 6.5×10^{10} Pa respectively.

In the absence of any buoyancy term in the mathematical formulation, the load sinks deeper and deeper into the body through time, the calculated deformation passing isostatic equilibrium at approximately 4×10^{4} yr and continuing indefinitely in agreement with the singular behaviour observed by Peltier (1974). This is obviously inconsistent with our intuitive expectation and neglecting both pre-stress advection and internal buoyancy renders our analytical model physically meaningless.

Both terms have a similar form and the same magnitude relative to the other entries of the governing matrix of the system, their relative importance and effect is not immediately obvious however. Figures 4.3, 4.4 and 4.5 give the results obtained for a semi-infinite visco-elastic half-space under a square ice sheet of side 1 000 km and 400 m thickness. The earth model used for these calculations consisted of an 80 km elastic lithosphere, an upper mantle viscosity of 10^{20} Pa s and a lower mantle viscosity of 10^{21} Pa s . The rigidity, bulk modulus, and density of the body were calculated from the PREM model of Dziewonski & Anderson (1981) averaged over four regions, the lithosphere, the upper-most mantle between depths of 80 km and 400 km, the transition
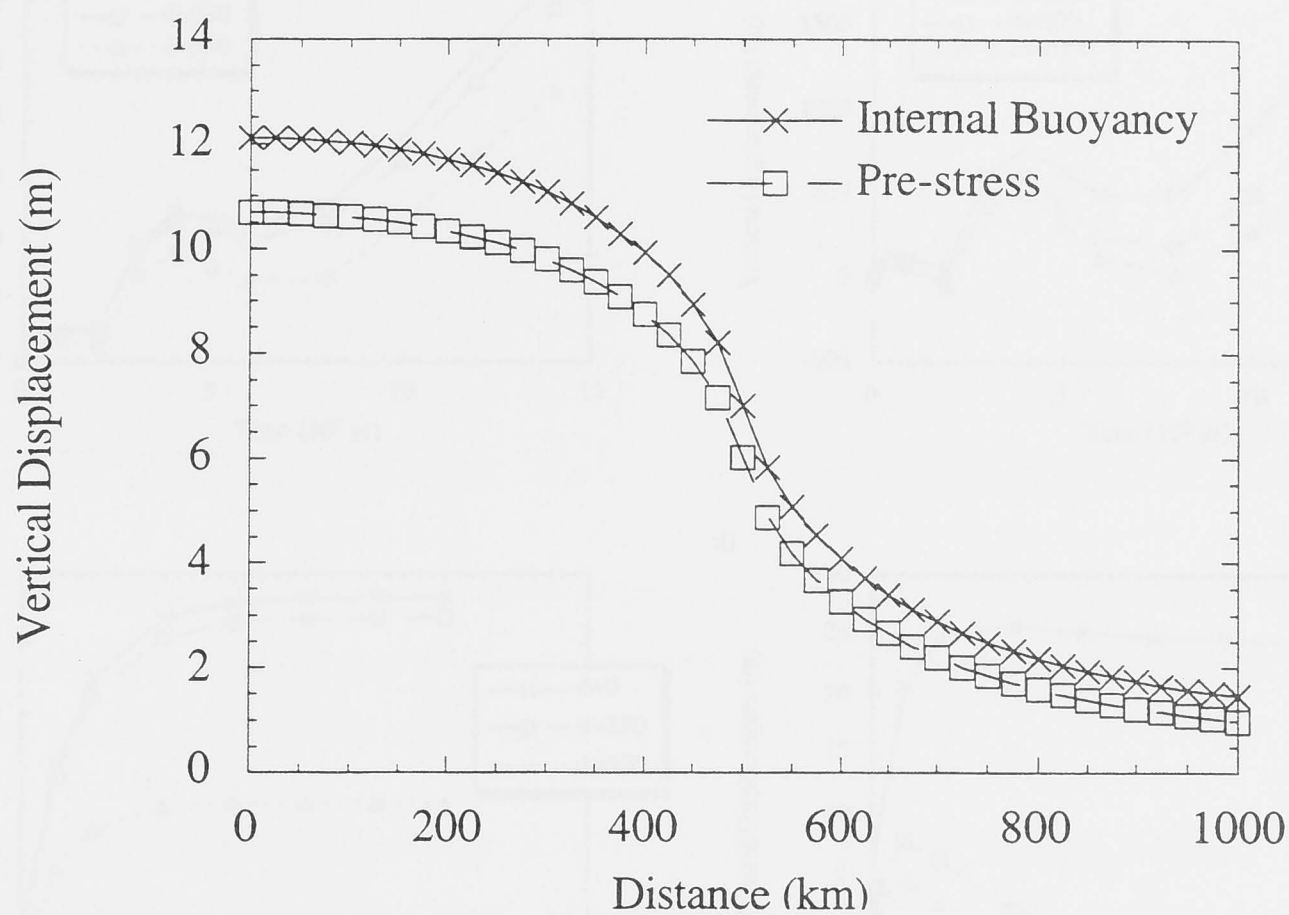
Figure 4.3: Comparison of elastic results for the formulation where pre-stress advection is included and internal buoyancy is neglected (solid line) as compared with the results for the case where the internal buoyancy term is included and pre-stress is neglected (dashed line)

zone, extending from 400 km to 670 km, and the lower mantle from 670 km down (in this case the lower mantle is an infinite layer, its physical properties averaged from PREM values for the lower mantle from the 670 km discontinuity to the core mantle boundary). The figures compare the results for the case where pre-stress advection is included and internal buoyancy is neglected as against the case where internal buoyancy is included and pre-stress is neglected. Figure 4.3 shows the results for both cases immediately after the application of the load, comparing the vertical displacement as function of x_1.

Qualitatively the two curves are very similar, with the internal buoyancy term producing a slightly larger vertical displacement over the surface of the body, the difference between the two curves decreasing steadily as the edge of the grid is approached. At this point the behaviour of both models is quite reasonable.

Figure 4.4 compares results through time for the origin and points at distances of 250 km, 500 km, 600 km, 800 km, and 1 000 km from the centre of the load along the x_1-axis, while figure 4.5 shows the corresponding cross-sections of deformation taken along the x_1-axis at 2×10^3 yr, 5×10^3 yr, and 10^4 yr after the application of the load, the infinite limit is also given for the case with pre-stress.

The results for the case where internal buoyancy is included without pre-stress advection are quite dramatic. In this instance a given parcel of material inside the body
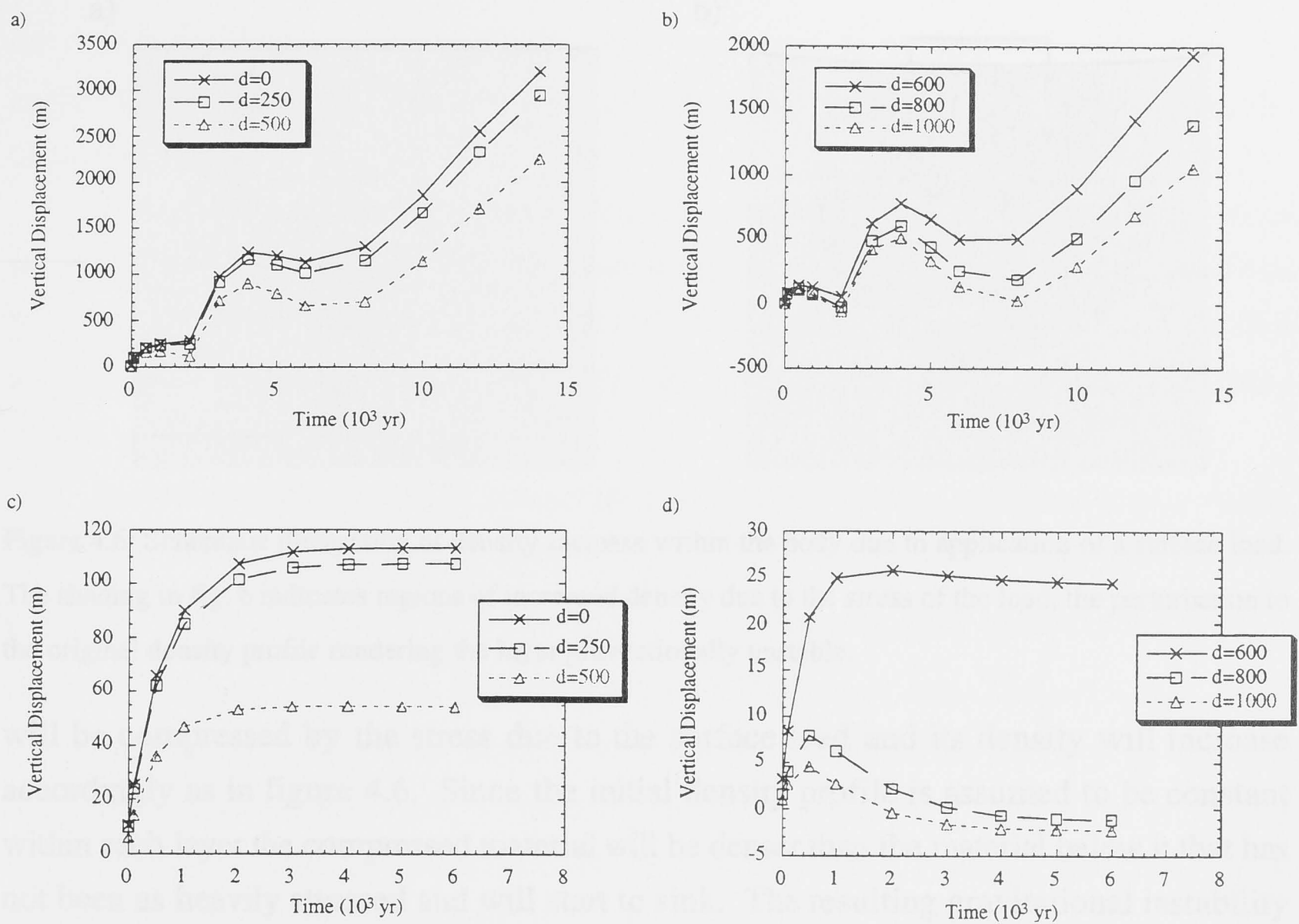
a)

b)

c)

d)

Figure 4.4: Comparison of deformation curves through time for the case where internal buoyancy (figures (a) and (b)), and pre-stress advection (figures (c) and (d)) are included in visco-elastic calculations. Curves for figures (a) and (c) are taken at the origin and distances of 250 km, and 500 km along the x_1 -axis. For figures (b) and (d) the curves were taken at distances 600 km, 800 km, and 1 000 km along the x_1 -axis.
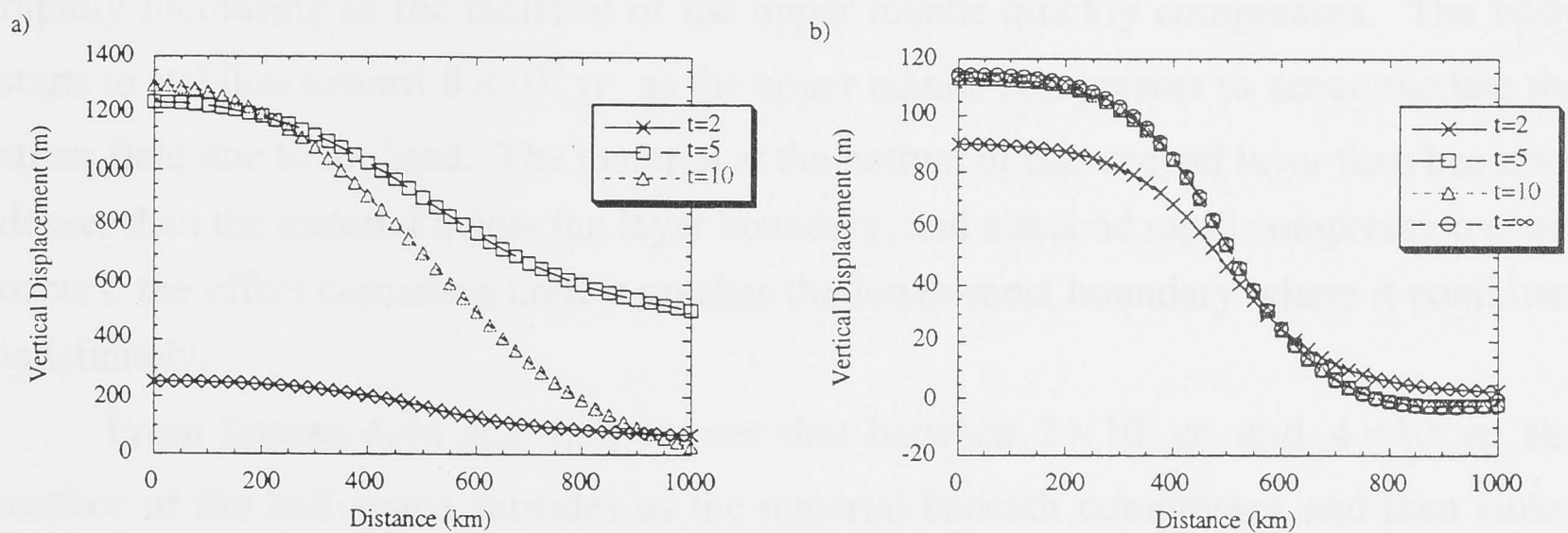
a)

b)

Figure 4.5: Cross-sections of deformation for the case where a) internal buoyancy and b) pre-stress advection are included in visco-elastic calculations. Curves taken at 2×10^3 yr, 5×10^3 yr, and 10^4 yr , with the infinite limit included in fig. (b).

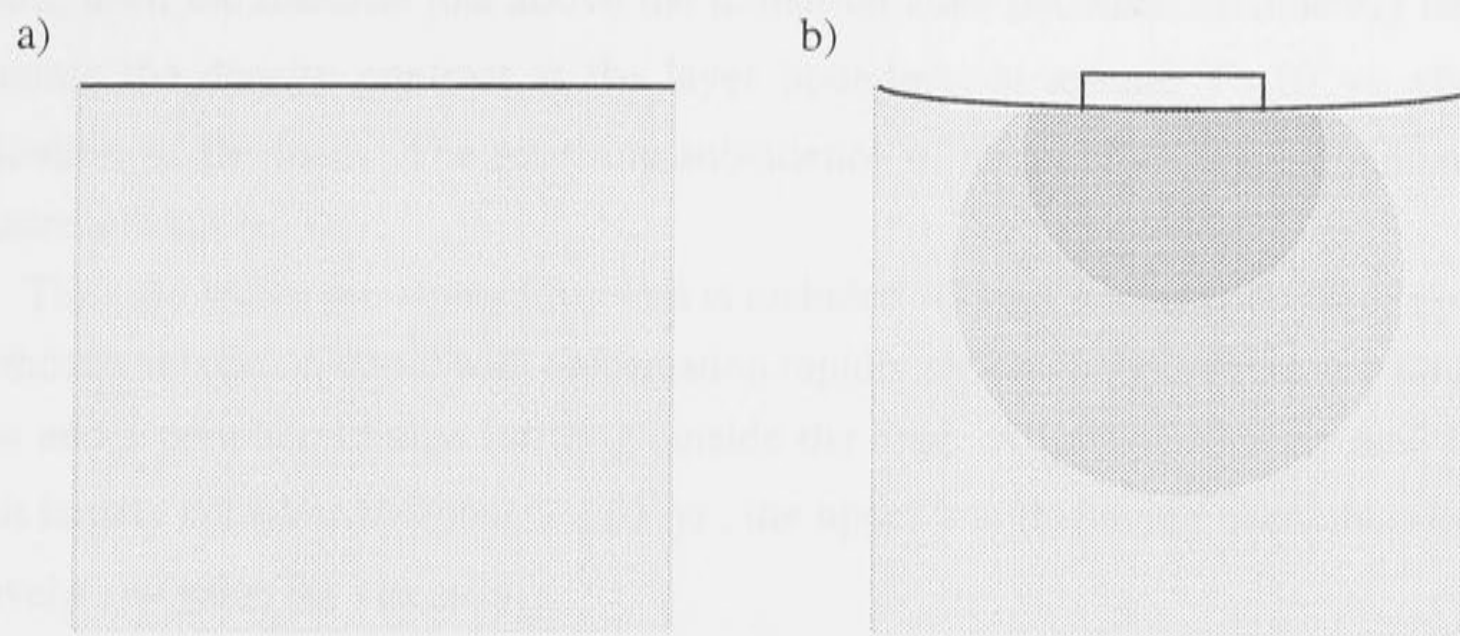a)   b)

Figure 4.6: Schematic illustration of density increase within the body due to application of a surface load. The shading in fig. b indicates regions of increased density due to the stress of the load, the perturbation to the original density profile rendering the layer gravitationally unstable.

will be compressed by the stress due to the surface load and its density will increase accordingly as in figure 4.6. Since the initial density profile is assumed to be constant within each layer the compressed material will be denser than the material below it that has not been as heavily stressed and will start to sink. The resulting gravitational instability leads to disproportionately large surface displacements.

The deformation curves through time for this case show the cascade-style effect of the internal buoyancy term, initially the body deforms very similarly to the case where pre-stress is included. At about 2×10^3 yr after the application of the load however, the density of the material at the bottom of the uppermost layer has increased to the point where it is as dense as the material below the layer boundary and deformation starts rapidly increasing as the material of the upper mantle quickly compresses. The body starts to stabilise toward 8×10^3 yr as the upper mantle compresses to accommodate the stress field due to the load. The material at the bottom of this second layer then becomes denser than the material below the layer boundary, and a second rapid compression event occurs, the effect cascading until it reaches the lower-most boundary where it continues indefinitely.

From figures 4.4a and 4.5a we see that between 2×10^3 yr and 4×10^3 yr the surface of the half-space subsides as the material beneath compresses and then sinks. This subsidence induces significant horizontal flow in the compressed upper mantle to accommodate the new stress-field, which acts to reduce vertical deformation by allowing the material of the layer to move laterally from the neighbourhood of the load to regions of lower stress, in the process of which it expands and vertical displacement is reduced. The upper mantle moves rapidly toward a gravitationally stable configuration from 4×10^3 yr

onward, until the material just above the transition zone becomes sufficiently dense to overcome the density contrast at the layer boundary, at around 7×10^3 yr after the application of the load. The resulting subsidence of the surface layer dominates the displacement curve.

The case where pre-stress advection is included without internal buoyancy produces an orthodox relaxation curve with deformation rapidly approaching the isostatic limit from below and a peripheral bulge forming outside the load. Adjustment to the new surface load is largely complete by about 5×10^3 yr, the upper mantle having been chosen with a relatively low value for viscosity.

Including both pre-stress advection and internal buoyancy introduces a subtle numerical problem. From the form of (4.1.16) we see that the eigenvalues of the governing matrix are real for $\rho g \left(\mu \left(\lambda + 2\mu \right) \right)^{-1/2} < \alpha$. For very small values of the Laplace transform variable, s, we see from (1.3.14) that $\tilde{\mu}^*(s) \approx \eta s$, and $\tilde{\lambda}^*(s) \approx \lambda + \tfrac{2}{3}\mu$. For parameter values typical when dealing with realistic earth models we have $\eta s \ll \mu$ and imaginary eigenvalues result. These eigenvalues are purely imaginary and their exponentials consequently do not decay or increase with depth, attacking the formalism of the reflection-transmission analysis that underpins the wave propagation procedure. This may be avoided by keeping the effective wave number, α, sufficiently large, which in turn requires that the grid-size be kept correspondingly small.

Figures 4.7 and 4.8 compare the results of calculations for a body in which pre-stress advection is included and the effect of internal buoyancy is alternately included and neglected. For these models we used the the same grid size as in the previous case, 512×512 data points, with a grid-spacing of 0.5 km rather than 25 km so that the zero edge condition will not be valid for anything but extremely small loads. The qualitative behaviour of the results should be largely unaffected however and they provide a useful comparison of the nature, effect, and relative importance of each of the terms in the inertia equation. The results shown were calculated for an ice load 400 m thick of side 100 km for an earth model similar to that considered above except that the depth of the layer boundaries were uniformly decreased by a factor of ten to allow viscous effects to become significant. For this scale of load, an 80 km lithosphere would result in deformation curves dominated by the elastic component, which we saw in the comparison of pre-stress and internal buoyancy above, is not sufficient to distinguish between two rival techniques. To allow the effect of each term in the visco-elastic regime to be assessed we have moved to a rheological model with an 8 km thick elastic lithosphere, a transition zone at a depth of 40 km, and a 67 km discontinuity. The rheological parameters throughout each region were taken equal to those in the corresponding region of the previous earth model.
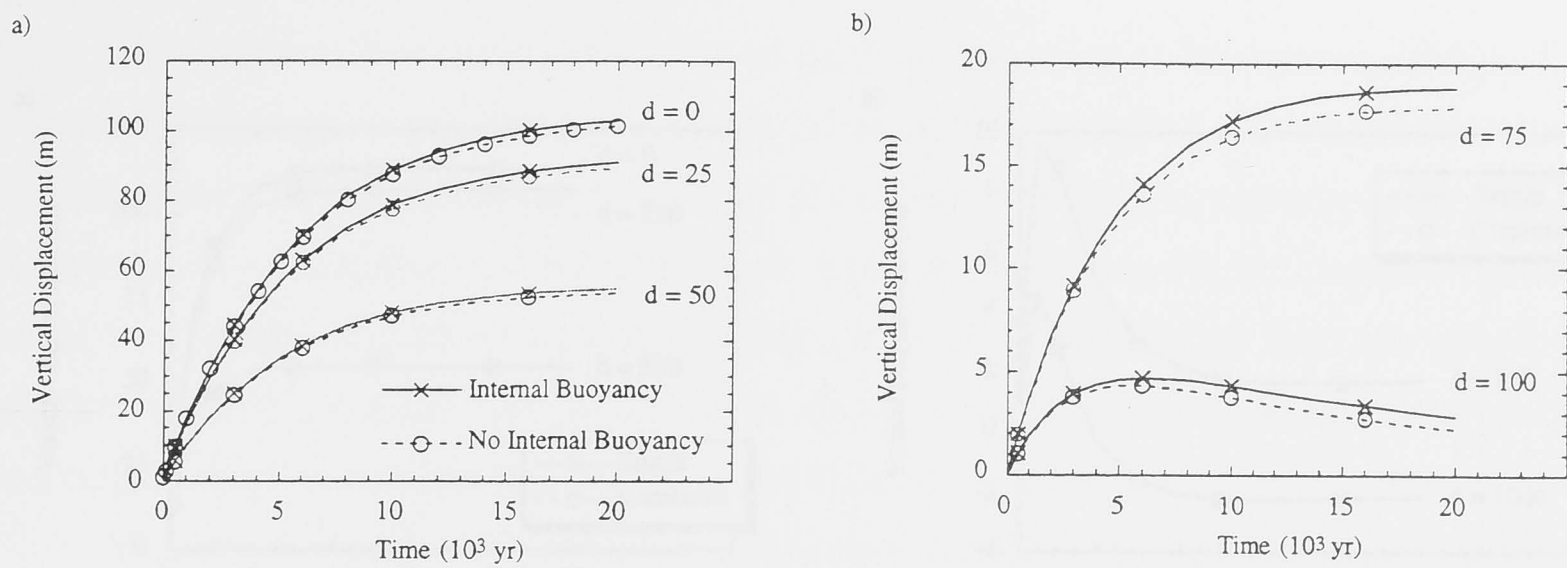
a)

b)

Figure 4.7: Comparison of deformation curves through time for visco-elastic models with pre-stress only (dashed lines) and both pre-stress and internal buoyancy (solid lines). Curves in fig. (a) are given for the origin, and at distances 25 km and 50 km along the -axis. The curves in fig. (b) are given for points at distances 75 km and 100 km along the x_1 -axis.
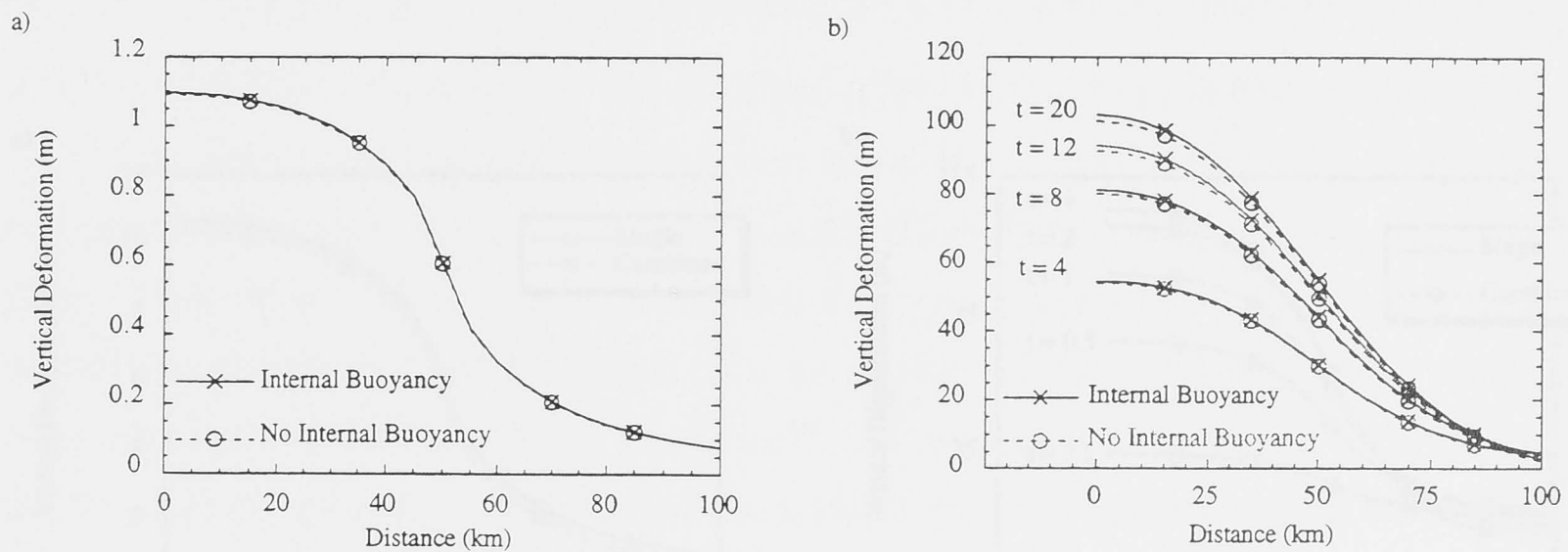
a)

b)

Figure 4.8: Comparison of cross-sections of deformation for earth models with pre-stress advection only (dashed lines), and both pre-stress advection and internal buoyancy (solid lines). Fig. (a) shows the comparison for the elastic case, and Fig. (b) the visco-elastic case. The curves for fig. (b) were taken at times 4×10^3 yr, 8×10^3 yr, 1.2×10^4 yr and 2×10^4 yr after the application of the load.

The agreement between the two sets of results is almost exact for short time scales and is nowhere larger than a few percent. The amount of vertical deformation that occurs at a fixed point inside the body will be a function of the total vertical stress at that point, which will include the stress due to the surface load and the weight of the overlying material. The amount of mantle material above a certain point is itself determined by the amount of vertical displacement that has occurred, the greater the deformation, the less overlying material, and the lower the resulting stress. Large vertical stresses are therefore compensated to some extent by the deformations they produce and vice versa so that the relationship between stress and displacement is damped by negative feedback in the form of the pre-stress advection term. Neglecting pre-stress advection removes the damping term from the system, with catastrophic results in the visco-elastic case.
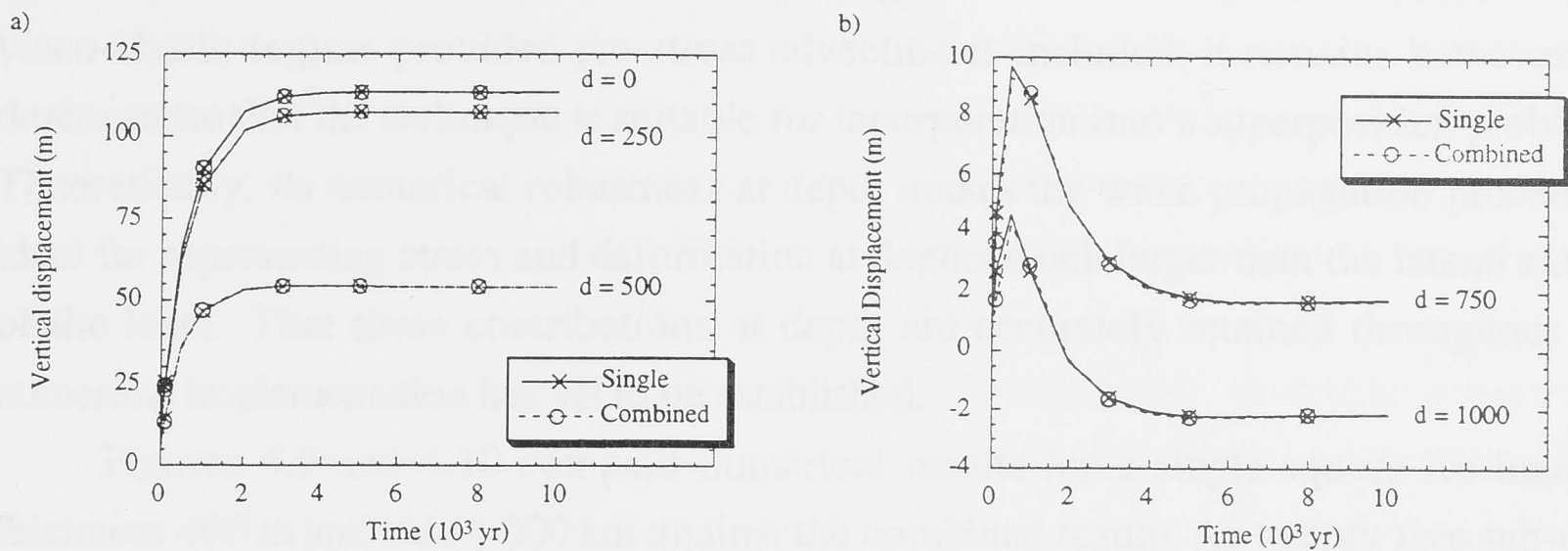
Figure 4.9: Comparison of deformation curves through time calculated from the combined contribution of 25 sub-unit loads of radius 200 km (dashed lines) and a single load of side 1 000 km (solid lines). Curves in fig. (a) are given for the origin, and at distances 250 km and 500 km along the -axis. The curves in fig. (b) are given for points at distances 750 km and 1000 km along the x_1 -axis.
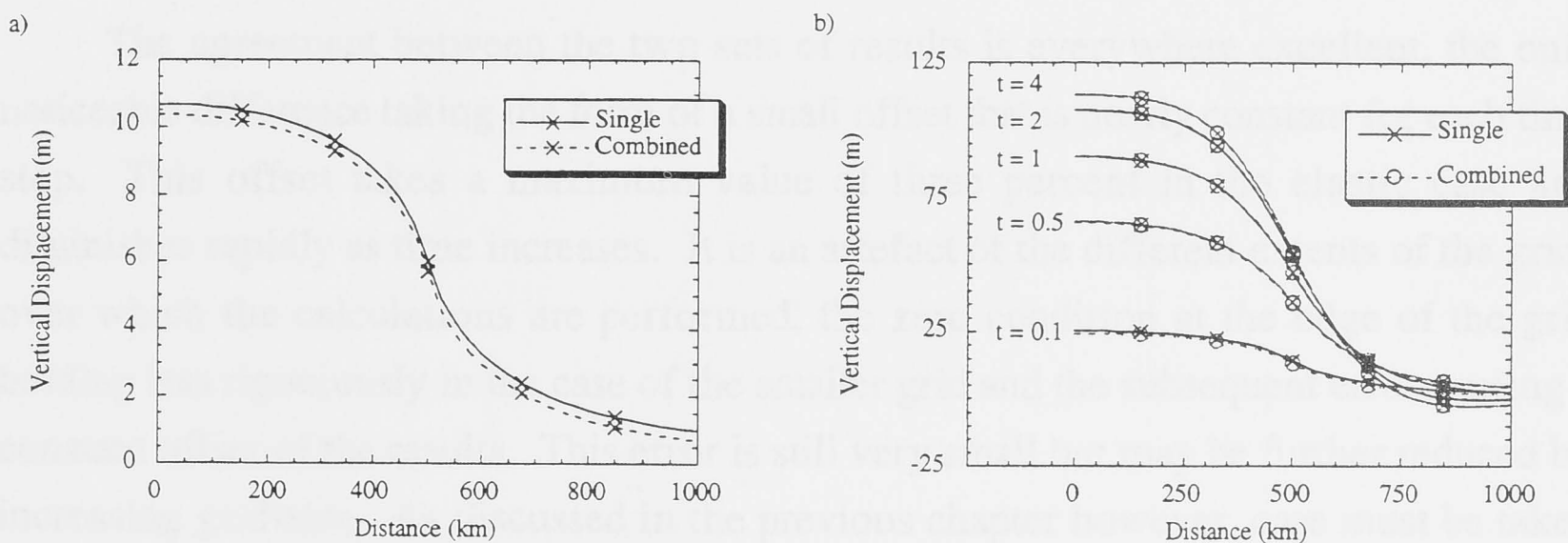

Figure 4.10: Comparison of cross-sections of deformation calculated from the combined contribution of 25 sub-unit loads of width 200 km (dashed lines) and a single load of side 1 000 km (solid lines). Fig. (a) shows the comparison for the elastic case, and Fig. (b) the visco-elastic case, with curves taken at times 10^2 yr, 5×10^2 yr, 10^3 yr, 2×10^3 yr and 4×10^{34} yr after the application of the load.

Neglecting internal buoyancy removes the effect of compression of the body, for small deformations this will not be a significant contribution, several hundred metres of deformation spread through the top few hundred kilometres of the mantle represents only a fractional increase in density. In an unstable or nearly unstable system however, this term provides positive feedback, large vertical displacements produce significantly increased densities, which in turn produce increased vertical stresses as the compressed material sinks. In the absence of pre-stress, the effects of the internal buoyancy term yield spectacular but clearly unrealistic results for the visco-elastic case, as the instability introduced by neglecting pre-stress is magnified.

The numerical accuracy of the wave propagation scheme has been established in the visco-elastic regime provided pre-stress advection is included, it remains however, to demonstrate that the technique is suitable for incorporation into a superposition problem. Theoretically, its numerical robustness at depth makes the wave propagation procedure ideal for representing stress and deformation at depths much larger than the lateral extent of the load. That these contributions at depth are accurately retained throughout the numerical implementation has yet to be established.

Figures 4.9 and 4.10 compare numerical results for a single square ice load of thickness 400 m and side 1 000 km against the combined results for twenty five sub-unit loads of thickness 400 m and side 200 km. The results given are for the same earth model as used for figures 4.4 and 4.5 with the pre-stress term included, both sets of calculations were performed over a grid of 512×512 data points with a grid-spacing of 25 km for the single load and 5 km for the combined loads. Figure 4.9 shows relaxation curves through time for fixed points on the x_1-axis, while figure 4.10 compares cross-sections of vertical displacement taken along the x_1-axis for fixed times after the application of the load.

The agreement between the two sets of results is everywhere excellent, the only noticeable difference taking the form of a small offset that is nearly constant for each time step. This offset takes a maximum value of three percent in the elastic case and diminishes rapidly as time increases. It is an artefact of the different extents of the grids over which the calculations are performed, the zero condition at the edge of the grid holding less rigourously in the case of the smaller grid and the subsequent error causing a constant offset of the results. This error is still very small but may be further reduced by increasing grid-size. As discussed in the previous chapter however, care must be taken not to increase grid-spacing to the point of losing resolution of the load.

4.2 The Case of an Incompressible Half-space

One popular simplification of glacial rebound problems is the assumption that the earth is an incompressible body. In the case of spherical modelling this approximation allows the time-dependent Love numbers to be calculated analytically using the normal mode analysis of Peltier (1985) while in the flat-earth procedures it considerably simplifies the algebra involved.

The usefulness of this class of model for comparison with analytical solutions is indisputable and in this section the theory of the two more sophisticated propagator matrix procedures will be adapted to the incompressible case.

In an incompressible body dilatation, Δ, defined in (1.5.4) is taken to be zero, $\lambda \to \infty$, and the quantity $(\lambda + \mu)\Delta$ is taken to be finite in limit (which makes sense of (2.1.3) and all subsequently dependent equations).

This obviously effects the governing matrix A given in (4.1.4) which in this case takes the form:

$$A = \begin{bmatrix} 0 & 0 & 0 & v_1 & \dfrac{1}{\mu} & 0 & 0 \\ 0 & 0 & 0 & v_2 & 0 & \dfrac{1}{\mu} & 0 \\ -v_1 & -v_2 & 0 & 0 & 0 & 0 \\ \mu\left(4\,v_1^2 + v_2^2\right) & 3\mu\,v_1 v_2 & \rho g v_1 \delta_1 & 0 & 0 & v_1 \\ 3\mu\,v_1 v_2 & \mu\left(v_1^2 + 4\,v_2^2\right) & \rho g v_2 \delta_1 & 0 & 0 & v_2 \\ \rho g v_1 \delta_1 & \rho g v_2 \delta_1 & 0 & -v_1 & -v_2 & 0 \end{bmatrix} \tag{4.2.1}$$

The non-zero entries in a_{61} and a_{62} result from substitution of the entries from the third row of the matrix for the $\rho g \partial_3$ term at a_{63}.

Cast in this form A has the characteristic equation:

$$\det\left(A - \alpha_i I\right) = \left(\alpha_i^2 - \alpha^2\right)^3 \tag{4.2.2}$$

regardless of the value of δ_1, and has a degenerate system of eigenvalues (as was pointed out for the two-dimensional case by Wolf 1985b), so that it becomes necessary to employ the Jordan form technique outlined in chapter 2.

Using standard techniques we deduce that the diagonalising matrix for A is:

$$
D = \begin{bmatrix}
v_2\beta_1 & v_1\beta_2 & {}^{v_1\beta_2}\!/_{2\alpha} & v_2\beta_1 & v_1\beta_2 & -{}^{v_1\beta_2}\!/_{2\alpha} \\
-v_1\beta_1 & v_2\beta_2 & {}^{v_2\beta_2}\!/_{2\alpha} & -v_1\beta_1 & v_2\beta_2 & -{}^{v_2\beta_2}\!/_{2\alpha} \\
0 & -\alpha\beta_2 & {}^{\beta_2}\!/_2 & 0 & \alpha\beta_2 & {}^{\beta_2}\!/_2 \\
\mu v_2\beta_1\alpha & 2\mu v_1\beta_2\alpha & \mu v_1\beta_2 & -\mu v_2\beta_1\alpha & -2\mu v_1\beta_2\alpha & \mu v_1\beta_2 \\
-\mu v_1\beta_1\alpha & 2\mu v_2\beta_2\alpha & \mu v_2\beta_2 & \mu v_1\beta_1\alpha & -2\mu v_2\beta_2\alpha & \mu v_2\beta_2 \\
0 & 2\alpha\beta_2(\kappa-\mu\alpha) & (\kappa-\mu\alpha)\beta_2 & 0 & -2\alpha\beta_2(\kappa+\mu\alpha) & (\kappa+\mu\alpha)\beta_2
\end{bmatrix}
$$

$$(4.2.3)$$

Where $\kappa = \dfrac{\rho g \delta_1}{2}$ and β_1 and β_2 are again chosen to make the system orthonormal.

The inverse of the diagonalising matrix then takes the form:

$$
D^{-1} = \begin{bmatrix}
\mu v_2\beta_1 & -\mu v_1\beta_1 & 0 & v_2\beta_1 & -v_1\beta_1 & 0 \\
\mu v_1\beta_2 & \mu v_2\beta_2 & -(\mu\alpha+\kappa)\beta_2 & {}^{v_1\beta_2}\!/_{2\alpha} & {}^{v_2\beta_2}\!/_{2\alpha} & -{}^{\beta_2}\!/_2 \\
2\mu v_1\beta_2\alpha & 2\mu v_2\beta_2\alpha & 2\alpha\beta_2(\kappa+\mu\alpha) & v_1\beta_2 & v_2\beta_2 & -\alpha\beta_2 \\
\mu v_2\beta_1 & -\mu v_1\beta_1 & 0 & -v_2\beta_1 & v_1\beta_1 & 0 \\
\mu v_1\beta_2 & \mu v_2\beta_2 & (\mu\alpha-\kappa)\beta_2 & -{}^{v_1\beta_2}\!/_{2\alpha} & -{}^{v_2\beta_2}\!/_{2\alpha} & -{}^{\beta_2}\!/_2 \\
-2\mu v_1\beta_2\alpha & -2\mu v_2\beta_2\alpha & 2\alpha\beta_2(\mu\alpha-\kappa) & v_1\beta_2 & v_2\beta_2 & \alpha\beta_2
\end{bmatrix}
$$

$$(4.2.5)$$

In this case the vector coefficients are defined so that:

$$
\beta_1^{-2} = 2\mu\alpha^3 \qquad\qquad \beta_2^{-2} = 4\mu\alpha^2
$$

$$(4.2.6)$$

and are also independent of δ_1.

4.3 Discussion

Neglecting pre-stress advection significantly simplifies the analytical treatment of elastic deformation, and has become standard in many engineering applications. Even in the elastic regime however, this neglect can lead to singularities in the algebraic solutions obtained. The similar form of the internal buoyancy term raises the possibility that it too may have a significant effect on the physical meaningfulness of model results.

The analytical complexity of including both terms has prompted many workers to simplify the formalism of the problem by neglecting internal buoyancy and adopting a simplified form for the contribution of the pre-stress term (as in Nakiboglu & Lambeck 1982). The validity of neglecting internal buoyancy had yet to be established however, and in this chapter the formalism of the conventional and wave propagator matrix procedures was extended to include both pre-stress advection and internal buoyancy, allowing their individual contributions to be examined.

The pre-stress advection term was found to provide negative feedback between stress and displacement, and to be critically important in the visco-elastic case, forcing the deformation to equilibrium over long time-scales, in accordance with previous treatments of the issue (Peltier 1974, Wolf 1985c,d, 1994). In contrast, internal buoyancy produces positive feedback between stress and deformation, and when included without pre-stress further reduces the stability of the system to produce strikingly non-physical results.

The results obtained for the case where both terms are included in our formulation demonstrate that, despite its strong analytical similarity, the effect of internal buoyancy is not significant over any time-scale in the flat-earth case, provided pre-stress is included. The numerical and physical accuracy of the wave propagator matrix procedure is guaranteed by incorporating pre-stress, and largely unaffected by neglecting the internal buoyancy term, allowing us to circumvent the numerical limitations of the technique when pre-stress and internal buoyancy are both incorporated. This accuracy is reflected in the technique's excellent stability and performance in superposition problems, the error introduced into the results for the composite load quickly becoming negligibly small, and never becoming significant compared with observational uncertainty.

Chapter 5

CONCLUSION

5.0   Discussion

Recent advances in dating techniques, data collection, and computer technology have made possible super-high resolution modelling of the earth's response to the melting of Holocene and latest Pleistocene ice sheets and the concomitant change in sea-level. Detailed modelling of these ice sheets can place strong constraints on both the evolution of the ice sheets and the earth's response to loading problems of this scale. The progress of deglaciation is in itself an important palaeo-climatic indicator and in regions such as the Barents Sea, North Sea and the Irish Sea where rising sea-levels have obliterated much of the geomorpholigical evidence of glacial advance and retreat, numerical inversion of the rebound data can provide valuable constraints on the history of the deglaciation process. In the current work I have examined the suitability of available modelling procedure to these high resolution problems and discussed the limitations and advantages of each, particularly their suitability for use as part of a numerical inversion scheme.

In chapter 1 I reviewed the formalism for the global spherical harmonic technique and demonstrated the excessive numerical cost of achieving high resolution using this procedure. The Spherical Cap Harmonic Analysis (SCHA) and Adjusted Spherical Harmonic Analysis (ASHA) schemes were also modified to a form appropriate for modelling deformation rather than the geomagnetic field for which they were first developed. The SCHA technique was demonstrated to be subject to significant numerical instability due to the size and complexity of the least squares problem required to calculate the coefficients of the spherical harmonic expansion, though the complexity of the technique could be greatly reduced by an appropriate choice of angular radius of the cap. The ASHA procedure offers an apparently simpler formulation but at the cost of physical meaningfulness. Scaling the angular radius of the load requires in turn that the physical response parameters of the earth be altered in a consistent fashion to avoid exaggerating the effect of sphericity or the width of the load. The consequence of this is that the rheology of the translated sphere will not be isotropic, attacking one of the central assumptions of the the procedure by which the Love numbers are calculated. The spherical harmonic formulations have therefore not been further developed in this work.

In view of the limitations of these spherical methods when applied to high-resolution problems, attention was next given to flat earth models in which the earth is taken to be a flat, semi-infinite half-space. In chapter 2 the mathematical formalism for the basic, conventional, and wave propagator matrix procedures for a flat semi-infinite half-space were developed in three-dimensional Cartesian coordinates. This change of coordinate systems significantly complicated the analytical development of each procedure

and for simplicity pre-stress advection, internal buoyancy, and gravitational perturbation terms were initially neglected. The added complexity of the Cartesian formulation is rewarded by the greater power, resolution, and flexibility of the new coordinate system, which may more readily be adapted to accommodate arbitrary load geometries than the two-dimensional cylindrical polar coordinate systems used in previous treatments. The stability of these flat-earth techniques at depth was shown to depend on the ratio between the depth of the bottom-most layer boundary and the spacing of the grid over which the calculations are performed. The basic technique was shown to fail when this dimensionless depth reached 70, while the conventional procedure was stable down to a depth of 150. The greater analytic sophistication of the wave propagator matrix technique guarantees complete and stable decoupling of increasing and decreasing exponential terms in the problem; for a 1 km grid spacing the scheme did not fail for any value of dimensionless depth up to 5 000, comparable with the radius of the earth.

A further advantage of the wave propagation technique is that transmission of the surface stress-displacement field into the body is stable with depth, the same is not true for the basic and classical procedures where the propagator matrices include exponentially growing terms. Though each of the flat-earth techniques agreed well with the analytical results for a uniform half-space, only the wave propagator was sufficiently well behaved with depth to be used as part of a scheme relying on superposition of individual loads.

Numerical inversion of the Fourier and Laplace transforms is an integral part of calculations for a visco-elastic half-space and can introduce significant numerical error unless the inversion routines and their associated parameters are chosen appropriately. In order to maintain the accuracy of the wave propagator technique, the Fourier transform requires a fine enough grid spacing that the load is well defined, and a large enough grid that the assumption of zero deformation at its edge is valid. The latter requirement was demonstrated to be the more significant, the numerical results for a square load becoming accurate to within a fraction of a percent for a grid of lateral extent 20 times that of the load, and to within three percent for a grid half that size. Grid spacings up to 20 percent of the width of the load produced good agreement with the analytical results, provided points at the edge and corner of the load were scaled appropriately.

Inversion of the Laplace transform is complicated by numerical instability at very small frequencies, a feature common to calculations for both the spherical and flat earth cases. The inversion schemes investigated in chapter 3 were all adversely affected by the sensitivity of these calculations. The secular determinant required for the normal mode method exhibits elaborately intricate variations for compressible earth models with either a thin lithosphere or a low upper mantle viscosity, rendering the technique unreliable for this class of rheology. Despite the greater mathematical rigour of its derivation, and its accuracy over short time scales, the normal mode procedure exhibited oscillatory

behaviour of substantially larger amplitude on long time scales than the collocation scheme for a simplistic four layer incompressible model.

The bilinear transform technique produced excellent results for time-scales less than 8×10^3 yr years in the incompressible case but broke down very rapidly thereafter. The magnitude of the scaling parameter was found to impact on the accuracy of the integrals used to calculate the coefficients in the Chebyshev series, and the technique could not be extended to longer time-scales.

The results for the Legendre approximation gave initial errors of up to ten percent but rapidly converged with the results for the other techniques by about 2×10^3 yr to give good agreement for the incompressible case. The maximum degree of the approximation was limited by the stability of the linear system used to calculate the coefficients of the approximating series. This maximum degree was substantially reduced in the compressible case where the scheme began to exhibit suspect numerical stability. Despite this, the results for the Legendre approximation provided a useful comparison for the collocation procedure in the compressible case. The agreement between the two was good though the collocation technique exhibited no signs of numerical instability apart from small amplitude oscillations over very long time-scales (5×10^4 yr to 10^5 yr). The effect of these oscillations on sea-level calculations was demonstrated for an axially symmetric incompressible earth by comparison with results for the normal mode scheme and shown to be significantly smaller than observational uncertainty.

In chapter 4 the formalism of the conventional and wave propagator matrix techniques was modified to include both the pre-stress advection and internal buoyancy terms. Pre-stress advection was shown to be crucially important in the visco-elastic case where it damps the system and forces deformation toward isostatic equilibrium on long time-scales. Its effect in the elastic case was also considered in response to the poor analytical behaviour of algebraic solutions to Boussinesq's problem. The internal buoyancy term was demonstrated to further reduce numerical stability in the absence of pre-stress advection, and did not significantly affect the results for earth models that already included the pre-stress term, justifying its neglect in the flat earth case.

Previous treatments of a flat visco-elastic half-space have been restricted to two dimensional stress systems, allowing only strip or cylindrical loads to be considered. Failure to decouple the growing and decaying exponential terms has further limited the results of these studies by introducing significant numerical instability at depths greater than the width of the load being modelled. Neither limitation affects the validity of the flat earth formulation for large-scale problems but has precluded the possibility of high resolution modelling or incorporation into a superposition scheme, since the contribution at depth will be lost.

The development of a numerically robust flat earth scheme capable of representing arbitrary load geometries greatly facilitates the development of a direct inversion scheme for rebound data, and dramatically simplifies high resolution forward modelling, particularly at depth.

BIBLIOGRAPHY

Amelung, F. & Wolf, D., 1994. Viscoelastic Perturbations of the Earth: Significance of the Incremental Gravitational Force in Models of Glacial Isostasy, *Geophys. J.*, **117**: 864-879.

Abramowitz, M. & Stegun, I. A., 1972. *Handbook of Mathematical Functions with Formulas, Graphs, and Mathematical Tables*, Dover Publications, New York.

Biot, M. A., 1965. *Mechanics of Incremental Deformations*, John Wiley & Sons.

Bloom, M. A., 1967. Pleistocene Shorelines: A New Test of Isostasy. *Geol. Soc. Am. Bull.*, **18**:1477-1494.

Braun, M., 1983. *Differential Equations and their Applications*, Springer Verlag, New York.

Boyce, W. R. & DiPrima, R. C., 1977. *Elementary Differential Equationa and Boundary Value Problems*, John Wiley & Sons.

Cathles, L. M., 1975. *The Viscosity of the Earth's Mantle*, Princeton University Press, Princeton.

Dahlen, F. A., 1974. On the Static Deformation of an Earth Model with a Fluid Core, *Geophys. J. R. Astr. Soc.*, **36**: 461-485.

Dahlen, F. A. & Fels, S. B., 1978. A Physical Explanation of the Static Core Paradox, *Geophys. J. R. Astr. Soc.*, **55**: 317-331.

Dvies, B. & Martin, B., 1979. Numerical Inversion of the Laplace Transform a Survey and Comparison of Methods, *J. Comp. Phys.*, **33**: 1-32.

De Santis, A., 1991. Translated Origin Spherical Cap Harmonic Analysis, *Geophys. J. Int.*, **106**: 253-263.

De Santis, A., 1992. Conventional Spherical Harmonic Analysis for Regional Modelling of the Geomagnetic Field, *Geophys. Res. Letters*, **19**: 1065-1067.

Dziewonski, A. M. & Anderson, D. L., 1981. Preliminary Reference Earth Model, *Phys. Earth Planet. Int.*, **25**: 297-356.

Erdélyi, A., 1943. *Phil. Mag.*, **34**: 533-537.

Fang, M. & Hager, B. H., 1994. A Singularity Free Approach to Post Glacial Rebound Calculations, *Geophys. Res. Letters*, **21**: 2131-2134.

Farrell, W. E., 1972. Deformation of the Earth by Surface Loads, *Rev. Geophys. Space Phys*, **10**: 761-797.

Farrell, W. E. & Clark, J. A., 1976. On Postglacial Sea-Level, *Geophys. J. R. Astr. Soc.*, **46**: 647-667.

Firth, C. R. & Haggart, B. A., 1989. Loch Lommond Stadial and Flandrian Shorelines in the Inner Moray Firth Area, Scotland, *J. Quaternary Sci.*, **4**: 37-50.

Fung, Y. C., 1965. *Foundations of Solid Mechanics*, Prentice-Hall, New Jersey.

Gantmacher, F. R. (translated into English by Hirsch, K. A.), 1960. *The Theory of Matrices*, Chelsea, New York.

Gasperini, P. & Sabadini, R., 1989. Lateral Heterogeneities in Mantle Viscosity and Post-Glacial Rebound, *Geophys. J.*, **98**: 413-428.

Gilbarg, D. & Trudinger, N. S., 1983. *Elliptic Partial Differential Equations of Second Order*, Springer Verlag, Berlin.

Gradshteyn, I. S. & Ryzhik, I. M., 1980. *Table of Integrals, Series and Products*, Academic Press, London.

Goodbody, A. M., 1982. *Cartesian Tensors with Applications to Mechanics, Fluid Mechanics and Elasticity*, Halsted Press, New York.

Haggart, B. A., 1986. Relative Sea-Level Change in the Beauly Firth, Scotland, *Boreas*, **15**: 191-207.

Haines, G. V., 1985. Spherical Cap Harmonic Analysis, *J. Geophys. Res.*, **90**: 2583-2591.

Haskell, N. A., 1935. The Motion of a Viscous Fluid under a Surface Load, *Physics*, **6**: 265-269.

Jeffreys, H., 1976. *The Earth: Its Origin, History and Physical Constitution*, Cambridge University Press, Cambridge.

Johnston, P. J., 1993. *Deformation of the Earth by Surface Loads*, Doctoral thesis, Australian National University, Canberra.

Johnston, P. J., Lambeck, K. & Wolf, D., 1997. Material vs. Isobaric Internal Boundaries in the Earth and their Influence on Postglacial Rebound, *In Press.*

Kaufmann, G., 1991. *Auswirkungen Adiabatischer und Chemischer Dichtegradienten auf das Relaxationsverhalten eienes Maxwell-Halbraums*, Diploma thesis, Westfälische Wilhelms-Universitat, Münster.

Kennett, B. L. N., 1981. Elastic Wave Propagation in Stratified Media, *Advances in Applied Mechanics*, **21**: 80-167

Kreyszig, E., 1983. *Advanced Engineering Mathematics*, John Wiley & Sons, New York.

Krylov, V. I. & Skoblya, N. S. (translated into English by Yankovsky, G.), 1977. *A Handbook of Methods of Approximate Fourier Transform and Inversion of the Laplace Transformation*, Mir Publishers, Moscow.

Lambeck, K., 1993a. Glacial Rebound of the British Isles - I. Preliminary Model Results, *Geophys. J. Int.*, **115**: 941-959.

Lambeck, K., 1993b. Glacial Rebound of the British Isles - II. A High-Resolution, High-Precision Model, *Geophys. J. Int.*, **115**: 960-990.

Lambeck, K., Johnston, P. J., Smither, C. & Nakada, M. 1996. Glacial Rebound of the British Isles - III. Constraints on Mantle Viscosity, *Geophys. J. Int.*, **125**: 340-354.

Lambeck, K., Smither, C. & Johnston, P. J. 1997. Glacial Rebound of Northern Europe, *Geophys. J. Int.*, In Press.

Lanczos, C., 1957. *Applied Analysis*, Pitman, London.

Longman, I. M., 1962. A Green's Function for Determining the Deformation of the Earth under Surface Mass Loads: 1. Theory, *J. Geophys. Res.*, **67**: 845-850.

Longman, I. M., 1963. A Green's Function for Determining the Deformation of the Earth under Surface Mass Loads: 2. Computations and Numerical Results, *J. Geophys. Res.*, **68**: 485-496.

Love, A. E. H., 1911. *Some Problems of Geodynamcs,* Cambridge University Press, Cambridge.

Love, A. E. H., 1927. *A Treatise on the Mathematical Theory of Elasticity*, Dover Publications, New York.

Love, A. E. H., 1929. On Stress Produced in a Semi-infinite Solid by Pressure on Part of the Boundary, *Trans. Roy. Soc. Lond.*, **228**:378-420.

McConnell, R. K., 1965. Isostatic Adjustment in a Layered Earth, *J. Geophys. Res.*, **70**: 5171-5188.

McConnell, R. K., 1968. Viscosity of the Mantle from Time Spectra of Isostatic Adjustment, *J. Geophys. Res.*, **73**: 7089-7105.

Mitrovica, J. X. & Peltier, W. R., 1991. A Complete Formalism for the Inversion of Post-Glacial Rebound Data: Resolving Power Analysis, *Geophys. J. Int.*, **104**: 267-288.

Mitrovica, J. X. & Peltier, W. R., 1992. A Comparison of Methods for the Inversion of Viscoelastic Relaxation Spectra, *Geophys. J. Int.*, **108**: 410-414.

Nakada, M. & Lambeck, K., 1987. Glacial Rebound and Relative Sea-Level Variations: A New Appraisal, *Geophys. J. R. Astr. Soc.*, **90**: 171-224.

Nakiboglu, S. M. & Lambeck, K., 1982. A Study of the Earth's Response to Loading with Application to Lake Bonneville, *Geophys. J. R. Astr. Soc.*, **70**: 577-620.

Papoulis, A., 1956. , *Quart. Appl. Math.*, **14**: 405-414.

Piessens, R., 1972. A New Numerical Method for the Inversion of the Laplace Transform, *J. Inst. Math. Applic.*, **10**: 185-192.

Peltier, W. R., 1974. The Impulse Response of a Maxwell Earth, *Rev. Geophys. Space Phys.*, **12**: 649-669.

Peltier, W. R., 1976. Glacial Isostatic Adjustment II: The Inverse Problem, *Geophys. J. R. Astr. Soc.*, **46**: 669-705.

Peltier, W. R., 1982. Dynamics of the Ice Age Earth, *Adv. Geophys.*, **24**: 1-146.

Peltier, W. R., 1985. The LAGEOS Consraint on Deep Mantle Viscosity: Results from a new Normal Mode Method for Inversion of Viscoelastic Relaxation Spectra, *J. Geophys. Res.*, **90**: 9411-9421.

Peltier, W. R. & Andrews, J. T., 1976. Glacial Isostatic Adjustment I: The Forward Problem, *Geophys. J. R. Astr. Soc.*, **46**: 605-646.

Press, W. H., Flannery, B. P., Tukolsky, S. A. & Vetterling, W. T., 1986. *Numerical Recipes: The Art of Scientific Computing*, Cambridge University Press.

Quinlan, G. & Beaumont, C., 1982. The Deglaciation of Atlantic Canada as Reconstructed from the Postglacial Relative Sea-Level Record, *Can.. J. Earth Sci.*, **19**: 2232-2246.

Ranalli, G., 1982. Deformation Maps in Grain Size-Stress Space as a Tool to Investigate Mantle Rheology. *Phys. Earth Plant. Inte.*, **29**: 42-50.

Rainville, Earl D., 1960. *Special Functions*, MacMillan, New York.

Saada, A. S., 1974. *Elasticity: Theory and Applications*, Pergamon Press, New York.

Schapery, R. A., 1962. Approximate Methods of Transform Inversion for Viscoelastic Stress Analysis, *Proc. 4th Nat. Congr. Appl. Mech.*, pages 1075-1085.

Sissons, J. B., 1974. The Quaternary in Scotland: A Review, *Scot. J. Geol.*, **10**:311-337.

Sissons, J. B., 1981. The Last Scottish Ice Sheet: Facts and Speculative Discussion, *Boreas*, **10**:1-17.

Sneddon, I. N., 1951. *Fourier Series*, McGraw-Hill, New York.

Spiegel, M. R., 1968. *Mathematical Handbook of Formulas and Tables*, McGraw-Hill.

Strang, G., 1980. *Linear Algebra and its Application*, Academic Press, London.

Timoshenko, S. P. & Goodier, J. N., 1970. *Theory of Elasticity*, McGraw-Hill, New York.

Timoshenko, S. P. & Woinowsky-Krieger, S., 1959. *Theory of Plates and Shells*, McGraw-Hill, New York.

Vermeersen, L. L. A., Sabadini, R. & Spada, G., 1996a. Compressible Rotational Deformation, *Geophys. J. Int.*, **126**: 735-761.

Vermeersen, L. L. A., Sabadini, R. & Spada, G., 1996b. Analytical Visco-ELastic Relaxation Modes, *Geophys. Res. Letters*, **23**: 697-700.

Wolf, D., 1984. The Relaxation of Spherical and Flat Maxwell Earth Models and Effects due to the Presence of the Lithosphere, *J. Geophys.*, **56**: 24-33.

Wolf, D., 1985a. The Normal Modes of a Uniform, Compressible Maxwell Half-Space, *J. Geophys.*, **56**: 100-105.

Wolf, D., 1985b. The Normal Modes of a Layered, Incompressible Maxwell Half-Space, *J. Geophys.*, **57**: 106-117.

Wolf, D., 1985c. Thick Plate Flexure Re-examined,*Geophys. J. R. Astr. Soc.*, **80**: 265-273.

Wolf, D., 1985d. On Boussinesq's Problem for a Maxwell Continua Subject to an External Gravity Field, *Geophys. J. R. Astr. Soc.*, **80**: 275-279..

Wolf, D., 1991. Viscoelastodynamics of a Stratified, Compressible Planet: Incremental Field Equations and Short- and Long-Time Asymptotes, *Geophys. J. Int.*, **104**: 401-417.

Wolf, D., 1994. *Gravitational Viscoelastodynamics for a Hydrostatic Planet*, Thesis, Institut für Planetologie, Westfälische Wilhelms-Universität, Münster.

Wu, P., 1978. *The Response of a Maxwell Earth to Applied Surface Mass Loads: Glacial Isostatic Adjustment*, Master's thesis, University of Toronto.

Wu, P., 1992. Deformation of an Incompressible Viscoelastic Flat Earth with Power-Law Creep, *Geophys. J. Int.*, **108**: 35-51.

Wu, P. & Peltier, W. R., 1982. Viscous Gravitational Relaxation, *Geophys. J. R. Astr. Soc.*, **70**: 435-485.

Wu, P. & Peltier, W. R., 1983. Glacial Isostatic Adjustment and the Free Air Gravity Anomaly as a Constraint on Deep Mantle Viscosity, *Geophys. J. R. Astr. Soc.*, **74**: 377-450.

Wu, P. & Peltier, W. R., 1984. Pleistocene Deglaciation and the Earth's Rotation: A New Analysis, *Geophys. J. R. Astr. Soc.*, **76**: 753-791.

Appendix A

PROPAGATOR MATRIX ENTRIES

A.0 Introduction

For the purposes of comparison the entries of the basic and conventional propagator matrices are given here for a 3-dimensional Cartesian coordinate system with neither pre-stress nor dilatation included. The effect of these terms may be incorporated for the converntional technique using the formalism of chapter 4 however.

For ease of notation we suppress the quantity n, the number of the body-layer in which the propagator matrix is being calculated, layer-dependence instead being indicated simply by the Lamé parameters λ and μ. We will also retain the definition for α given in chapter 2, so that $\alpha^2 = v_1^2 + v_2^2$ where v_1 and v_2 are the wavenumbers for the problem.

As discussed in section 2.5, in a practical implementation of the conventional technique a scaling factor of $e^{-\alpha h_{N-1}}$ may be introduced to increase the procedure's numerical stability. This factor is not included here but may be be trivially incorporated into any numerical scheme based on these entries. Similar attempts at scaling the classical propagator technique are not productive since they do not prevent the immense variation in magnitude of the matrix entries themselves.

A.1 Basic Propagator Matrix Entries

Defining constants:

$$\kappa_0 = \frac{\lambda + 3\mu}{\lambda + \mu} \qquad\qquad \kappa_1 = \frac{\mu}{\lambda + \mu} \qquad\qquad \kappa_2 = \frac{\lambda + 2\mu}{\lambda + \mu}$$

the entries of the matrix $M(z) = (m_{ij})$ defined by (2.2.8) and (2.2.9) are given:

$$m_{11} = e^{\alpha z} \qquad m_{31} = -\frac{v_1 e^{\alpha z}}{\alpha} \qquad m_{51} = \frac{\mu}{\alpha} v_1 v_2 e^{\alpha z}$$

$$m_{12} = 0 \qquad m_{32} = -\frac{v_2 e^{\alpha z}}{\alpha} \qquad m_{52} = \frac{\mu}{\alpha}\left(v_1^2 + 2 v_2^2\right) e^{\alpha z}$$

$$m_{13} = v_1 z e^{\alpha z} \qquad m_{33} = \left[\kappa_0 - \alpha z\right] e^{\alpha z} \qquad m_{53} = 2\mu v_1 \left[\alpha z - \kappa_1\right] e^{\alpha z}$$

$$m_{14} = e^{-\alpha z} \qquad m_{34} = \frac{v_1 e^{-\alpha z}}{\alpha} \qquad m_{54} = -\frac{\mu}{\alpha} v_1 v_2 e^{-\alpha z}$$

$$m_{15} = 0 \qquad m_{35} = \frac{v_2 e^{-\alpha z}}{\alpha} \qquad m_{55} = -\frac{\mu}{\alpha}\left(v_1^2 + 2 v_2^2\right) e^{-\alpha z}$$

$$m_{16} = v_1 z e^{-\alpha z} \qquad m_{36} = \left[\kappa_0 + \alpha z\right] e^{-\alpha z} \qquad m_{56} = -2\mu v_2 \left[\alpha z + \kappa_1\right] e^{-\alpha z}$$

$$m_{21} = 0 \qquad m_{41} = \frac{\mu}{\alpha}\left(2 v_1^2 + v_2^2\right) e^{\alpha z} \qquad m_{61} = -2\mu v_1 e^{\alpha z}$$

$$m_{22} = e^{\alpha z} \qquad m_{42} = \frac{\mu}{\alpha} v_1 v_2 e^{\alpha z} \qquad m_{62} = -2\mu v_2 e^{\alpha z}$$

$$m_{23} = v_2 z e^{\alpha z} \qquad m_{43} = 2\mu v_1 \left[\alpha z - \kappa_1\right] e^{\alpha z} \qquad m_{63} = -2\mu\alpha\left[\alpha z - \kappa_2\right] e^{\alpha z}$$

$$m_{24} = 0 \qquad m_{44} = -\frac{\mu}{\alpha}\left(2 v_1^2 + v_2^2\right) e^{-\alpha z} \qquad m_{64} = -2\mu v_1 e^{-\alpha z}$$

$$m_{25} = e^{-\alpha z} \qquad m_{45} = -\frac{\mu}{\alpha} v_1 v_2 e^{-\alpha z} \qquad m_{65} = -2\mu v_2 e^{-\alpha z}$$

$$m_{26} = v_2 z e^{-\alpha z} \qquad m_{46} = -2\mu v_1 \left[\alpha z + \kappa_1\right] e^{-\alpha z} \quad m_{66} = -2\mu\alpha\left[\alpha z + \kappa_2\right] e^{-\alpha z}$$

A.2 Conventional Propagator Matrix Entries

If we define constants:

$$\kappa_3 = \frac{1}{\lambda + 2\mu} \qquad \kappa_4 = (\lambda + \mu)\kappa_3 \qquad \kappa_5 = (\lambda + 3\mu)\kappa_3 \qquad \kappa_6 = \mu\kappa_3$$

and quantities:

$$sh = \sinh(\alpha x) \qquad\qquad ch = \cosh(\alpha x)$$

where sinh and cosh are the standard hyperbolic trigonometric functions (see for example Spiegel, 1968) and x is some scalar quantity, then using the techniques of section 2.3.1 the entries of the matrix $e^{Ax} = N(x) = (n_{ij})$ for the matrix A defined in (2.3.4) can be shown to be:

$$n_{11} = ch + \kappa_4 v_1^2 x \frac{sh}{\alpha} \qquad\qquad n_{12} = \kappa_4 v_1 v_2 x \frac{sh}{\alpha}$$

$$n_{13} = v_1\left[\kappa_4 x ch + \kappa_6 \frac{sh}{\alpha}\right] \qquad n_{14} = \frac{1}{2\mu\alpha^2}\left[\kappa_4 x v_1^2 ch + \left(2 v_2^2 + \kappa_5 v_1^2\right)\frac{sh}{\alpha}\right]$$

$$n_{15} = \frac{\kappa_4 v_1 v_2}{2\mu\alpha^2}\left[x ch - \frac{sh}{\alpha}\right] \qquad n_{16} = \frac{\kappa_4 v_1 x}{2\mu\alpha} sh$$

$$n_{21} = \kappa_4 v_1 v_2 x \frac{sh}{\alpha} \qquad\qquad n_{22} = ch + \kappa_4 v_2^2 x \frac{sh}{\alpha}$$

$$n_{23} = v_2\left[\kappa_4 x ch + \kappa_6 \frac{sh}{\alpha}\right] \qquad n_{24} = \frac{\kappa_4 v_1 v_2}{2\mu\alpha^2}\left[x ch - \frac{sh}{\alpha}\right]$$

$$n_{25} = \frac{1}{2\mu\alpha^2}\left[\kappa_4 x v_2^2 ch + \left(2 v_1^2 + \kappa_5 v_2^2\right)\frac{sh}{\alpha}\right] \qquad n_{26} = \frac{\kappa_4 v_2 x}{2\mu\alpha} sh$$

$$n_{31} = -v_1\left[\kappa_4 x ch - \kappa_6 \frac{sh}{\alpha}\right] \qquad n_{32} = -v_2\left[\kappa_4 x ch - \kappa_6 \frac{sh}{\alpha}\right]$$

$$n_{33} = ch - \kappa_4 \alpha x sh \qquad\qquad n_{34} = -\frac{\kappa_4 v_1 x}{2\mu\alpha} sh$$

$$n_{35} = -\frac{\kappa_4 v_2 x}{2\mu\alpha} sh \qquad\qquad n_{36} = -\frac{1}{2\mu\alpha}\left[\kappa_4 \alpha x ch - \kappa_5 sh\right]$$

$$n_{41} = \mu \left[2\,\kappa_4\,x\,v_1^2\,ch \;+\; \left(v_2^2 + 2\,\kappa_4\,v_1^2 \right) \frac{sh}{\alpha} \right] \qquad n_{42} = \mu\,v_1\,v_2 \left[2\,\kappa_4\,x\,ch \;+\; \lambda\,\kappa_3\,\frac{sh}{\alpha} \right]$$

$$n_{43} = 2\,\mu\,x\,v_1\,\kappa_4\,\alpha\,sh \qquad\qquad n_{44} = ch \;+\; x\,\kappa_4\,v_1^2\,\frac{sh}{\alpha}$$

$$n_{45} = \kappa_4\,v_1\,v_2\,x\,\frac{sh}{\alpha} \qquad\qquad n_{46} = v_1 \left[\kappa_4\,x\,ch \;-\; \kappa_6\,\frac{sh}{\alpha} \right]$$

$$n_{51} = \mu\,v_1\,v_2 \left[2\,\kappa_4\,x\,ch \;+\; \lambda\,\kappa_3\,\frac{sh}{\alpha} \right] \qquad n_{52} = \mu \left[2\,\kappa_4\,x\,v_2^2\,ch \;+\; \left(v_1^2 + 2\,\kappa_4\,v_2^2 \right) \frac{sh}{\alpha} \right]$$

$$n_{53} = 2\,\mu\,x\,v_2\,\kappa_4\,\alpha\,sh \qquad\qquad n_{54} = \kappa_4\,v_1\,v_2\,x\,\frac{sh}{\alpha}$$

$$n_{55} = ch \;+\; x\,\kappa_4\,v_2^2\,\frac{sh}{\alpha} \qquad\qquad n_{56} = v_2 \left[\kappa_4\,x\,ch \;-\; \kappa_6\,\frac{sh}{\alpha} \right]$$

$$n_{61} = -2\,\mu\,\kappa_4\,v_1\,\alpha\,x\,sh \qquad\qquad n_{62} = -2\,\mu\,\kappa_4\,v_2\,\alpha\,x\,sh$$

$$n_{63} = -2\,\mu\,\kappa_4\,\alpha \left[\alpha\,x\,ch - sh \right] \qquad n_{64} = -v_1 \left[\kappa_4\,x\,ch \;+\; \kappa_6\,\frac{sh}{\alpha} \right]$$

$$n_{65} = -v_2 \left[\kappa_4\,x\,ch \;+\; \kappa_6\,\frac{sh}{\alpha} \right] \qquad n_{66} = ch \;-\; \kappa_4\,\alpha\,x\,sh$$

A.3   Comparison

Neglecting all terms including v_2 in either of the previous sections yields 2×2 matrices that correspond to those given by Wolf (1984) and McConnell (1965). Following McConnell's derivation, using the variables defined in (2.2.1) renders the two dimensional Cartesian case exactly analogous to the cylindrical polar formulation under the assumption of axial symmetry which is the case that Wolf considers.

Comparing the form of the two matrices we see that the propagator matrix in the case of the basic technique has very large variations in the magnitude of its entries, rendering it numerically degenerate once depth becomes large. This is particularly serious given the matrix manipulations required in equation (2.2.11). The propagator matrix in the conventional technique is not prone to this problem directly but for large values of x the sinh and cosh terms become indistinguishable and degeneracy ensues.